



NTNU – Trondheim
Norwegian University of
Science and Technology

Optimize Resistance to buckling under external hydrostatic Pressure of thin walled Composite Tubes

Eivind Hugaas

Mechanical Engineering

Submission date: June 2014

Supervisor: Andreas Echtermeyer, IPM

Norwegian University of Science and Technology
Department of Engineering Design and Materials

THE NORWEGIAN UNIVERSITY
OF SCIENCE AND TECHNOLOGY
DEPARTMENT OF ENGINEERING DESIGN
AND MATERIALS

**MASTER THESIS SPRING 2014
FOR
STUD.TECHN. EIVIND HUGAAS**

Optimize resistance to buckling under external hydrostatic pressure of thin walled composite tubes

Optimalisere knekkemotstanden for tynnveggede komposittrør utsatt for hydrostatisk ytre trykk

Composite tubes are widely used as pressure pipes. This study will investigate how such tubes should be made to withstand hydrostatic external pressure. The effect of different layouts shall be investigated by finite element modeling and by experiments. Calculation methods shall be developed to predict buckling behavior. The methods shall be used to optimize the tube structure. Experiments shall be done to validate the approach.

Three weeks after start of the thesis work, an A3 sheet illustrating the work is to be handed in. A template for this presentation is available on the IPM's web site under the menu "Masteroppgave" (<http://www.ntnu.no/ipm/masteroppgave>). This sheet should be updated one week before the Master's thesis is submitted.

Performing a risk assessment of the planned work is obligatory. Known main activities must be risk assessed before they start, and the form must be handed in within 3 weeks of receiving the problem text. The form must be signed by your supervisor. All projects are to be assessed, even theoretical and virtual. Risk assessment is a running activity, and must be carried out before starting any activity that might lead to injury to humans or damage to materials/equipment or the external environment. Copies of signed risk assessments should also be included as an appendix of the finished project report.

The thesis should include the signed problem text, and be written as a research report with summary both in English and Norwegian, conclusion, literature references, table of contents, etc. During preparation of the text, the candidate should make efforts to create a well arranged and well written report. To ease the evaluation of the thesis, it is important to cross-reference text, tables and figures. For evaluation of the work a thorough discussion of results is appreciated.

The thesis shall be submitted electronically via DAIM, NTNU's system for Digital Archiving and Submission of Master's thesis.



Torgeir Welo
Head of Division



Andreas Echtermeyer
Professor/Supervisor

Abstract

Composite tubes are a very good alternative to steel tubes in applications requiring low weight and high stiffness. For composite tubes to replace traditional steel tubes in demanding environments, such as in the subsea petroleum industry, more research on their behavior has to be made to qualify the performance. This thesis seeks to expand that knowledge by investigating the buckling behavior of composite tubes subjected to external hydrostatic pressure. To find a method of correctly predicting the stress and strain states on the tubes, a comparison between FEA and previously acquired strain data from external hydrostatic pressure testing of a composite tube has been carried out. The composite tube had a length of 600 mm and a diameter of 100 mm and was filament wound with a layup of $[89^{\circ}_1/12.7^{\circ}_1/45^{\circ}_1]$ and instrumented with optical fiber to acquire the strain data. It was found that by modeling the cross section of the tube elliptic with 0.46 % ("0.46 % ovality") of the mean diameter added and subtracted to the major and minor diameter of the ellipse respectively, a very good match between FEA and the strain data was found. Using the same ovality, seven different layups were analyzed to find an optimal layup for withstanding external hydrostatic pressure. Based on the optimal layup assessment, the most optimal layup, $[89^{\circ}_2/12.7^{\circ}_1/89^{\circ}_2]$, was produced. The tube was cut into lengths of 300, 400 and 600 mm to assess the buckling behavior and FEA matching's dependency on length. The tubes were instrumented with optical fiber for strain measurements and tested in an autoclave. It was found that the $[89^{\circ}_2/12.7^{\circ}_1/89^{\circ}_2]$ layup performed well having a buckling pressure of 9.75 bar for the 600 mm long tube, 2.79 times that of the $[89^{\circ}_1/12.7^{\circ}_1/45^{\circ}_1]$ layup, despite being just 33.5 % thicker. To achieve a good match in FEA for the $[89^{\circ}_2/12.7^{\circ}_1/89^{\circ}_2]$ layup, the fiber direction E-modulus had to be increased by 12 % to 37738 MPa, compared to the predicted E-modulus from volume fraction scaling. The high E-modulus was concluded as being due to low void content coming from post winding compression of the tubes with peel ply. The ovality needed to achieve matching for the 600 mm long tube was 0.01%. Based on the matching of the shorter tubes it was concluded that longer tubes with the same layup will need an ovality close to 0.01% to simulate correct strain behavior.

Sammendrag

Komposittrør er ett godt alternativ til stålrør i applikasjoner som krever lav vekt og høy stivhet. For at komposittrør skal kunne erstatte tradisjonelle stålrør i ekstreme omgivelser, sånn som kan finnes i oljeindustrien, må mer forskning til for å kvalifisere ytelsen til slike rør. Denne master oppgaven søker å utvide kunnskapen om ytelsen ved å undersøke knekking av komposittrør utsatt for ytre hydrostatisk trykk. For å finne en god metode å forutsi spenninger og tøyninger i rørene har det blitt gjort en sammenligning av FEA og allerede eksisterende tøyningmålinger fra testing av ett komposittrør. Komposittrøret hadde en lengde på 600 mm og en diameter på 100 mm og ble produsert med filament winding med en $[89^{\circ}_1/12.7^{\circ}_1/45^{\circ}_1]$ fiberstruktur, tøyningmålingene ble gjort med optiske fiber. Ved å modellere røret elliptisk med 0.46 % ("0.46 % ovalitet") av normaldiameteren lagt til og trekt fra største og minste diameter i ellipsen, ble det funnet godt samsvar mellom FEA og tøyningmålingene. Ved å bruke den samme ovaliteten ble sju forskjellige fiberstrukturer analysert og sammenlignet for å finne en optimal fiberstruktur med hensyn på maks trykk. Det ble funnet at $[89^{\circ}_2/12.7^{\circ}_1/89^{\circ}_2]$ fiberstruktur var det mest optimale og det ble derfor produsert ett rør med denne fiberstrukturen. Røret ble kuttet i lengder på 300 mm, 400 mm og 600 mm for å undersøke rørets og FE analysens avhengighet av lengde. Rørene ble instrumentert med optiske fiber før de ble testet i en autoklave. Det ble funnet at $[89^{\circ}_2/12.7^{\circ}_1/89^{\circ}_2]$ fiberstrukturens ytelse var god, med ett makstrykk på 9.75 bar for det 600 mm lange røret, 2.79 ganger mer enn for $[89^{\circ}_1/12.7^{\circ}_1/45^{\circ}_1]$ fiberstrukturen, selvom det bare var 33 % tykkere. For å få godt samsvar mellom FEA og $[89^{\circ}_2/12.7^{\circ}_1/89^{\circ}_2]$ fiberstrukturen måtte E-modulen i fiberretning økes med 12 % til 37738 MPa, sammenlignet med E-modulen slik den ble fastsatt gjennom volumfraksjonsskalering. Den høye E-modulen ble konkludert at skyldtes lav andel av luftinneslutninger i fiberstrukturen fra kompresjon med peel ply etter ferdig vikling av røret, som i sin tur skviste ut luftinneslutninger. Ovaliteten for samsvar i FEA for det 600 mm lange røret var på 0.01 %. Basert på testing av de to kortere rørene ble det konkludert med at lengere rør med samme geometri og fiberstruktur vil trenge en ovalitet nærme 0.01 % for å forutsi korrekte tøyninger.

Preface

This work is a master's thesis at NTNU carried out in the Spring of 2014 to investigate optimal filament wound layups on tubes when subjected to external hydrostatic pressure. Besides finding, producing and testing a possible optimal layup, the thesis also aims to find a method to match FEA strain results with strain measured with optical fiber on the tubes. During the Autumn of 2013 a preparatory project (project thesis) was carried out as preparation for the master's thesis to investigate how filament wound tubes buckle compared to FEA and to validate if optical fiber can measure strain on the tubes while being submerged. It was found, during the project thesis, that the optical fiber performed well and that work has to be done to achieve a better match between FEA and the optical fiber. The work to find a good method of achieving a good FEA match with the optical fiber strain measurements from the project thesis was made into a paper that can be found in the appendix.

Trondheim, 2014-06-10

A handwritten signature in black ink, reading "Eivind Hugaas". The signature is written in a cursive style and is positioned above a horizontal dotted line.

Eivind Hugaas

Acknowledgment

I would like to thank the following persons for their great help during the work.

MSc Carl-Magnus Midtbø, PhD student Jon Harald Lambert Grave, Associate Professor Nils Petter Vedvik and the student group in room 230.

I would also like to thank my supervisor for his contribution to my work.

Professor Andreas Echtermeyer

A handwritten signature in cursive script, reading "Eivind Magnus". The signature is written in black ink and is positioned above a horizontal dotted line.

E. H.

Table of contents

Problem description	i
Abstract	iii
Sammendrag	v
Preface	vii
Acknowledgment	ix
Table of contents	xi
List of figures	xiv
List of tables	xvi
List of symbols	xix
Abbreviations	xxi
1 Introduction	1
1.1 Introduction	1
1.2 Problem Formulation	2
1.3 Filament winding	2
1.4 Optical fiber strain measuring	3
1.5 Earlier work	4
1.6 Winding angle and layer definition	6
1.6.1 Winding angle definition	6
1.6.2 Layer and ply definition	7

xi

TABLE OF CONTENTS

1.7	Theory	8
1.7.1	Riks analysis	8
1.7.2	Linear buckling analysis	9
2	FEA	11
2.1	Geometry and mesh	12
2.2	Layup and material properties	13
2.3	Loads and boundary conditions	15
2.4	Riks and linear buckling analysis parameters	16
2.4.1	Riks analysis	16
2.4.2	Linear buckling analysis	16
2.5	Optimal Layup assessment	16
2.5.1	Conclusion and choice of layup for production	23
2.6	Analysis on produced layup	23
2.6.1	Length sensitivity analysis	24
3	Tube design and production	27
3.1	Design, material and winding layup	27
3.2	Winding machine setup	28
3.2.1	Winding machine programming	28
3.3	Mandrel treatment and curing	28
4	Test setup and method	31
4.1	Endcaps	33
4.2	Fiber instrumentation and equipment	34
4.2.1	Autoclave interface	36
4.3	Pressure equipment and manometer	36
4.4	Test method	37
5	Material investigation	39
5.1	Burn-off testing	39
5.2	Thickness measurements	40

5.3	Microscopy	40
5.4	Scaling of material properties	41
6	Results	45
6.1	Data acquisition details and comment on result presentation	46
6.2	600 mm long tube	47
6.2.1	Pressure test	47
6.2.2	FEA match	48
6.3	400 mm long tube	49
6.3.1	FEA match	49
6.4	300 mm long tube	51
6.5	Length sensitivity	52
6.6	Comparison table	54
7	Discussion	65
7.1	Optimal layup behavior	65
7.2	FEA comparison and length sensitivity	70
8	Conclusion and recommendations for further work	75
8.1	Conclusion	75
8.2	Recommendations for further work	77
A	Paper	81
B	Graphs	95
B.1	Strain measurements from 600 mm long tube test nr. 1	96
B.2	Strain measurements from 600 mm long tube test nr. 2	99
B.3	Strain measurements from 400 mm long tube test nr. 1	102
B.4	Strain measurements from 400 mm long tube test nr. 2	103
B.5	Strain measurements from 300 mm long tube	104
B.6	Pressure readings from the 600 mm long tube	105
B.7	Pressure readings from the 400 mm long tube	107
B.8	Pressure readings from the 300 mm long tube	109

TABLE OF CONTENTS

B.9 LPF curve	110
C Tables	111
C.1 Layer thickness	112
C.2 Material properties	113
C.3 Material background information	114
C.4 Clock times for optical fiber strain readings readings	115
D Pictures	117
D.1 Microscopy pictures	118
D.2 layups for the optimal layup assessment	129
D.3 Failure Criteria	133
D.4 Deformation plots and tangential strain path start points	135
E Risk assessments	139
E.1 Risk assessment of thesis	140
E.2 Risk assessment of filament winding	143
E.3 Risk assessment of testing	147
E.4 Risk assessment explanation	151

List of Figures

1.1	Messenger et. al. test rig.	5
1.2	Cylindrical coordinate system.	7
2.1	FEA constraints and loads.	15
2.2	Tangential FEA strain at 3.41 bar for the $[89^{\circ}_1/12.7^{\circ}_1/45^{\circ}_1]$ layup	18
2.3	Axial FEA strain at 3.41 bar for the $[89^{\circ}_1/12.7^{\circ}_1/45^{\circ}_1]$ layup.	19
2.4	Pressure VS Arc length for assessed layups.	21
2.5	$[89^{\circ}_2/12.7^{\circ}_1/89^{\circ}_2]$ layup visualization.	24
2.6	Length sensitivity analysis on produced layup pre testing.	26
3.1	Tube with peel ply applied.	29
4.1	The autoclave.	32
4.2	End caps	33
4.3	Endcap applied with stickytape.	33
4.4	Tubes with optical fiber pretest.	35
4.5	T-fitting with pressure hose and fiber escaping through end cap.	36
5.1	Perillo's ring compression test setup.	43
5.2	Perillo's ring compression test setup as modeled in FEA.	44

6.1	Fixed constraints on the 400 mm long tube.	51
6.2	Tubes post testing.	56
6.3	Strain at 150 mm on the 600 mm long tube, test nr. 1.	57
6.4	Strain at 300 mm on the 600 mm long tube, test nr. 1.	57
6.5	Strain at 450 mm on the 600 mm long tube, test nr. 1.	58
6.6	Strain at 150 mm on the 600 mm long tube, test nr. 2.	59
6.7	Strain at 300 mm on the 600 mm long tube, test nr. 2.	59
6.8	Strain at 450 mm on the 600 mm long tube, test nr. 2.	60
6.9	Strain at 200 mm on the 400 mm long tube, test nr. 1.	60
6.10	Strain at 200 mm on the 400 mm long tube, test nr. 2.	61
6.11	Strain at 150 mm on the 300 mm long tube.	61
6.12	Tsai-wu failure criterion for the 600 mm long tube.	62
6.13	Tsai-wu failure criterion in the top ply on the 600 mm long tube.	62
6.14	Length sensitivity analysis	63
6.15	Strain energy.	63
7.1	Shear strain comparison.	67

List of Tables

1	Complete list of symbols	xix
2.1	Material properties from project thesis.	13
2.2	Layups for the optimal layup assessment	14
2.3	Optimal layup assessment results.	22
2.4	$[89^{\circ}_2/12.7^{\circ}_1/89^{\circ}_2]$ layup	24
3.1	Filament winding parameters	28
5.1	Burn-off test result with volume fractions.	39
5.2	Thickness measurement of the $[89^{\circ}_2/12.7^{\circ}_1/89^{\circ}_2]$ layup.	40
5.3	Layer thickness.	41
5.4	Scaled material properties.	42
6.1	Result comparison table	55

List of symbols

Table 1: Complete list of symbols

Symbol	Description
1	When used in context with direction, this denotes the fiber direction of the ply.
2	When used in context with direction, this denotes the transvers fiber direction of the ply.
12	When used in context with direction, this denotes shear in 12 direction.
E_1	Modulus of elasticity in the 1 direction for the composite material.
E_2	Modulus of elasticity in the 2 direction for the composite material.
E_3	Modulus of elasticity in the 3 direction for the composite material.
ν_{12}	Poisson's number for the 12 direction of the composite material.
ν_{13}	Poisson's number for the 13 direction of the composite material.
ν_{23}	Poisson's number for the 23 direction of the composite material.
G_{12}	Shear modulus for the 12 direction for the composite material.
X_T	Tensile strength in the longitudinal direction for the composite material.
X_C	Compressive strength in the longitudinal direction for the composite material.
Y_T	Tensile strength in the transverse direction for the composite material.
Y_C	Compressive strength in the transverse direction for the composite material.

S_{12}	Shear strength in the 12 direction.
S_{13}	Shear strength in the 13 direction.
S_{23}	Shear strength in the 23 direction.
E_{1f}	Modulus of elasticity in the longitudinal direction of the fiber.
E_{2f}	Modulus of elasticity in the transverse direction of the fiber.
E_m	Modulus of elasticity in the matrix material.
V_f	Volume fraction.
t	Total thickness of the filament winded tube.

Abbreviations

NTNU	Norwegian University of Science and Technology
FWM	Filament Winding Machine
FW	Filament Winding
LPF	Load Proportionality Factor
GFRP	Glass Fiber Reinforced Polymer
FE	Finite Element
FEA	Finite Element Analysis
UD	Uni Directional
FBG	Fiber Bragg Gratings
OBR	Optical Backscatter Reflectometry

Introduction

1.1 Introduction

Composite tubes are seen today in many different applications due to a high strength to weight ratio. There is an increasing interest in replacing steel tubes that operate in high pressure and high temperature environments with composite tubes [14]. Such applications include, most notably, drilling risers and drill strings for the subsea oil industry [22]. Replacing steel risers and steel drill strings with composite tubes when drilling deep wells at deep waters will greatly cut the weight of the equipment and will also have the benefit of requiring less buoyancy elements built into the structures. When performing operations at deep waters, the critical design pressure may be, as opposed to tubes operating in shallow waters, the external pressure. In order for composite tubes to be qualified for high external pressure, they need to be thoroughly tested so as to qualify not only the material, but also the analysis tools, design methodology and production methods. This thesis will focus mainly on the analysis tools and the design of such tubes when subjected to external pressure. Firstly, the thesis aims at developing a method in FEA to accurately predict the behavior of thin walled GFRP tubes subjected to external pressure. Secondly, the thesis aims at using the FEA method to find an optimal layout that can withstand relatively high external pressure.

1.2 Problem Formulation

The problem to be investigated is firstly to find a way of matching previously acquired strain readings from external hydrostatic pressure testing of filament wound tubes with FEA. The strain readings were acquired from optical fiber glued circumferentially on the outer surface of a GFRP filament wound tube subjected to external hydrostatic pressure in NTNU's autoclave. After having found a good matching method, the method is to be used to find good candidates for an optimal layup with high buckling pressure and a low failure exposure factor. Secondly, the most optimal layup is to be produced and subjected to external hydrostatic pressure while being monitored with optical fiber to measure strain. Lastly, the data from the optical fibers are to be compared with FEA to investigate further the matching method. Due to the fact that applications for such tubes will likely be in context of long tubes, as for the subsea oil industry, finding how the end effect affects buckling is also to be studied. The end effect will be assessed by testing tubes of different lengths and comparing this with FEA predictions. The goal of the end effect assessment is to be able to accurately analyze long tube sections based on FEA matching parameters taken from testing on shorter tube sections.

1.3 Filament winding

Filament winding is a composite material production method where fibers are continuously applied on a mandrel over time. This is done by having the mandrel rotate while the fiber is being wound onto it from a CNC type machine. The filament winding machines of today are multi axis CNC machines that operate according to a preprogrammed path [22]. Before the fiber is wound on to the mandrel, the fiber is coated with epoxy, usually by passing through an epoxy bath built into the filament winding machine. When the epoxy has hardened, the mandrel is usually withdrawn and only the composite shell is left [22]. The mandrel can also be left as a part of the wound structure. The fibers can be wound with different angles in different layers, resulting in a product with very tailored mechanical properties. Modern machines can wind not only straight tubes, but also structures with advanced rotational geometry. It also ex-

ists filament winding machines where the mandrel is stationary and the fiber is wound onto it by having the surrounding machine rotating. By the last method continuous tubes and pipes of theoretically infinite length can be wound [22].

1.4 Optical fiber strain measuring

To measure strain on the tubes, optical fiber was used. The use of optical fiber to measure strain allows for monitoring and measuring of strain fields instead of strain at single points, as for classic strain gauges and fiber bragg gratings. In the paper in Appendix A a short description of the equipment and how it works can be found. For an extensive and more in depth description, see the the OBR 4600 User Manual [2] along with M. Haaheim's master's thesis [16], where NTNU's optical fiber equipment was verified and tested in the context of strain measuring on composites.

1.5 Earlier work

As a preparation for the work in this master's thesis, a project thesis focusing on comparing FEA with strain results from optical fibers on tubes subjected to external hydrostatic pressure was carried out in the Autumn of 2013. In the project thesis, a tube with a layup of $[89^{\circ}_1/12.7^{\circ}_1/45^{\circ}_1]$ was instrumented with optical fibers to measure strain and then tested for external hydrostatic pressure in an autoclave. Besides, a FEA analysis was carried out, but the match between FEA and test results was found to be poor and improvements to the FEA was suggested to achieve a better match. The project thesis was also intended to investigate how well the optical fiber performed when being submerged. Since the optical fiber proved to give reliable strain readings it was decided to proceed with the same testing method for the tubes in the master's thesis. Based on the conclusions and recommendations in the project thesis, part of the master's thesis was made to focus on developing a FEA matching method. The work for finding a matching method with the optical fiber strain measurements from the project thesis has been written as a paper and can be found in Appendix A.

Most relevant study conducted so far on buckling of composite tubes from external hydrostatic pressure and finding optimal layups is Messenger et. al. [24]. Messenger et. al. found a layup optimization model for carbon fiber and glass fiber filament wound tubes with the goal of increasing the resistance against buckling. The study was based on comparing FEA with test results of tubes with different layups. The optimization model consisted of an algorithm coupled with a FEA buckling analysis to give the best possible layup with regards to buckling pressure with a given geometry of the tube. For thin tubes, the layup that proved the most optimal in FEA and in the tests was that of $[90^{\circ}_3/15^{\circ}_2/90^{\circ}_2]$. Of special interest was the study's use of a test rig that enabled visual inspection of the tube during testing by having the tube constrained to the outside of the pressure cylinder. The test rig is shown sketched in Figure 1.1.

Though Messenger et. al. found a model for predicting optimal layups, only visual inspection was carried out to investigate how and when the tubes buckled. No strain measurements was carried out and only the buckling mode and buckling pressure was investigated.

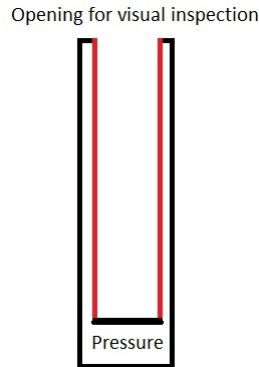


Figure 1.1: Schematic sketch of the Messenger et. al. [24] test rig. Red is the tube while black represents the pressure vessel and the endcap at one end.

A study that investigated the strain development in composite tubes subjected to external pressure was that of D. Choqueuse [14] et. al.. The study investigated the buckling behavior of composite reinforced steel tubes subjected to external hydrostatic pressure. The steel tubes to be tested were filament wound with carbon fiber in the hoop direction. The tubes had an 8 mm layer of filament wound carbon fiber over a 5 mm thick steel tube with inner diameter of 124 mm and length of 520 mm. To measure the strain during testing, optical fiber bragg gratings were used and were embedded into the filament wound layer. Pressure was applied in a water autoclave. To study the buckling shape, a FEA analysis was carried out and matched with the strain readings from the fiber bragg gratings. The results showed that reinforcing of the tubes could increase the buckling pressure with as much as 50% with pressures between 414 and 583 bar (large scatter). Due to delamination between the steel and the CFRP, some unusual buckling modes occurred that was not initially predicted by the FEA. However, by modifying the boundary conditions between the layers, agreement between FEA and test results were found. The study reported that the FBG worked well up to 200 bar, whereafter the FBG had "significant decreases in performance".

Though D. Choqueuse managed to attain strain readings with FBG, it only gave strain at single points, as opposed to optical fiber that provides strain fields. Also, with optical fiber, noise occurring at spots along the length of the fiber does not necessarily corrupt

the readings where the fiber is damage free with no noise.

The studies mentioned are very relevant with regards to when filament wound tubes buckle, but they do not mention much on how the tubes deform before and after buckling, which this thesis will investigate further.

1.6 Winding angle and layer definition

1.6.1 Winding angle definition

The winding angle has been defined by a cylindrical coordinate system on the outer surface of the filament wound tube. The cylindrical coordinate system has the abscissa axis along the length of the center axis of the tube and the ordinate axis tangential to the outer circumference of the tube. All winding angles in the thesis are given as a rotation around the normal vector of the tube's surface (z-axis) with the abscissa axis as reference and positive rotation defined in direction of the ordinate. Figure 1.2 shows how the winding angle is defined. It is important to be aware that 0° or 90° winding angles are impossible to achieve due to the nature of the filament winding process. Even though an exact 90° (hoop direction) layer is impossible, whenever a "hoop winding" is referenced to it means a layer that is close to 90° (usually 89°). Likewise " 0° " layers will be in some contexts referenced to as helical layers (usually 12.7°). What angles are possible to achieve, especially when using small angles, depends in large on the geometry of the mandrel. A long and thin mandrel can take smaller angles than a short mandrel with a large diameter.

Due to the nature of the filament winding process, all layers, apart from the hoop layers, are balanced. This is due to that the fiber has to "turn around" at each end of the mandrel when angles smaller than 90° are used. The end result is a fiber structure resembling that of a woven laminate with equal amount of fibers with a positive and negative winding angle.

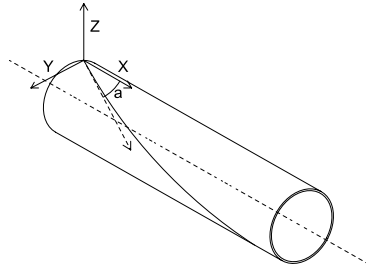


Figure 1.2: The cylindrical coordinate system shown on a tube with one winding at angle α .

1.6.2 Layer and ply definition

The layers and plies are numbered from inside of tube to the outer surface. If referenced to, layer number one (1) is therefore always the inside surface of the tube/bottom of the layup. Likewise, when a layup is referred to in the written form, such as $[89^\circ_1/12.7^\circ_1/45^\circ_1]$, the inner/bottom layer is the first layer in the formula. For the $[89^\circ_1/12.7^\circ_1/45^\circ_1]$ layup, the bottom layer is therefore the 89° layer. In most scientific context today, a layer usually refers to a part of a laminate with unidirectional material direction that stretches over the whole of the laminate. A ply on the other hand is often used for layers on the structure which only covers part of the laminate [25]. Since the tubes in this thesis haven't got any variation in the number of layers along the tube, layer and ply can therefore, according to the normal definition above, be interchanged. However, due to the way the layups are modelled in the FEA, differentiating between the two have been done in the context of this thesis. In the FEA, each layer (such as the 12.7° layer of a $[12.7^\circ_n/45^\circ_n]$ layup) consists of many thinner balanced layers with equal thickness ($[12.7^\circ/-12.7^\circ]_n$). To differentiate between the balanced layers and the layer as a whole, ply denotes one single balanced layer (a 12.7° or -12.7° layer), while layer denotes the layer as a whole (such as the 12.7° layer of a $[12.7^\circ_n/45^\circ_n]$ layup).

1.7 Theory

1.7.1 Riks analysis

Riks analysis in Abaqus is used to model static equilibrium phases during unstable stiffness response of a structure when the loading is proportional [11]. This means that as long as the loads applied are defined by a single variable, such as the external pressure on tubes, a Riks analysis can provide incremental solutions of the load even though the stiffness of the structure is decreasing with increasing deformation. Riks analysis can thus handle when a structure goes from being stable, to when it starts exhibiting a nonlinear deformation/load curve, for buckling this is the case. While a linear buckling analysis can give at what load the structure will suddenly go from stable to unstable, Riks analysis can show how the deformation unfolds if the loading is applied gradually (incrementally). Incrementation of load in Riks analysis is decided by the analysis, and load is applied so that the structure gets a stable deformation even though the structural stiffness decreases [11]. The key output from a Riks analysis, which is always given as default, is the load proportionality factor (LPF) and the arc length. The arc length is a measure of deformation used by Abaqus to give an estimate of the structure's total deformation in each increment.

A Riks analysis won't show an unstable response if it's used to analyze a "perfect" structure with loads that won't cause any instability. For such a "perfect" structure a Riks analysis will simply self-abort at an early stage because the loads will increase to infinity without any instability occurring. As an example, a Riks analysis will increase the loads to infinity if a beam subjected to axial compression (euler buckling [18]) is analyzed. However, if the beam has got a very slight curvature, the bending forces will at some load cause instability and the beam will buckle. A Riks analysis will, in the beam example, be able to detect at what load the instability (buckling) occurs, and then adjust the load so that deformation after the beam has buckled can gradually proceed. The same goes for a tube, where a slight ovality (elliptical shape) will induce bending strains that at some point will cause a buckling behavior.

1.7.2 Linear buckling analysis

Linear buckling analysis in Abaquss is based on linear pertubation and is used to give an estimate of critical load for instability of "perfect" structures [10]. While a Riks analysis needs an imperfection to induce instability, a linear buckling analysis predicts the buckling load like an Eigenvalue problem, or more easy to comprehend, like classical a Euler buckling problem [10].

Chapter 2

FEA

The FEA and the modeling of the tubes was carried out with Abaqus/CAE 6.12-1. The main intention with the FEA was firstly to try and match optic fiber strain results from the project thesis [17] with FEA results by developing a method for doing this. Secondly, the intention was to do an assessment on several proposed layups to try and find an optimal layup for withstanding external hydrostatic pressure. Lastly, the matching method was to be reviewed through testing of tubes with the optimal layup. As part of the optimal layup testing, an assessment on how the matching method can be applied to give accurate strain and buckling pressure predictions on longer tubes was to be carried out, a so called length sensitivity analysis. All the above was carried out and the comparison with the results from the project thesis was written as a paper that can be found in Appendix A, as mentioned in Section 1.5. The layup that proved to be the most optimal was the $[89^{\circ}_2/12.7^{\circ}_1/89^{\circ}_2]$ layup, which was produced and tested with optic fiber. The optic fiber strain results were compared with FEA to validate and further refine the matching method and investigate the length sensitivity, as can be found in the results chapter, Chapter 6.

2.1 Geometry and mesh

The tubes for the optimal layup assessment were modeled as simple circle 2D shell profile extrudes of 100 mm in diameter (slightly elliptic for the Riks analysis, see below) and 600 mm length. For the lengths in the analysis of the produced layups, see section 2.6.

All tubes were meshed with SR4 elements set to 2.0 mm in size, the mesh is shown in the paper in Appendix A along with a mesh sensitivity analysis. Since the effect of increasing the mesh size can be seen, in the paper, to be very small, no further investigation of mesh size was carried out for the other analyzed layups. The imperfection required for the Riks analysis to induce instability was introduced by modeling the tubes slightly elliptic. To give a measure of the elliptic shape, "ovality" has been introduced and defined as percentage of the nominal diameter added and subtracted to the major and minor ellipse diameter respectively. The tubes in the Riks analysis assessing the optimal layups had 0.46 % ovality, that is 0.46 mm added and subtracted, as found through the matching in the paper.

2.2 Layup and material properties

In order to model the wound layup, several balanced plies were used for each layer on the tubes, apart from the hoop layers. By using several balanced plies, the layups were modeled as woven laminates, this might not be exactly true for filament wound tubes, but for this case it is considered a good approach. Validating this approach is the good match between FEA and optic fiber strain results found in the paper. Abaqus' composite layup with conventional shell was the method used for setting up the layups with plies and material directions.

To analyze somewhat realistic layups in the optimal layup assessment, the layer thicknesses of the assessed laminates' layers were based on what was measured on the tube with the $[89^\circ_1/12.7^\circ_1/45^\circ_1]$ layup in the project thesis, shown in the paper. Besides the layer thicknesses, the material properties used in the FEA for the optimal layup assessment were also the same as the volume fraction scaled properties used for the $[89^\circ_1/12.7^\circ_1/45^\circ_1]$ layup. The material properties are reported in Table 2.1 and the layups in the optimal layup assessment with layer thicknesses are reported in Table 2.2.

Table 2.1: Scaled material properties from the project thesis as used in the optimal layup assessment.

Parameter	Scaled value (unscaled value)	Unit
E_1	37.537 (38.6)	GPA
E_2	11.0	GPA
ν_{12}	0.3	-
G_{12}	3.07	GPA
X_T	831.46 (855.0)	MPA
X_C	402.60 (414.0)	MPA
Y_T	39.0	MPA
Y_C	112.0	MPA
S_{12}	42.0	MPA

Table 2.2: Table showing the different layups in the optimal layup assessment.

Nr.**	Layup	Total Thickness	Layer thickness
1	$[89^\circ_2/12.7^\circ_1/89^\circ_2]$	1.702	0.51/0.69/0.51
2	$[89^\circ_1/12.7^\circ_n/89^\circ_1]$	1.702	0.26/1.19*/0.26
3	$[89^\circ_n]$	1.675*	1.675*
4	$[89^\circ_1/12.7^\circ_1/45^\circ_1]$	1.675	0.26/0.71/0.70
5	$[12.7^\circ_n]$	1.675*	1.675*
6	$[12.7^\circ_n/89^\circ_n/12.7^\circ_n]$	1.675	0.278*/1.12*/0.278*
7	$[55^\circ_n]$	1.675*	1.675*

*Thickness of layer not based on measurements from $[89^\circ_1/12.7^\circ_1/45^\circ_1]$ layup, but set to fit the total thickness of the other laminates. **Nr. refers to layup visualization from Abaqus in Appendix D.2.

2.3 Loads and boundary conditions

The tube ends were pinned (freely supported) to two reference points set one at each end of the tubes along the central axis using rigid body constraints. The tube ends were pinned (and not fixed) to the reference points due to little support from the endcaps. Besides the rigid body constraints, one side was constrained to absolute translation in all directions to avoid singular solution errors in the FEA. The two reference points can be seen in Figure 2.1 as RP-1 and RP-2, and the absolute constraint can be seen around the end edge at the RP-1 side of the tube. The tubes had an external pressure of 10 bar (1 MPa) applied on the outer surface, as well as a point load of 8364.68 N applied in RP-2 to simulate the pressure on the end caps. Both the pressure and point load is visible in Figure 2.1. The force of 8364.68 N was calculated as in Equation 2.1 by multiplying the pressure with the projected area.

$$F(t) = (\pi \times (r + t)^2 \times 10 \text{ bar}) = (\pi \times (50 \text{ mm} + 1.6 \text{ mm})^2 \times 10 \text{ bar}) = 8364.68 \text{ N} \quad (2.1)$$

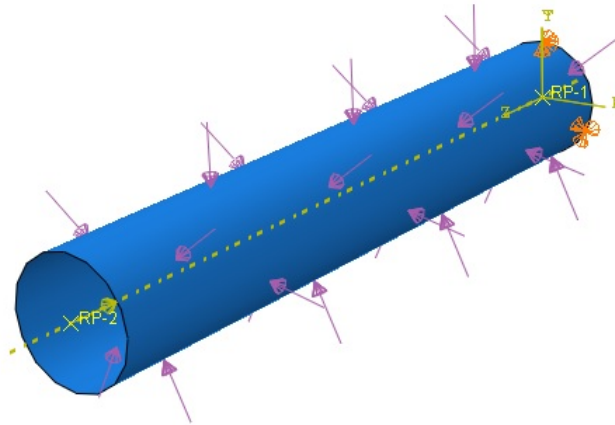


Figure 2.1: The tube as constrained with all loads applied. The yellow arrow is the point load from the end cap pressure and the purple arrows indicate the pressure load. The orange triads indicate the absolute translation constraint to avoid singular solution errors in FEA. RP-1 and RP-2 are the reference points which the ends of the tube are pinned to. At the RP-1 side can be seen the cylindrical coordinate system used for the tube.

2.4 Riks and linear buckling analysis parameters

2.4.1 Riks analysis

The Riks analysis was run with non linear geometry (Nlgeom set to ON in Abaqus). Further, the minimum and maximum arc length increment was set to 0.00001 and 1 respectively, while the initial arc length was set to 0.01.

2.4.2 Linear buckling analysis

The linear buckling analysis was run with Subspace eigensolver and all eigenvalues requested. Also, four vectors per iteration were used and maximum number of iterations was set to 30.

2.5 Optimal Layup assessment

To assess what layup would be the most optimal for withstanding the highest pressure before buckling, seven different layups were analyzed with Riks analysis and then compared with each other. The layups were chosen based on engineering common sense, FEA strain results, sandwich theory and the layups suggested by T. Messenger et. al. [24]. The layups were modeled as shown in Table 2.2 with the FEA results in Table 2.3. Based on what was observed in the project thesis, the most critical failure that would ultimately lead to a degradation of the stiffness of the tube was considered to be matrix cracking/matrix failure. Therefore, the failure criteria that were employed were the Tsai-Wu (interaction coefficient set to zero) and Max Stress with the strength in fiber direction increased by a thousand times (for both criteria). This approach was chosen so as to only reveal matrix failure, as suggested by DNV [3]. Since matrix cracking in the top ply initiates leakage, this ply was investigated together with the max exposure factor of the failure criteria through the thickness, as can be seen in Table 2.3. The failure criteria were all gathered from the middle circumference of the tubes where all the tubes had the peak exposure factor, neglecting high stresses at the ends due to over-rigid constraints.

Due to the tubes being modeled with 0.46 % ovality, the tubes develop a two lobe deformation pattern almost from the start, which at some point gets so pronounced that the tubes lose structural stiffness and buckle. With this deformation pattern the strains on the tubes, axial and tangential (neglecting through thickness strains), get inhomogeneous over the surface and through the thickness of the tube. This causes the stress and strain states on the tubes to deviate quite a lot from traditional hoop stress vs axial stress of a pressurized tube theory, which applies very accurately for internal pressure. This in turn causes layups that perform well when subjected to internal pressure to perform surprisingly bad. As a good example, the $[55^\circ_n]$ layup, which is considered a good layup for internal pressure [24], performs very badly. The poor performance of the $[55^\circ_n]$ layup was also pointed out by T. Messenger et. al. [24].

To improve understanding of the strain states on the tubes, the FEA of the $[89^\circ_1/12.7^\circ_1/45^\circ_1]$ layup was investigated. Due to the two lobe buckling mode occurring for all the assessed layups (with 600 mm tube length) and due to the laminate theory approach in Abaqus [9], the axial and tangential strain states on the tubes will all follow the same pattern. Therefore, investigating only one layup is substantial to get a good idea of the strain states in all the other layups. However, the strains will have a varying overall magnitude depending on the laminate stiffness matrix components, in turn decided by the material and layup. Figure 2.2 shows the tangential and axial strain in the top and bottom ply at the middle circumference (300 mm) of the tube plotted at the same pressure as the graphs in the paper, 3.41 bar. Also plotted is the strain coming from uniform deformation. The top and bottom ply tangential strain in Figure 2.2 can be seen to be opposite of each other, proving a strong bending component through the thickness. When the pressure increases further, the amplitude of the tangential strain curves increases at a much higher rate than the mean value. The amplitude increase results in a further bending strain increase, this can be seen in Figure 12 in the paper which shows the strain on the tube after buckling. Interestingly, but also logic, is that the strain coming from uniform deformation coincides with where the strain curves for top and bottom cross. The axial strain, visible in both Figure 2.2 and Figure 2.3 is distributed as relatively uniform compression at the lobes and tension in the creases

through the thickness, indicating little bending. The reason for the axial strain to have little bending is due to the two lobe deformation pattern constraining the axial strain so it doesn't develop any pronounced bending strains through the thickness. It can be seen in Figure 2.3 that there are some very high axial bending strains at the ends due to the FEA's idealization of the freely supported end constraints. However, the bending strain quickly diminishes straight after the ends due to the geometrical constraint caused by the two lobe deformation pattern. Also visible in the axial strain plot along the tube is the axial strain from uniform deformation, as also plotted in Figure 2.2. As for the circumferential plot it coincides with the strain where the curves cross. Looking at the strain from uniform deformation it can be seen that the buckling shape strain has got much higher peak values, indicating that there is a big difference in max buckling/burst pressure between internal and external (by nature even deformation) hydrostatic pressure.

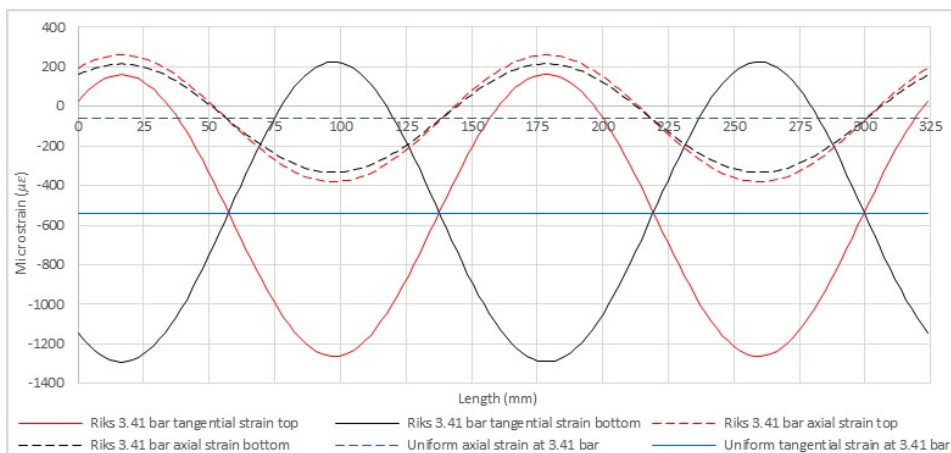


Figure 2.2: Tangential and axial strain around the middle circumference in the top and bottom ply of the $[89^{\circ}_1/12.7^{\circ}_1/45^{\circ}_1]$ layup at 3.41 bar. The tangential strain curve for the top ply can also be found in the paper, compared with optical strain measurements. As can be seen, the tangential strain has a very big bending component with opposite curves for the top and bottom ply while the axial strain has a very small bending component through the thickness. Also plotted is the strain at 3.41 bar from uniform deformation and it can be seen to coincide with where the respective buckling shape strain curves cross.

The strain states come to show in the optimal layup analysis, where a layup consisting of just 89° layers gives a relatively high buckling pressure due to good resistance

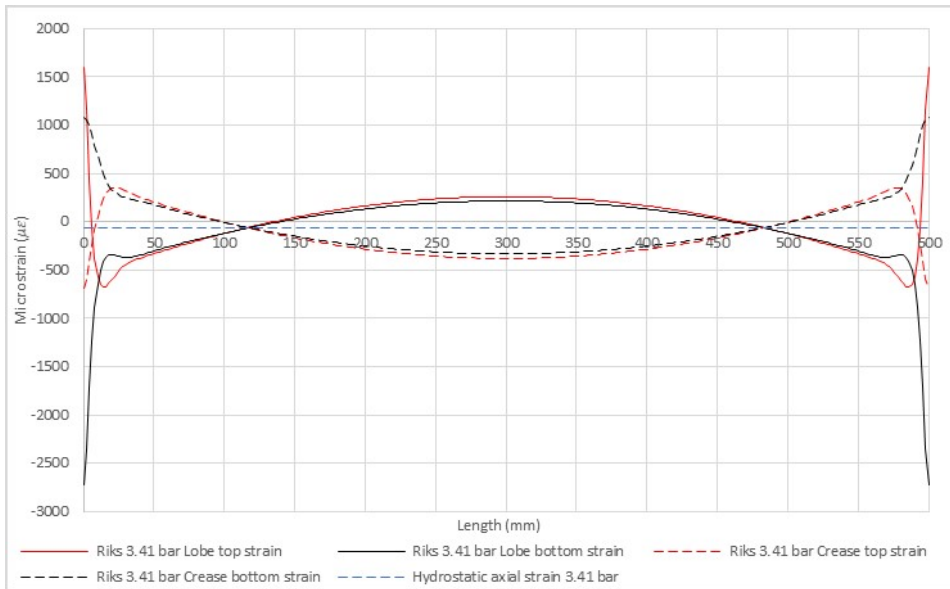


Figure 2.3: Axial strain along the length in the top and bottom ply of the $[89^{\circ}_1/12.7^{\circ}_1/45^{\circ}_1]$ layup at 3.41 bar for both the lobe, at 18 and 178 mm in Figure 2.2, and the crease shape at 98 and 262 mm. As can be seen, the axial strain has a very big bending component with opposite curves at the ends of the tube, where there is a lot of bending torque from idealized over-rigid constraints in the FEA. The reason why there is no bending strain through the thickness in the rest of the tube is due to the two lobe deformation shape constraining the strain. Also plotted is the strain at 3.41 bar from uniform deformation and it can be seen to coincide with where the respective buckling shape strain curves cross, as for Figure 2.2.

against the high tangential strains. However, the failure criteria show high exposure factors for this simple layup due to the weak matrix in the axial direction. By introducing a 12.7° layer, as in the $[89^{\circ}_2/12.7^{\circ}_1/89^{\circ}_2]$ layup, the exposure factor drops while the buckling pressure increases. This can be explained by the layup acting somehow as a sandwich structure, with high bending stiffness. The 89° layers keeps the tube from buckling from tangential bending strain, while the 12.7° layer stiffens the tube in the axial direction and hinders strain to build up in the weak transverse (matrix) direction of the 89° layers. To further validate the sandwich approach, the $[12.7^{\circ}_n/89^{\circ}_n/12.7^{\circ}_n]$ layup shows a very low buckling pressure. The $[12.7^{\circ}_n/89^{\circ}_n/12.7^{\circ}_n]$ layup's low buckling pressure is due to the fact that the outer layers lack the tangential bending stiffness to keep it from buckling, while the 89° layer adds little stiffness in the axial direction.

For most of the layups, the failure will occur in the top ply of the top layer at the

lobes, apart from the layups with many 12.7° layers, which show a tendency for the Tsai-Wu criterion to reveal failure in the bottom of the 12.7° layer. The reason for the failure to occur in the bottom 12.7° ply comes from the fact that the tangential bending strain initiate matrix failure as opposed to the axial strain, which initiates it for the 89° layers. Seeing as the tangential bending strain is at its peak value on the outer and inner surfaces of the tubes, it wont cause any harm to the 12.7° layers as long as they are constrained to the middle layers, as shown with the $[89^\circ_2/12.7^\circ_1/89^\circ_2]$ layup. However, if increasing the thickness of the 12.7° layer, as with the $[89^\circ_1/12.7^\circ_2/89^\circ_1]$ layup, it can be seen that the relative thickness of the 12.7° layers causes the layup to fail by tangential strain in the 12.7° layers, instead of failure from axial strain in the 89° layers. The failure from tangential strain in the 12.7° layers causes matrix compression failure instead of matrix cracking. As opposed to the axial strain, which has got quite even compression/tension magnitude at the lobes and at the creases, the tangential strain has got a much larger compression magnitude occurring at the creases, as can be seen in Figure 2.2. The high compression magnitude results in matrix compression failure when the critical strain is the tangential. Even though, as stated, the most critical failure is matrix cracking in the top ply from a leakage point of view, a failure of the underlying 12.7° layers will cause a reduction in stiffness leading to failure of the other layers.

The reason for the different failure locations for the Tsai-Wu and the Max stress, as seen in Table 2.3, is likely du to the fact that the Tsai-Wu takes into account the interaction between the axial and tangential strains. On the other hand, the max stress criterion only looks at the individual components one by one [19].

An important aspect of the results in Table 2.3 is at what arc length the tubes buckle. This is graphically presented in Figure 2.4 for the $[12.7^\circ_n]$, $[89^\circ_n]$, $[55^\circ_n]$ and $[89^\circ_2/12.7^\circ_1/89^\circ_2]$ layups. It can be seen that the $[89^\circ_2/12.7^\circ_1/89^\circ_2]$ layup withstands high pressure for a relatively long deformation (arc length) interval before reaching buckling pressure compared to the other layups. Even though the exposure factors in Table 2.3 show values above 1 at the buckling pressure for all the layups, the exposure factors very close to buckling pressure is a good deal lower due to the long deformation interval with low stiffness when approaching the buckling pressure. Since the

$[89^{\circ}_2/12.7^{\circ}_1/89^{\circ}_2]$ layup have the most pronounced arc length interval close to buckling, it shows quite low exposure factors at pressures close to the buckling pressure. By studying the FEA results in Abaqus for the $[89^{\circ}_2/12.7^{\circ}_1/89^{\circ}_2]$ layup it shows that at 4.95 bar, 0.14 bar below buckling pressure, the exposure factors of the max stress and Tsai-Wu criteria are respectively 0.49 and 0.45, more than half the value at buckling pressure.

Comparing the $[89^{\circ}_2/12.7^{\circ}_1/89^{\circ}_2]$ layup with that found to be the most optimal by T. Messenger et. al. [24], the $[90^{\circ}_3/15^{\circ}_1/90^{\circ}_2]$ layup, the two can be seen to be very similar. The similarity supports that the $[89^{\circ}_2/12.7^{\circ}_1/89^{\circ}_2]$ layup is the most optimal layup given the layer thicknesses and tube geometry used in this assessment.

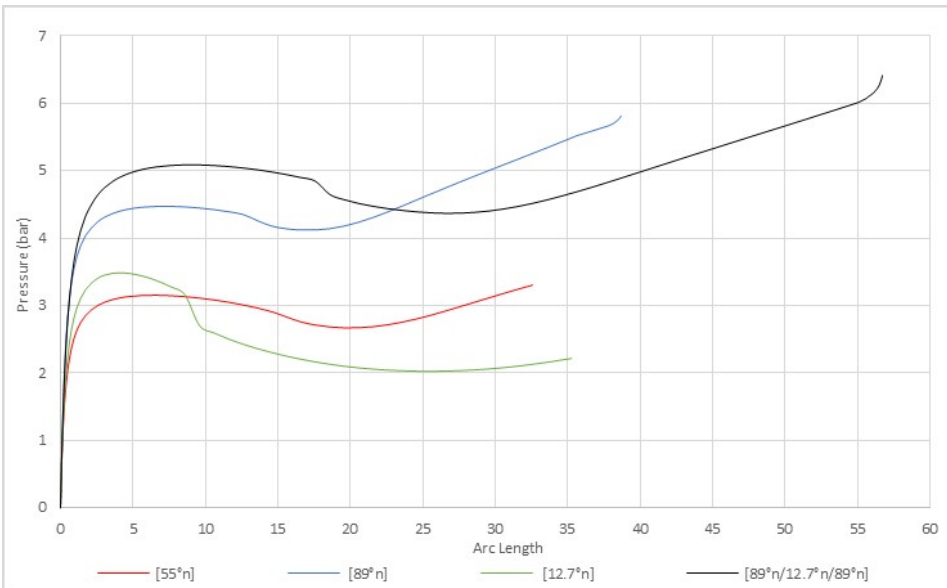


Figure 2.4: The pressure vs arc length graphs for the $[12.7^{\circ}_n]$, $[89^{\circ}_n]$, $[55^{\circ}_n]$ and $[89^{\circ}_2/12.7^{\circ}_1/89^{\circ}_2]$ layups. As can be seen, the $[89^{\circ}_2/12.7^{\circ}_1/89^{\circ}_2]$ layup withstand high pressure for a relatively long deformation (arc length) interval before reaching peak pressure.

Table 2.3: Table showing the optimal layup assessment results. The failure criteria are taken from peak pressure (buckling pressure) as seen in Figure 2.4. The table is sorted by what layup had the highest buckling pressure.

Nr.**	Layup (B to T)	Max P	MS Max	MS Top ply	MS Location	TW Max	TW Top ply	TW Location
1	[89° ₂ /12.7° ₁ /89° ₂]	5.09	1.04	1.04	Top ply	0.95	0.95	Top ply
2	[89° ₁ /12.7° _n /89° ₁]	4.8	0.93	0.93	Top ply	0.93	0.85	Bottom of Middle layer
3	[89° _n]	4.47	1.56	1.56	Top ply	1.56	1.56	Top ply
4	[89° ₁ /12.7° ₁ /45° ₁]	4.33	0.93	0.93	Top ply	0.87	0.87	Top ply
5	[12.7° _n]	3.48	1.14	0.59	B ply	1.16	0.60	Bottom ply
6	[12.7° _n /89° _n /12.7° _n]	3.40	1.34	1.34	Top ply	1.40	1.27	Bottom ply
7	[55° _n]	3.15	1.39	1.39	Top ply	1.29	1.29	Top ply

*Thickness of layers not based on measurements from project thesis. **Nr. refers to layup visualization from Abaqus in Appendix D.2.

2.5.1 Conclusion and choice of layup for production

The layup that proved to perform best was the $[89^\circ_2/12.7^\circ_1/89^\circ_2]$ layup based on high buckling pressure and low failure exposure factors. The $[89^\circ_2/12.7^\circ_1/89^\circ_2]$ layup was therefore chosen as the layup to produce and test. The layup performed well mainly due to high resistance against tangential bending strains from the 89° layers, giving a high buckling pressure. Besides, the 12.7° layer hindered build up of strains in the weak transverse direction of the 89° layers, resulting in low failure exposure factors.

2.6 Analysis on produced layup

Two analysis types were used on the produced $[89^\circ_2/12.7^\circ_1/89^\circ_2]$ layup. Riks analysis was used to compare with the results from the optical fibers, and linear buckling analysis was used to assess the length sensitivity. The comparison between test results and FEA is to be found in the results chapter, Chapter 6.

To find accurate material properties and layer thicknesses for the FEA, a material investigation was carried out, see Chapter 5. The layup as modeled in FEA can be seen in Table 2.4 and in Figure 2.5 based on the layer thicknesses as reported in the mentioned material investigation. Due to increased thickness, the end cap force was increased to 8572.48 N as shown in Equation 2.2.

Due to the critical failure still being matrix cracking from a leakage point of view, the failure criteria approach suggested by DNV [3], as used for the optimal layup assessment, was applied. In this approach, fiber strength values are multiplied by 1000 to investigate only matrix cracking. Scaling of the fiber dominated strength X_T and X_C as done in the material investigation was therefore not relevant. Due to the max stress and Tsai-Wu failure criterion giving almost equal values in the optimal layup assessment, only the Tsai-Wu was applied for the analysis on the produced layup.

$$F(t) = (\pi \times (r + t)^2 \times 10 \text{ bar}) = (\pi \times (50 \text{ mm} + 2.237 \text{ mm})^2 \times 10 \text{ bar}) = 8572.48 \text{ N} \quad (2.2)$$

Table 2.4: Layup in the FEA of the produced $[89^\circ_2/12.7^\circ_1/89^\circ_2]$ layup with ply thicknesses derived from Table 5.3 in the material investigation in Chapter 5.

Ply number	Orientation (winding angle)	Layer thickness*	Ply thickness (mm)
10 (top)	89°	0.827	0.0.827
2 - 9 (middle)	12.7°	0.732	0.0.0916
1 (Bottom)	89°	0.678	0.678

*From Table 5.3

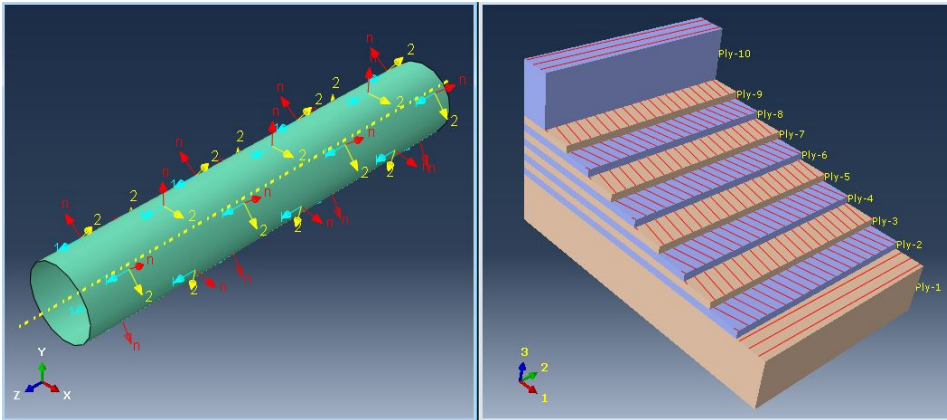


Figure 2.5: Layup in Abaqus showing direction of the material coordinate system, ply number and orientation of each ply for the produced $[89^\circ_2/12.7^\circ_1/89^\circ_2]$ layup. The ply number refers to Table 2.4.

2.6.1 Length sensitivity analysis

To see how the matching method could be applied to predict the buckling behavior of longer tubes, linear buckling analysis was run on many different tube lengths. The intention with running the analysis pre testing was to see how the end effect affects buckling pressure and if testing tubes in certain lengths would be beneficial for assessing it. The analysis were run with the updated material data from the material investigation. The resulting graph can be seen in Figure 2.6 and as can be seen, the end effect diminishes at around 800 mm, where the graph flattens. 800 mm is however beyond the maximum length of 600 mm that can be tested in the autoclave, so proving how the matching is beyond the end effect threshold value had to be done in other ways. Instead, testing of a tube of 400 mm length was decided as this would give information

on how the matching behaves at other lengths than 600 mm. Also visible in the graph is the change of curvature occurring at 350 mm. The change of curvature is caused by the buckling mode going from two lobe to three lobe. Since the mode change is caused by the length and thus the end effect, testing of a tube with predicted three lobe mode close to the mode change threshold length was also decided. Based on the above, the third tube was set to a length of 300 mm. Testing of a tube length predicted to have a three mode shape would also indicate if the tube from production actually has got a slight two lobe shape, as indicated by the good match with the elliptical two lobe shape in the paper. In other words, it can give an indication on whether or not the elliptical shape is an analysis parameter or an actual physical geometry.

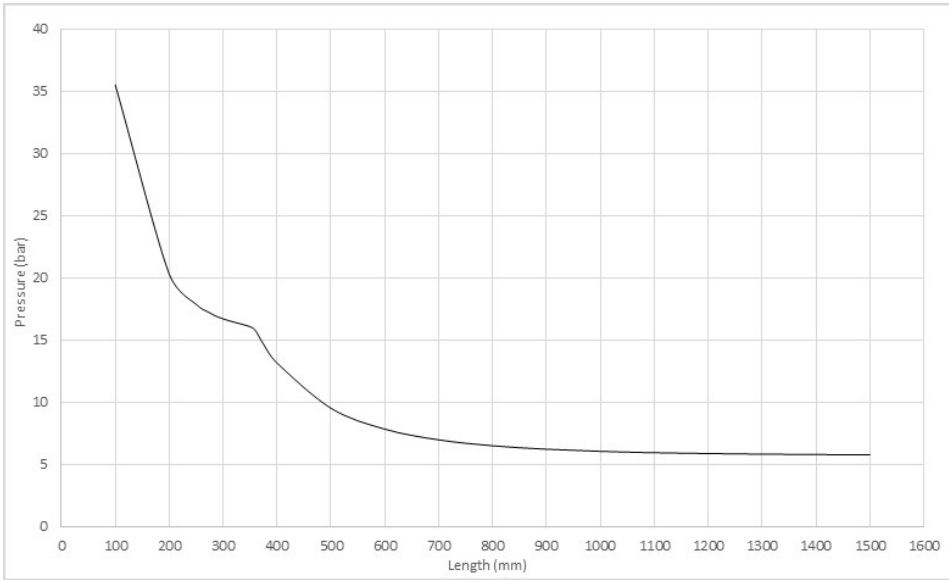


Figure 2.6: Length sensitivity analysis of the produced $[89^{\circ}_2/12.7^{\circ}_1/89^{\circ}_2]$ layup pre testing with material properties from the scaled material properties in T Table 5.4 and ply thicknesses as reported in Table 2.4.

Chapter 3

Tube design and production

3.1 Design, material and winding layup

The $[89^{\circ}_2/12.7^{\circ}_1/89^{\circ}_2]$ layup was chosen for production since it proved to be the most optimal layup amongst the assessed layups, as concluded in the optimal layup conclusion in Section 2.5.

For easy comparison with the results in the paper, the tube was cut into a length of 600 mm. Additionally, the tube was cut into lengths of 300 mm and 400 mm for assessing the FEA match at different tube lengths, as described in the length sensitivity analysis in Section 2.6.

The epoxy used for the tube was the EPIKOTE Resin MGS RIMR 135 with curing agent EPIKURE Curing agent RIMH 137 [6] and they were mixed according to the corresponding epoxy datasheet [6]. The fiber used was HiPer-Tex W2020 from 3B [7]. The fiber and epoxy was chosen based on the fact that NTNU had a lot of experience and relevant material data [21]. The steel mandrel that was used had a 2020 mm long cylindrical section with removable spheres at each end reducing the diameter to 22 mm for the attachment rod to the chuck and tailstock of the machine. The spheres were removable to allow for extraction of the finished tube from the mandrel.

3.2 Winding machine setup

The machine used for producing the tube was the FWM at NTNU. It is of the type MAW 20 LS 4/1 [20]. It has 4 degrees of freedom; mandrel rotation, wind eye rotation, horizontal carriage movement along the mandrel and horizontal carriage movement normal to the mandrel. The machine consists of two units; a tensioning unit and a filament winding unit. The tensioning unit is loaded with the fiber rolls and winds out fiber a preset tension while the filament winding unit winds it onto the mandrel while coating it with epoxy through an epoxy bath. All the layers were wound with a fiber tension of 15 N.

3.2.1 Winding machine programming

The program used for programming the winding path for the layup was the Winding Expert 1.185 from Mikrosam. The mandrel existed as a premade 3D model which was imported into the Winding Expert. Table 3.1 shows the winding program parameters of the different layers. After the program was finished it was exported to the FWM control program, Winding Commander 8.0, for running on the FW machine.

Table 3.1: Table showing the parameters used for the winding programs for the different layers. The hoop layer has no pattern as it can only be wound with an opening diameter of 100 mm (same as mandrel), and in only one way.

Layer	Coverage	Opening diameter (mm)	Fiber thickness (mm)	Pattern	Fiber tension (N)
12.7°	102.79 %	22	5	17/1*	15
89°	100	100 %	6	-	15

*90° dwell (Quarter turn of the mandrel in between each strand wound along the mandrel to hinder fiber slippage during winding).

3.3 Mandrel treatment and curing

Before winding, the mandrel was treated so as to ease release of the tube after curing of the epoxy. First, three layers of Zywx Flex-Z 3.0 [12] was applied with 15 minutes curing

time between each layer. During the 15 minute curing time a heat gun was used to heat the mandrel so as to cure the Zywax. Finally, a layer of Huntsman Renlease QV 5110 [8] release wax was applied. The curing of the epoxy was done by letting the mandrel stay in the machine turning at a low speed for 24 hours (room temperature), before moving it into an oven and letting it stay there turning for another 15 hours at 80°C.

In order for the tube to get a smooth surface peel ply [4] was applied straight after the tube was wound, before the epoxy was left to cure for 24 hours in room temperature. The peel ply was removed after the epoxy had hardened in room temperature, before the mandrel was put into the oven. Figure 3.1 shows a close up picture of the tube straight after the peel ply was applied.

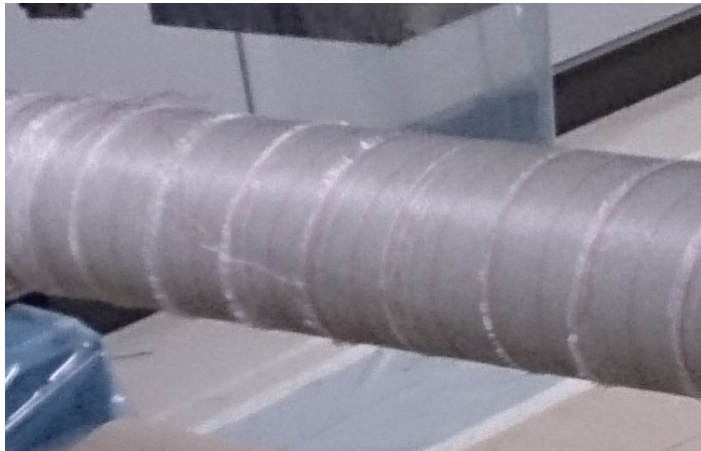


Figure 3.1: Tube with peel ply applied.

Chapter 4

Test setup and method

Testing of the tubes was conducted by sealing the ends of the tubes with steel endcaps and applying pressure by water in the autoclave at the Institute of Engineering Design and Materials at NTNU. Strain readings were acquired from optical fiber glued to the surface of the tubes with the signal wire from the fiber escaping from the autoclave through a T-fitting. Figure 4.1 shows the autoclave and a tube with signal wire for fiber, but without endcaps.



Figure 4.1: Autoclave and tube without endcaps, with the signal wire escaping the autoclave through the T-fitting seen on the left side of the autoclave.

4.1 Endcaps

The endcaps were secured and kept tight by applying stickytape [5] to the circumference and using bodyweight to secure them on the tube. Figure 4.2 shows the endcaps and Figure 4.3 shows one of the endcaps fitted to the tube with stickytape. The endcaps had a stick out of 10 mm as indicated in Figure 4.2



Figure 4.2: The two endcaps used for sealing the ends of the tube. Also shown is the stick out of 10 mm.



Figure 4.3: Endcap applied with stickytape. Also visible in the background is the T-fitting.

4.2 Fiber instrumentation and equipment

A single strain of fiber of 165 micron in diameter was used to measure strain on each of the tubes. The fiber was glued on to the surface of the tubes by use of cyanide optic fiber glue. Based on the experience from the project thesis and the paper and what was found in the length sensitivity analysis in Section 2.6, the following data acquisition requirements were set for the optical fiber.

- For easy comparison with the strain measured on the tube in the project thesis, measure strain at the same locations on the 600 mm long tube as for the tube in the project thesis.
- Measure strain on the 300 mm long tube so as to verify the change of buckling mode in the length sensitivity analysis.
- Measure strain on the 400 mm long tube to provide enough data for matching with Riks analysis.

To meet these requirements, the 600 mm long tube had the fiber laid in three circumferential turns with a spacing of 150 mm along the central axis, same as for the tube in the project thesis described in the paper. The 300 mm long tube only had the fiber applied at one single circumference on the middle of the tube, to easily and without generating too much data reveal if the buckling mode of the length sensitivity analysis occurred. The 400 mm long tube had the fiber also laid at one circumference on the middle of the tube based on that the middle circumference strain reading proved to be the critical reading for the matching in the paper. The equipment used for measuring signals from the fiber was NTNU's fiber optic equipment. Details concerning the optical fiber can be found in the paper in Appendix A and for more indepth knowledge, see M. Haaheim's master's thesis [16].

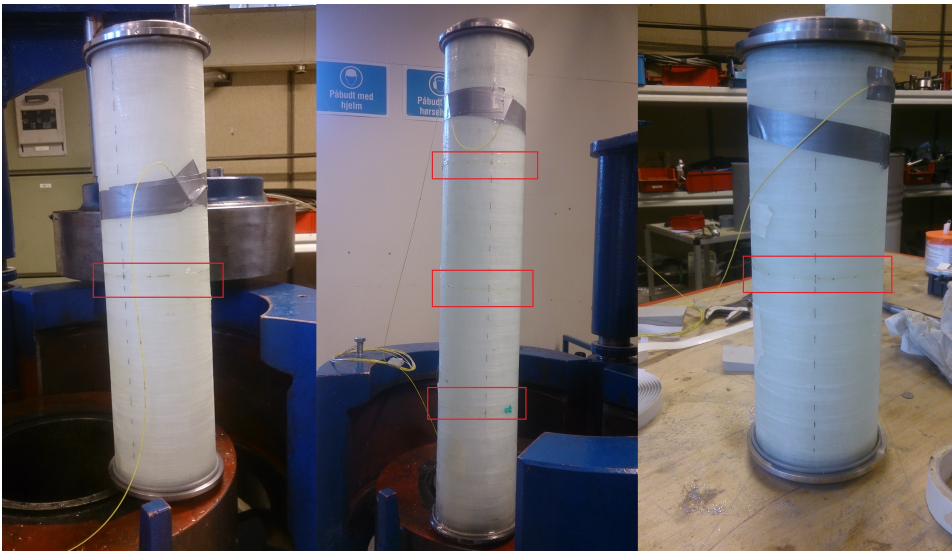


Figure 4.4: The 400 mm long tube (left), 600 mm long tube (middle) and 300 mm long tube (right) with endcaps. The 600 mm long tube had the fiber at 150 mm, 300 mm and 450 mm along the longitudinal axis. The other two tubes had the fiber at the middle at 150 mm for the 300 mm long tube and at 200 mm for the 400 mm long tube. The paths are outlined with red squares.

4.2.1 Autoclave interface

In order to get the signal wire securely out from the autoclave without leakage, a T-fitting was used together with an end cap. The end cap had a hole of 1 mm drilled for the signal wire. To keep the end cap water and pressure tight, Araldite Rapid was applied so that it filled up the inner cavity of the end cap, where the fiber went through. Figure 4.5 shows the T-fitting with the fiber escaping from the end cap and the pressure hose going into the T-fitting.

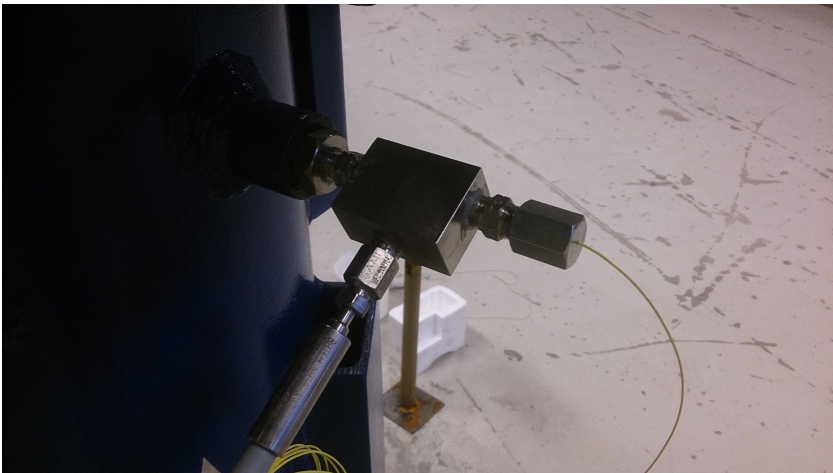


Figure 4.5: T-fitting with pressure hose and fiber escaping through end cap.

4.3 Pressure equipment and manometer

For pressurizing the autoclave, an air powered compressor was used. A LEO 3 manometer from Keller AG [1] was used to measure pressure. The manometer was connected to a laptop, via an USB interface, where pressure was recorded using software supplied by Keller AG.

4.4 Test method

The tubes were pressure tested by increasing the pressure incrementally until buckling. The increments were taken from Riks analysis of the $[89^\circ_2/12.7^\circ_1/89^\circ_2]$ layup with material properties and thickness data from the material investigation in Chapter 5 and an ovality of 0.46 % as in the optimal layup assessment. For the 300 mm long tube, expected to buckle as three lobe, the imperfection was not modelled as ovality, but introduced as shape import from linear buckling analysis and then scaled. The scale factor was set to 0.22, equivalent to ± 0.23 mm radial displacement as for the 0.46 % ovality. Having equal pressure increments in the tests as in the Riks analysis was done to ease the matching provided that the final, matched, Riks analysis not had to much deviation from the used Riks analysis. Before testing and pressurizing begun it was made sure that no air was left in the autoclave. The reference strain needed for the OBR software was, as for the paper, taken prior to submerging the tubes. Before each test nr. 2, the tubes were taken out of the autoclave and a new reference strain reading was carried out to cancel out any noise introduced during the pressurizing.

Material investigation

In order to obtain material and cross section data of the produced tube, a material investigation was carried out. The areas of interest for the investigation was the thickness of each layer and the volume fraction (of fibers) in each layer. To study this, a microscopy and a burn-off test was carried out on samples taken from uniform parts of the tube (no visible disturbance in the winding pattern).

5.1 Burn-off testing

The burn-off test was carried out by heating a sample of the tube put in a ceramic cup for 240 minutes at 500 C° and comparing the post and pre heating weights of the sample. Table 5.1 shows the result from the burn-off test. As can be seen in Table 5.1, the volume fraction of fiber was 0.54

Table 5.1: Burn-off test result with volume fractions.

Material	Weight (g)	Density (g/cm ³)	Volume fraction
Epoxy	9.0947	1.19*	0.46
Fiber	23.297	2.58**	0.54

*[6] **[7]

5.2 Thickness measurements

The tube's thickness was measured with a micrometer at ten different spots on the tube and then averaged. The results from the thickness measurements can be seen in Table 5.2. As can be seen, the standard deviation is very low, indicating a uniform thickness.

Table 5.2: Thickness measurement of the $[89^\circ_2/12.7^\circ_1/89^\circ_2]$ layup.

Tube	Average thickness (mm)	Standard deviation (mm)
$[89^\circ_2/12.7^\circ_1/89^\circ_2]$	2.237	0.048

5.3 Microscopy

A microscopy was carried out to examine the thickness of the individual layers, as reported in Table 5.3. The microscopy was carried out on a cross section of the tube ground with fine silica sand paper and the pictures from the microscope can be found in Appendix D.1. The red lines on the microscopy pictures indicate where the borders between the layers were considered to be, and these lines were in turn used to decide the relative thickness of each layer. The absolute thickness of each layer was found by scaling the relative thickness with the thickness of the tube as reported in Table 5.2. Looking at the standard deviations in Table 5.3 it can be seen to be within acceptable levels, meaning that enough pictures were taken.

In the project thesis, an investigation of the volume fraction in the individual layers was carried out by counting fibers within control areas on the microscopy pictures. It was discovered that the volume fractions in the individual layers (of the $[45^\circ_1/12.7^\circ_1/89^\circ_1]$ layup) were so even that any variation was within the standard deviation. Based on the experiences from the project thesis and the good match between results and FEA in the paper, no investigation of the individual layers' volume fractions were carried out.

Table 5.3: Thickness of each layer measured relatively from the microscopy pictures in Appendix D.1 and scaled with the measured layup thickness in Table 5.2.

Layer (location)	Layer thickness (mm)	Standard deviation (mm)
89° (outer)	0.827	0.034
12.7°	0.732	0.049
89° (inner)	0.678	0.029

5.4 Scaling of material properties

From Vedvik (2013) [25], the micro mechanical models expressed by Equation 5.1 and 5.3 gives the elastic modulus in the transverse (matrix direction) and longitudinal (fiber direction) material direction in a laminate as a linear relation with the volume fraction, shown with the generalization in Equation 5.2 and 5.4. By using Equation 5.1 and 5.3, scaling of the elastic moduli at a given volume fraction is possible if another volume fraction is found and either E_m or E_{1f} and E_{2f} is known. However, the material model for the transverse elastic modulus given in equation 5.3 is very poor [25], and therefore only the elastic modulus in the fiber direction was scaled.

After some the volume fraction for the layup was known through the burn-off test and the elastic properties for a volume fraction of 0.62 was given in the material properties, as can be found in Appendix C.2, the scaled elastic modulus for the layup could be found. Table 5.4 shows the relevant material data from Table C.2 in Appendix C.2, indicated by the unscaled values. For finding the elastic modulus of the in the longitudinal direction by scaling, the elastic modulus for the epoxy (matrix material, E_m) was used with a value of 2950 MPa [6]. E_{1f} could be used for scaling instead of E_m , but since the resulting difference of E_1 is small there has not been put any emphasis on which to choose.

Since the stresses and strains are linearly related and the strength of the laminate is governed by the strain in the fibers, the strength will change with the same fraction as the elastic modulus. Again, the linear scaling only applies for the longitudinal direction. Table 5.4 shows the scaled and unscaled values. However, due to the failure criteria used in FEA, the scaled material strengths were not applied, as mentioned in Section 2.6.

$$E_1 = E_{1f} V_f + E_m(1 - V_f) \quad (5.1)$$

$$E_1 = (E_{1f} - E_m) V_f + E_m = ax + b \quad (5.2)$$

$$\frac{1}{E_2} = \left(\frac{V_f}{E_{2f}}\right) + \left(\frac{1 - V_f}{E_m}\right) \quad (5.3)$$

$$\frac{1}{E_2} = \left(\frac{1}{E_{2f}} - \frac{1}{E_m}\right) V_f + \frac{1}{E_m} = ax + b \quad (5.4)$$

Table 5.4: Scaled material properties. Unscaled material properties are from G. Perillo [21] see Table C.2 in Appendix C.2 for complete material property table as reported by G. Perillo.

Parameter	Unscaled value	Scaled value	Unit
E_1	38.600	34.092	GPA
E_2	11.000		GPA
ν_{12}	0.3		-
G_{12}	3.070		GPA
X_T	855.0	755.15	MPA
X_C	414.0	365.65	MPA
Y_T	39.0		MPA
Y_C	112.0		MPA
S_{12}	42.0		MPA

The unscaled material data given in Table 5.4 from Appendix C.2 are from G. Perillo [21]. Perillo found the material data through FEA matching with filament wound ring compression testing. Due to the fact that Perillo had none of the required fixtures and testing equipment for directly deciding the material data for filament wound tubes, an alternative approach was chosen. Since material data was already available for vacuum infused samples, these were scaled by modeling a ring compression test in FEA and comparing it with actual ring compression testing. By adjusting the material data in the FEA until a good match was found between the displacement and force, the FW material data was found. Three tubes with different layups were tested and they all showed good FEA compliance with the found material data. The force was that which is

indicated in Figure 5.1 and the displacement was recorded at the same spot as the force, as can be seen in the graph in Figure 5.2 together with the FEA model. The filament wound material was found to have a volume fraction of 0.62, 14.8 % higher than for the vacuum infused samples at 0.54. Even though the volume fraction was higher, the E-moduli had to be reduced by 25 % compared to the volume fraction scaled values, as can be seen in the force/displacement graph. The total decrease in the E-modulus in fiber direction was 13.8 %, from 44.8 GPa to 38.6 GPa, however, a different scaling method was used than in this master's thesis and also more material data than just in the fiber direction was scaled. The decrease in E-moduli was concluded as being due to a higher void content, see G. Perillo's PhD thesis [21] for further information.

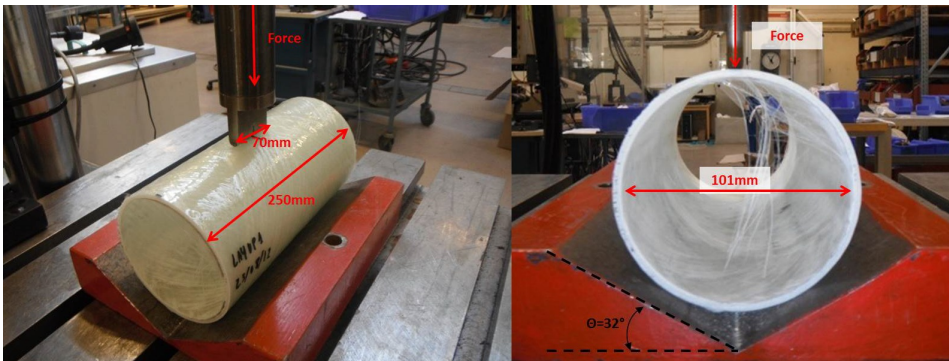


Figure 5.1: Perillo's ring compression test setup, the setup can be seen modelled in FEA in Figure 5.2. The figures are taken from G. Perillo's PhD thesis [21].

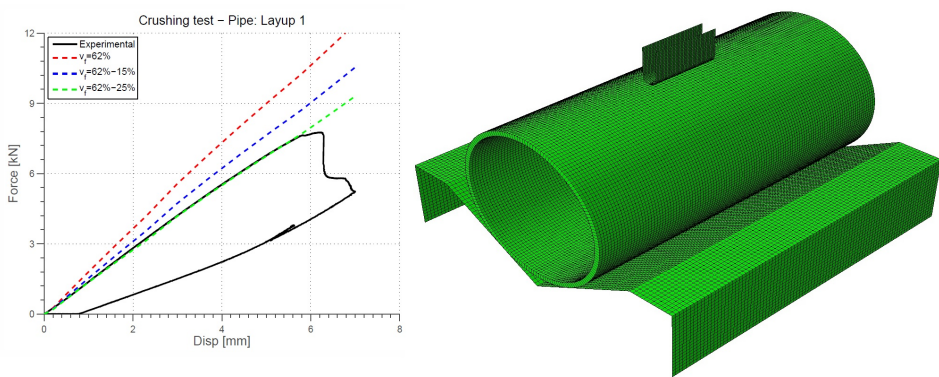


Figure 5.2: Perillo's ring compression test setup as modeled in FEA together with the force/displacement curve. The blue, red and green lines are with scaled material data with respect to volume fraction minus the percentage indicated to weigh up for higher void content. The figure is taken from G. Perillo's PhD thesis [21].

Chapter 6

Results

Here all the results will be presented along with accompanying figures and tables deemed relevant. In order to easily compare the results and for lookup for later work, Table 6.1 was made where the most relevant quantifiable results have been summarized.

To clarify potential misunderstandings it is pointed out that the FEA results represents the comparative value. This means that if a test result value is referenced to as a percentage or share of a corresponding FEA value, the FEA value represents 100 % or 1 respectively, unless otherwise stated. In such, a tube with a buckling pressure of 9 bar and with a FEA buckling pressure of 10 bar will be referenced to as having a buckling pressure of 90% of the FEA and not that the FEA predicted buckling at 111.1 % of the test. This approach was chosen due to the fact that the FEA is of great interest in the work in this master's thesis.

The results have been presented and sectioned based on the individual tube lengths behavior and how the FEA results compare with the tests. Some of the results refer to tables and figures put in the Appendix as they were not included in the main document due to space and relevance assessments. Due to the fact that no visual damage was observed on the tubes, the result section is very analytic and mainly based on the optic fiber strain readings, however, a picture of the tubes post testing have been included and can be seen in Figure 6.2. After all the test's it was observed that some water was

present inside the tubes.

6.1 Data acquisition details and comment on result presentation

The virtual strain gauge length and the gauge spacing in the OBR software was set to the same as in the readings from the paper, 5 mm and 1 mm respectively.

The starting point for the length axis in the tangential strain graphs relative to the deformation on the tubes is shown in Appendix D.4. To make the graphs showing both FEA and optic fiber strain more understandable, the strain measurements for roughly equal pressures in the FEA and the tests have been set to the same color differed by that the FEA got dashed lines. Strain readings that lack a corresponding match in FEA has been set to black, as an example this can be seen for the 14.00 bar post buckling reading in Figure 6.9. Likewise, if a FEA strain has got a high pressure compared to the tangential strain, but match well with one of the optical fiber strain readings, it has been set to black. As an example of the FEA reading being black is the 23.27 bar FEA strain curve in Figure 6.11.

The pressures for the optical strain measurements have been found through the pressure graphs in Appendix B.6, B.7 and B.8 by the clock time for when the optical fiber strain measurements were taken as stated in Appendix C.4. As can be seen in the pressure graphs, especially for test nr. 2 of the 400 mm tube in Figure B.17, some of the tubes had leakage at low pressures that diminished when pressure was increased. The leakages are likely due to end cap leakage that diminished when pressure and thus the end cap force was increased, tightening the end cap fit. Also visible in the pressure graphs is areas with substantial noise coming from running of the compressor. Due to the end cap leakage, it is hard to tell whether the water inside the tubes post testing came from leakage through the laminate or just from the end caps leaking. The water present in the tubes post testing has therefore not been assessed further when presenting or discussing possible leakage due to material failure.

6.2 600 mm long tube

6.2.1 Pressure test

The 600 mm long tube had a buckling pressure of 9.75 bar during test nr. 1. It was not possible to increase pressure beyond 9.75 bar, and when the compressor was switched off the pressure stabilized at 9.45 bar. For test nr. 2 the buckling occurred at 9.60 bar followed by a stable pressure at 8.85 bar when the compressor was switched off. Even though the pressure couldn't be increased, indicating a leakage, no failure was possible to spot on the tube visually after the tests, as mentioned. The buckling and post buckling pressures can be seen in the pressure graphs for the 600 mm long tube in Appendix B.6.

Though the tubes showed no visual sign of material failure, the relatively high strains post buckling in the strain graphs in Figure 6.4 and Figure 6.7 indicate buckling behavior. The stable pressure just below buckling pressure indicates that the tube developed a pressure dependent leakage enabling water to penetrate the tube and lower the pressure in the autoclave to a stable pressure. During the project thesis the same pattern was discovered, however it was followed by a drastic decrease in structural stiffness during the subsequent test indicated by much high strain at low pressures in the strain graphs. In the project thesis the leakage was therefore blamed on material failure reducing the stiffness through matrix cracking and delamination that allowed water to penetrate. However, such a pattern is not that obvious in the strain graphs of the 600 mm long tube. Even though a decrease in stiffness is not that prominent, it can be seen that the 9.30 bar reading of test nr. 2 in Figure 6.7 shows 8.14 % higher strains at 170 mm than the 9.32 bar reading of test nr. 1 in Figure 6.4, with $-1975 \mu\epsilon$ in test nr. 1 and $-2150 \mu\epsilon$ in test nr. 2. Looking at the strain graphs it can also be seen that the peak strain is 21.88 % higher during test nr. 1 than for test nr. 2 at 170 mm on the 300 mm reading. The reason for the higher peak strain in test nr. 1 is obviously due to higher pressure, but it can also indicate that the strain state in test nr. 1 caused material failure that led to the tube not reaching the same buckling pressure and the same strains during test nr. 2.

For reference, at 9.67 bar in the FEA, the radial deformation had a max (absolute) value of -1.97 mm (in the creases) around the middle circumference, as can be seen in Figure D.22. Also visible in Figure D.22 is the two lobe buckling mode, however, at a scale factor of 1. For a more pronounced visualization of the two lobe buckling mode see Figure 6.13, where it is scaled by a factor of 5.

6.2.2 FEA match

The FEA Riks analysis predicted buckling as well as material failure at 10.04 bar, yielding buckling pressure during testing at 97.1 % of the predicted pressure. Compared to the tube in the paper, which buckled at 80.8 % of the FEA predicted pressure, the $[89^{\circ}_2/12.7^{\circ}_1/89^{\circ}_2]$ layup can be said to be more predictable than the $[89^{\circ}_1/12.7^{\circ}_1/45^{\circ}_1]$ layup. However, only one tube was tested of each layup meaning that the statistical confidence is low. Regarding material failure, the Tsai-Wu failure criterion max envelope and top ply plots can be seen in Figure 6.12 and Figure 6.13 respectively. As can be seen in the failure plots, the most critical areas, the lobes, are the same in the max envelope as for the top ply, meaning failure is predicted to occur in the top ply at the lobes. The match between optical fiber readings and FEA can be seen in Figure 6.3, 6.4 and 6.5 for test nr. 1. Compared to the FEA matching in the paper it can be seen to be generally smaller deviations. Most notably, the match is better for the 150 mm and 450 mm readings, meaning that the pressure gradient along the tube due to the water column has got less impact on the tube, likely due to higher pressures. Also to be noted is that the strains close to buckling pressure shows a good match, this differs from the project thesis as it failed, as mentioned, at a lower fraction of the FEA predicted buckling pressure. Due to the fact that the difference in strains is only prominent for the peak strains in test nr. 2 compared to test nr. 1, the matching parameters used for test nr. 1 also matched well for test nr. 2, as can be seen in Figure 6.6, 6.7 and 6.8.

The good match was achieved through using an ovality of 0.01 %, a lot less than the 0.46 % used for the layup in the paper. Besides using the mentioned ovality, the longitudinal E-module had to be increased to 37738 MPa, corresponding to a volume fraction of 0.605.

6.3 400 mm long tube

Pressure test

The 400 mm long tube had a buckling pressure in the first test of 15.70 bar and 14.75 bar in test nr. 2, as can be seen in the pressure graphs in Appendix B.7. After buckling pressure was reached and the compressor switched off the pressure stabilized at 5.3 bar in test nr. 1, for test nr. 2 the test was stopped before a stable pressure was reached. As for the 600 mm long tube and as mentioned before for all the tube lengths, the 400 mm long tube showed no sign of material failure after the tests. Compared to the 600 mm long tube, the deviation in buckling pressure between test nr. 1 and nr. 2 was 0.8 bar bigger and the stable post buckling pressure was 56.0 % of the buckling pressure compared to 96.9 % for the 600 mm long tube. As for the 600 mm long tube the buckling comes to show through high strains post buckling, as can be seen in the strain graphs in Figure 6.9 and Figure 6.10. The buckling is very pronounced in test nr 1 with the 14.00 bar post buckling reading having a max absolute strain 31 % higher than the 15.00 bar reading with $-2100 \mu\epsilon$ at 15.00 bar and $-2750 \mu\epsilon$ at 14.00 bar post buckling at 170 mm. In test nr. 2 the 12.93 bar reading post buckling can be seen to almost match the 13.97 bar reading (pre buckling), indicating loss of structural stiffness due to buckling. Additionally, it can be seen that the 14.70 bar reading in test nr. 2 matches very well with the 14.00 bar post buckling reading of test nr. 1, indicating that the tube had buckled when the 14.70 bar reading was acquired.

For reference, at 15.23 bar in the FEA, the radial deformation had a max (absolute) value of -1.04 mm (in the creases) as can be seen in Figure D.23. Also visible in Figure D.23 is the two lobe buckling mode, however, at a scale factor of 1. For a more pronounced visualization of the two lobe buckling mode on the 400 mm long tube see Figure D.19, where it is scaled by a factor of 5.

6.3.1 FEA match

The FEA Riks analysis predicted buckling as well as material failure at 17.39 bar, yielding buckling pressure during testing at 90.3 % of the predicted pressure. The Tsai-Wu failure

plot was almost identical as for the 600 mm long tube, with the predicted failure in the top ply at the lobe(s). The failure plots can be seen in Appendix D.3. The match between the FEA and the optical fiber in test nr. 1 can be seen in Figure 6.9 to be better for the lower pressures than for the pressures close to buckling, however, this only goes for the creases, at the lobes it can be seen to be the opposite. This behaviour is clearly present in test nr. 1 if comparing the match for the optical fiber 12.80 bar reading (12.60 bar in FEA) with the optical fiber 15.00 bar reading (15.23 bar in FEA). The match in the creases (20 mm and 175 mm) can be seen to be better for the 12.80 bar reading than for the 15.00 bar reading, however, at the lobes the 15.00 bar reading have a much better match than the 12.80 bar reading. Even though the mentioned readings have pressures that does not correspond to well with the FEA pressure increments, it is a good example of the general trend. Looking at test nr. 2 in Figure 6.10 it can be seen that the match is better at the creases due to generally higher strains during test nr. 2. The higher strains indicate a loss of stiffness and coupled to the lower buckling pressure of test nr. 2 it is likely that material damage occurred during test nr. 1.

To achieve a good a match as possible in the FEA for the 400 mm long tube, the imperfection was introduced through import from linear buckling analysis instead of modeling an ovality as for the 600 mm long tube. The buckling shape from the linear buckling analysis was scaled with a scaling factor of 0.18, corresponding to a radial deformation/ovality of ± 0.23 mm/0.46 % as the radial deformation of the linear buckling analysis was ± 1.275 mm. Besides importing the linear buckling shape, the end caps had to be modeled as fixed and not freely supported to yield a stiff enough behavior. Figure 6.1 shows the fixed constraint. Besides using the fixed constraints, the same longitudinal E-modulus as for the 600 mm long tube of 37738 MPa had to be used to achieve a stiff enough behavior.

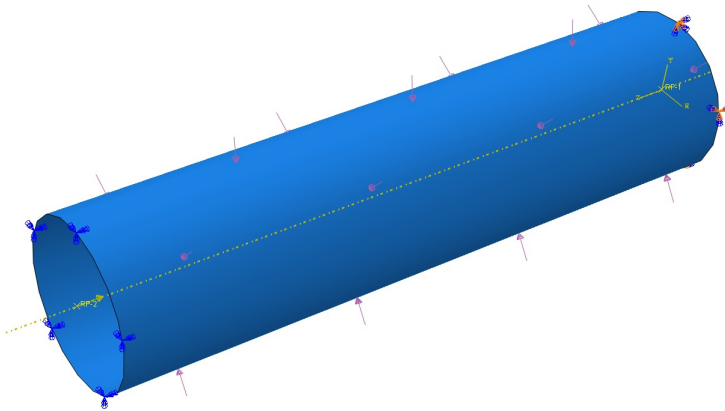


Figure 6.1: The fixed constraints on the 400 mm long tube needed for achieving matching between the FEA and the optical fiber strain results. The blue triads indicate the fixed constraint at each side of the tube.

6.4 300 mm long tube

Pressure test

The 300 mm long tube was only tested once and the buckling pressure during testing was 21.80 bar as can be seen in the pressure graph in Figure B.19. As for the other two tubes, a stable pressure was reached after the compressor was switched off. However, the stable pressure was relatively low at 5.00 bar (outside the pressure graph), 22.9 % of the buckling pressure. As for the other two tubes no material failure or damage was possible to spot visually on the tubes after testing, as mentioned. Supporting that the tube actually buckled is the very high strain of the 21.50 bar reading in the strain graph in Figure 6.11. The 21.50 bar reading also had a lot of noise as can be seen in the raw non smoothed reading in Figure B.9, indicating that the material underneath the optical fiber cracked and caused radiuses at the micro level introduced on the fiber causing noise. As can also be seen in the strain graph, the tube buckled as three lobe and not two lobe. An interesting observation concerning the three lobe mode is the difference in strain magnitude between the three lobes and creases. It can be seen that the strain magnitude increases from the lobe and crease between 0 mm and 125 mm to the lobe and crease between 275 mm and 325 mm. In other words it means that the creases and

lobes were of different size. However, the buckling pressure reading at 21.50 bar shows an evening out of the difference, indicating that the three lobe shape is more stable at high pressures/strains/deformations.

For reference, at 23.27 bar in the FEA, the radial deformation had a max (absolute) value of 1.68 mm (at the lobes) as can be seen in Figure D.24. Also visible in Figure D.24 is the three lobe buckling mode, however, at a scale factor of 1. For a more pronounced visualization of the three lobe buckling mode, see Figure D.21, where it is scaled by a factor of 5.

FEA match

As predicted by the linear buckling analysis carried out pre testing as seen in Section 2.6, the 300 mm long tube buckled as three lobe. The Riks analysis predicted buckling and material failure at 23.49 bar yielding buckling during testing at 92.8 % of the predicted pressure. Due to the mentioned increase in strain magnitude around the circumference, the matching also varies accordingly. It can be seen that the match is good for the crease and lobe between 275 mm and 325 mm and poorer for the lobe and crease between 0 mm and 120 mm. As for the 400 mm long tube, the Tsai-Wu failure plot was almost identical as for the 600 mm long tube, with the predicted failure in the top ply at the lobe(s). The failure plots can be seen in Appendix D.3.

Due to the three lobe buckling mode, matching through shape import from linear buckling analysis, as for the 400 mm long tube, was done to achieve a slight three lobe shape in the Riks analysis model. The scale factor was set to 0.052, which in terms of radial deformation/ovality is ± 0.054 mm/0.108 %. In order to achieve a stiff enough strain behavior, the tube had to be constrained as for the 400 mm long tube, fixed, and the same E-modulus of 37738 MPa had to be used.

6.5 Length sensitivity

After achieving a good match in the Riks analysis for the tubes, linear buckling analysis was run to investigate the end effect and the length sensitivity. Of special interest was

to try and answer why the 300 mm and 400 mm long tubes had to be modeled with fixed constraints. Many linear buckling analysis were run with both fixed and freely supported constraints on different tube lengths to assess the difference between the two constraints. Both the fixed and the freely supported analysis had the E-modulus found through the 600 mm long tube's matching of 37738 MPa, the resulting graph can be seen in Figure 6.14. Also plotted is the buckling pressures from the tests and the matched Riks analysis. As can be seen, the difference between the two constraints diminishes at about 900 mm tube length followed by a distinct flattening of the curves, meaning that the end effect no longer is present. As can be seen, both of the constraints' curves have a distinct change of curvature at short tube lengths indicating a change of buckling mode from two lobe to three lobe. The mode transformation was also shown in the length sensitivity analysis pre testing in Section 2.6.1. The fixed curve has got the transformation occurring at 360 mm versus 320 mm for the freely supported. The longer mode transformation threshold length for the fixed curve comes from that the end effect is more pronounced than for the freely supported. An interesting observation is how the buckling pressures from the tests comply best with the buckling pressures of the freely supported linear buckling analysis, while the strain measurements comply best with the fixed constrained Riks analysis for 300 and 400 mm long tubes.

In order to investigate further why the 300 mm long tube buckled as three lobe and the 400 and 600 mm as two lobe, Riks analysis with imposed unnatural modes were run on the 300 mm and 600 mm long tubes. The analysis were run with imposed three lobe shape on the 600 mm long tube from linear buckling analysis import and imposed two lobe shape on the 300 mm long tube from ovality modeling. With 0.01 % ovality the 300 mm long tube buckled as two lobe and with a scale factor of 0.052 the 600 mm long tube buckled as three lobe. The resulting graph can be seen in Figure 6.15. As can be seen, the strain energy is higher for the unnaturally occurring buckling modes. It can also be seen that the 600 mm long tube's strain energy deviation between the two modes is a lot bigger than for the 300 mm long tube.

6.6 Comparison table

Table 6.1: Result comparison table

Parameter	600 mm	400 mm	300 mm	Data source
Buckling pressure (bar)	9.75	15.70	21.80	Figure B.19, B.15 and B.11
Linear buckling analysis buckling pressure (bar)	10.33	16.10	22.87	Figure 6.14
- Pressure test comparison	94.4 %	97.5 %	94.3 %	
Riks analysis buckling pressure	10.04	17.39	23.49	Appendix B.9 or see Figure 6.14
- Pressure test comparison	97.1 %	90.3 %	92.8 %	
FEA matching parameters				
- Matching ovality	0.01 %	0.46 %	0.108 %	From Abaqus
- E-modulus in fiber direction	37738 MPa	37738 MPa	37738 MPa	From Abaqus
- Constraint	Freely supported	Fixed	Fixed	From Abaqus

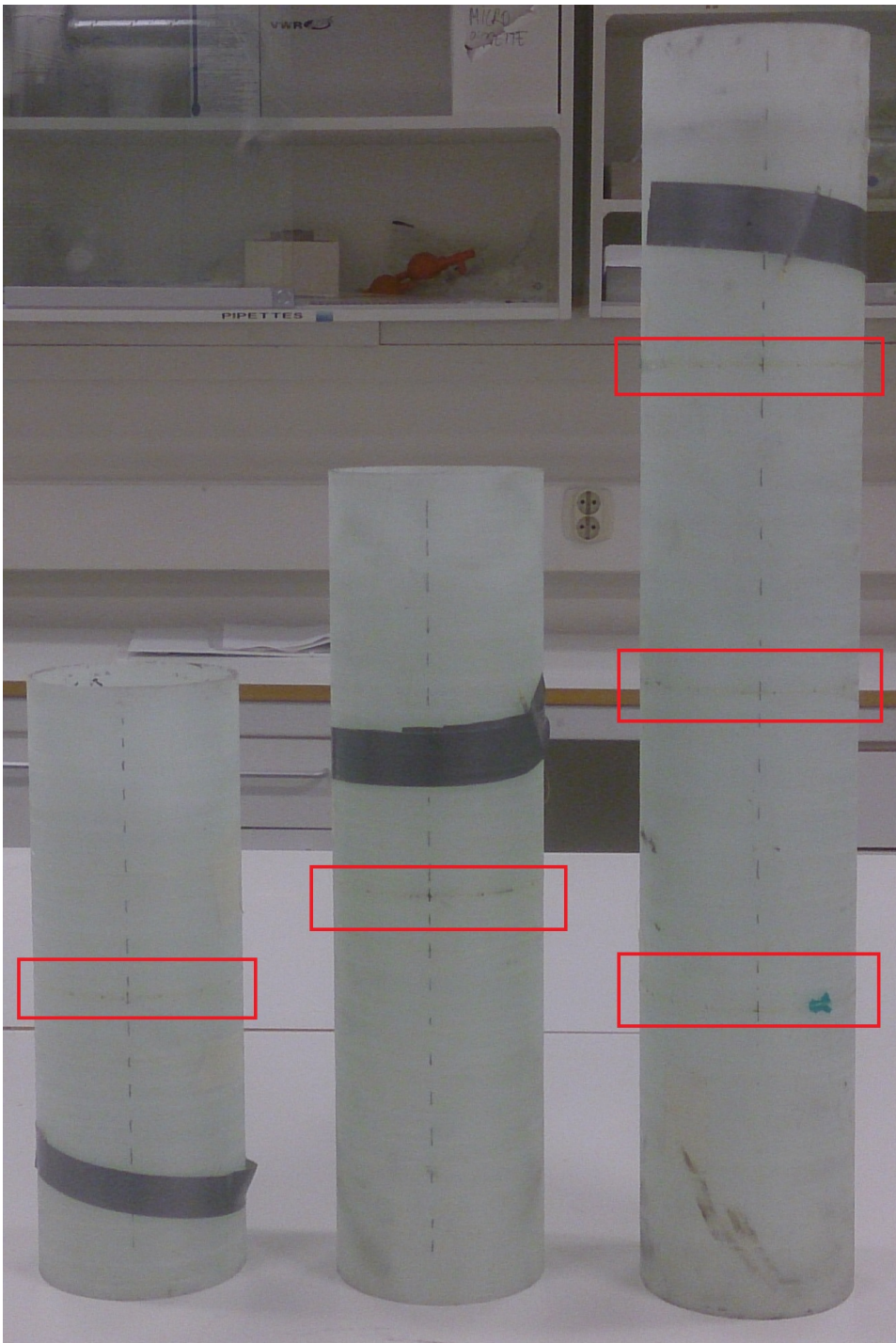


Figure 6.2: Picture of the tubes post testing with fiber paths highlighted with red squares.

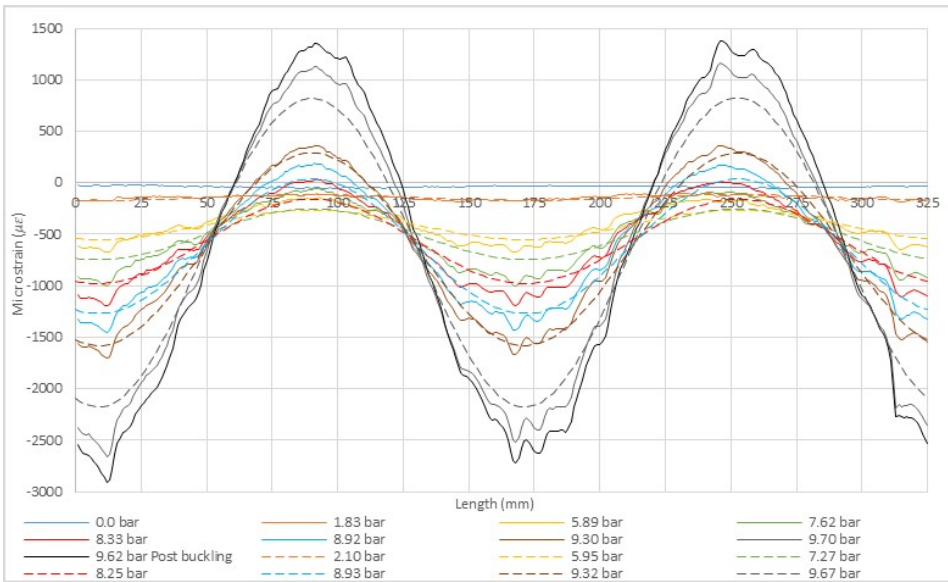


Figure 6.3: Strain measurements and FEA results at 150 mm on the 600 mm long tube from test nr. 1.

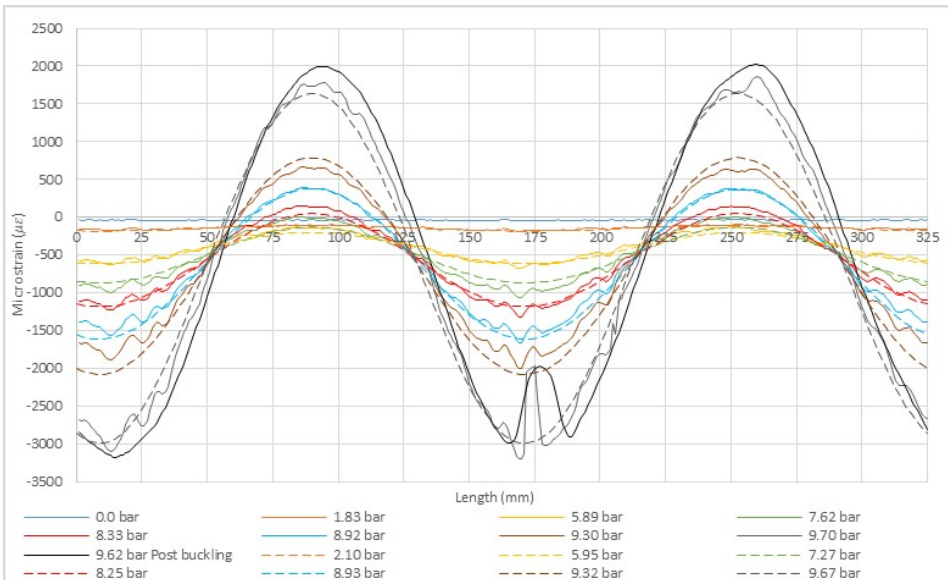


Figure 6.4: Strain measurements and FEA results at 300 mm on the 600 mm long tube from test nr. 1. The post buckling measurement have been smoothed, the original measurement can be found in the Appendix in Figure B.2.

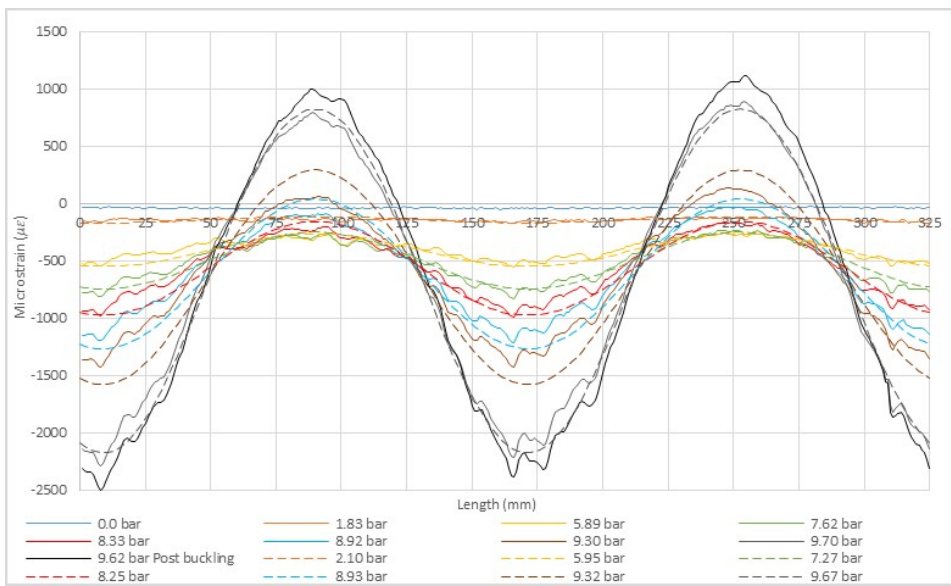


Figure 6.5: Strain measurements and FEA results at 450 mm on the 600 mm long tube from test nr. 1.

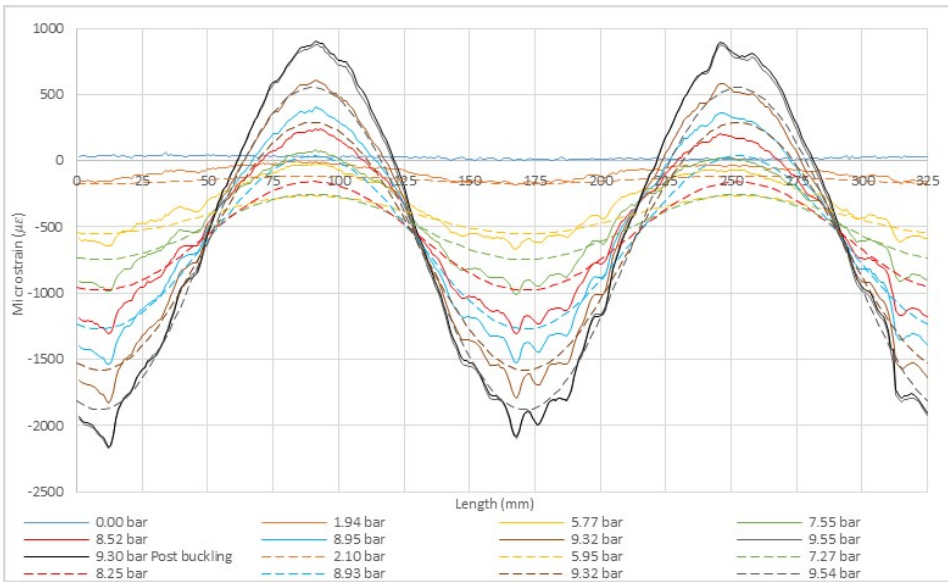


Figure 6.6: Strain measurements and FEA results at 150 mm on the 600 mm long tube from test nr. 2.

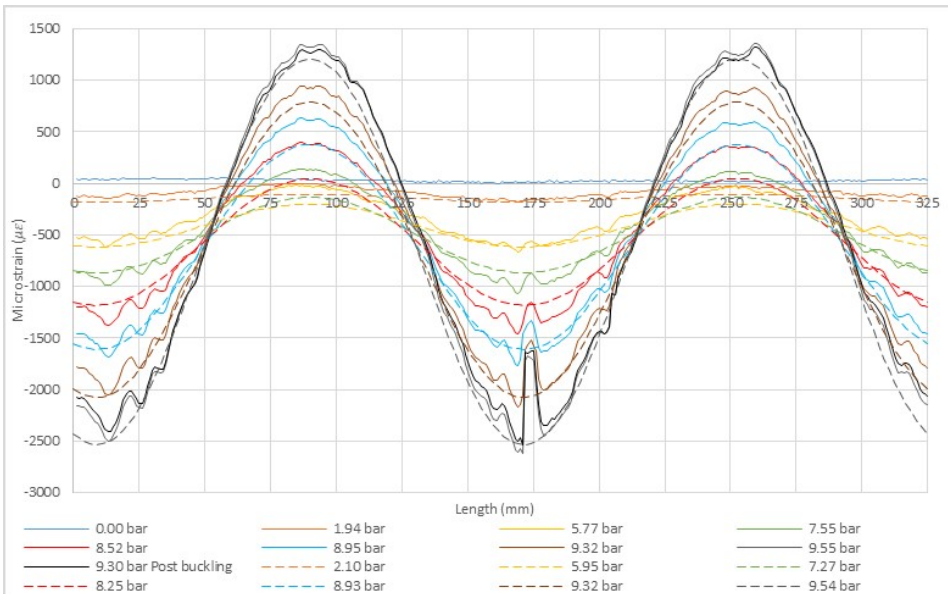


Figure 6.7: Strain measurements and FEA results at 300 mm on the 600 mm long tube from test nr. 2.

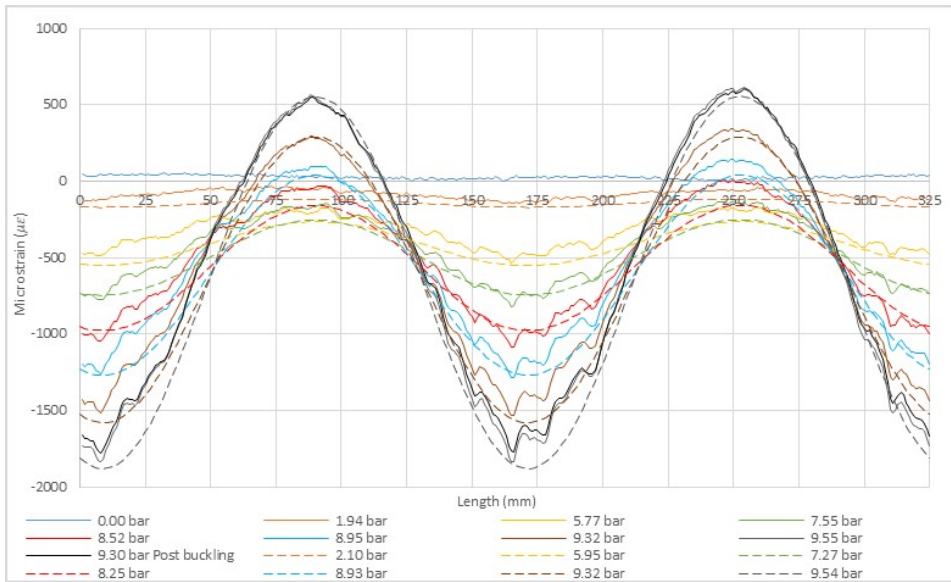


Figure 6.8: Strain measurements and FEA results at 450 mm on the 600 mm long tube from test nr. 2.

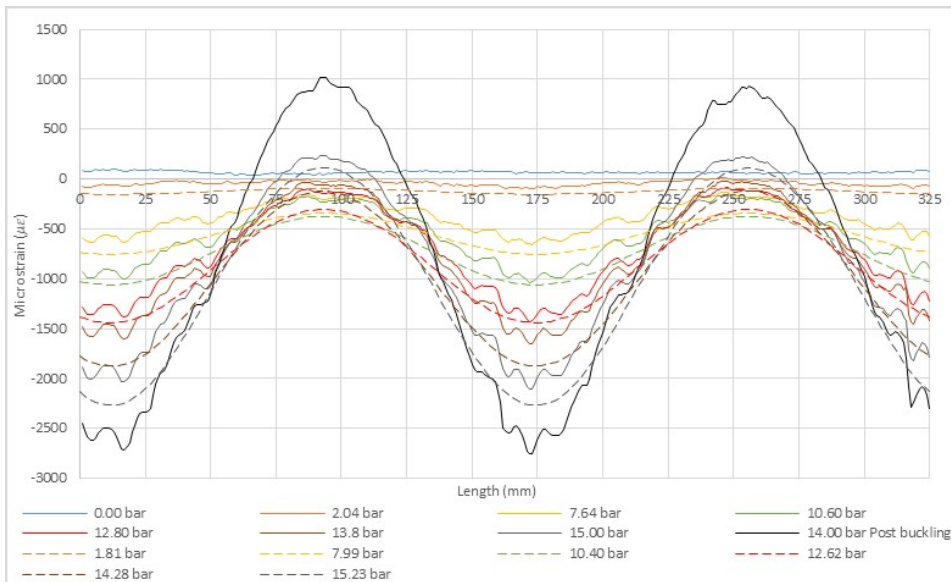


Figure 6.9: Strain measurements and FEA results at 200 mm on the 400 mm long tube from test nr. 1.

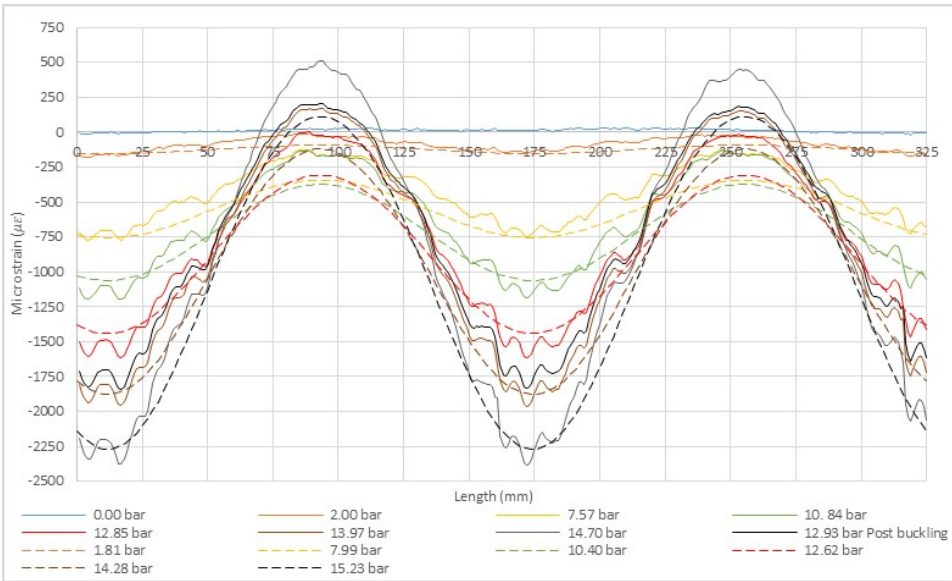


Figure 6.10: Strain measurements and FEA results at 200 mm on the 400 mm long tube from test nr. 2.

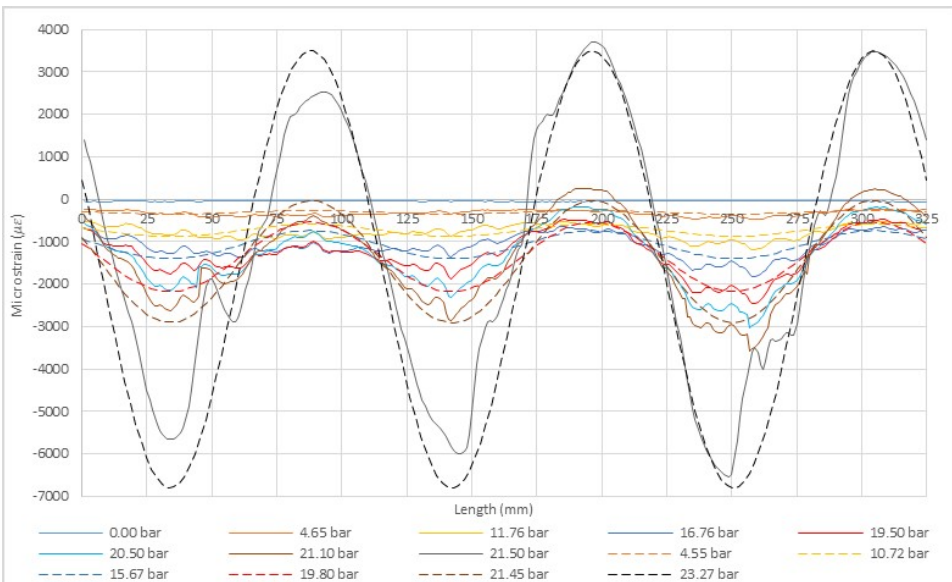


Figure 6.11: Strain measurements and FEA results at 150 mm on the 300 mm long tube. As can be seen the tube has got a three lobe buckling mode, indicated by the three peaks of the strain curve. The post buckling measurement have been smoothed, the original measurement can be found in the Appendix in Figure B.9.

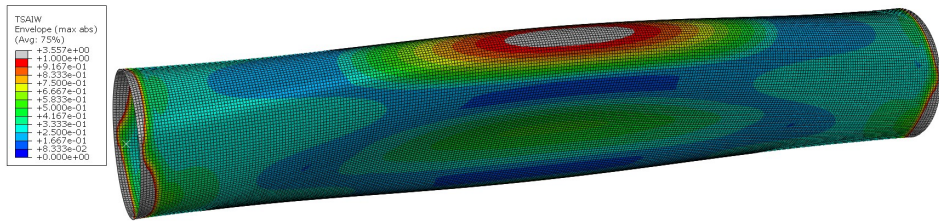


Figure 6.12: Max exposure factor of the Tsai-wu failure criterion through the thickness for the 600 mm long tube at the failure (and buckling) pressure of 10.04 bar.

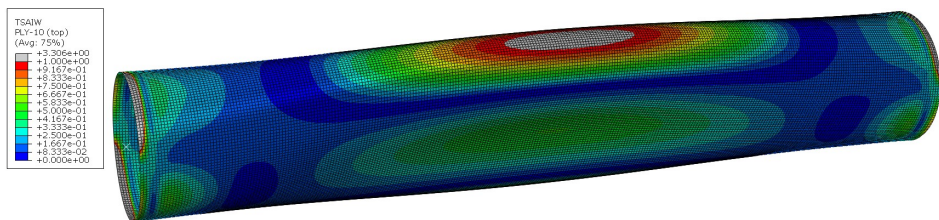


Figure 6.13: Tsai-wu failure criterion on the 600 mm long tube at the top of the top ply at the failure (and buckling) pressure of 10.04 bar. As can be seen, the most exposed area at the top of the lobe is also the most exposed area when looking at the max envelope in Figure 6.12.

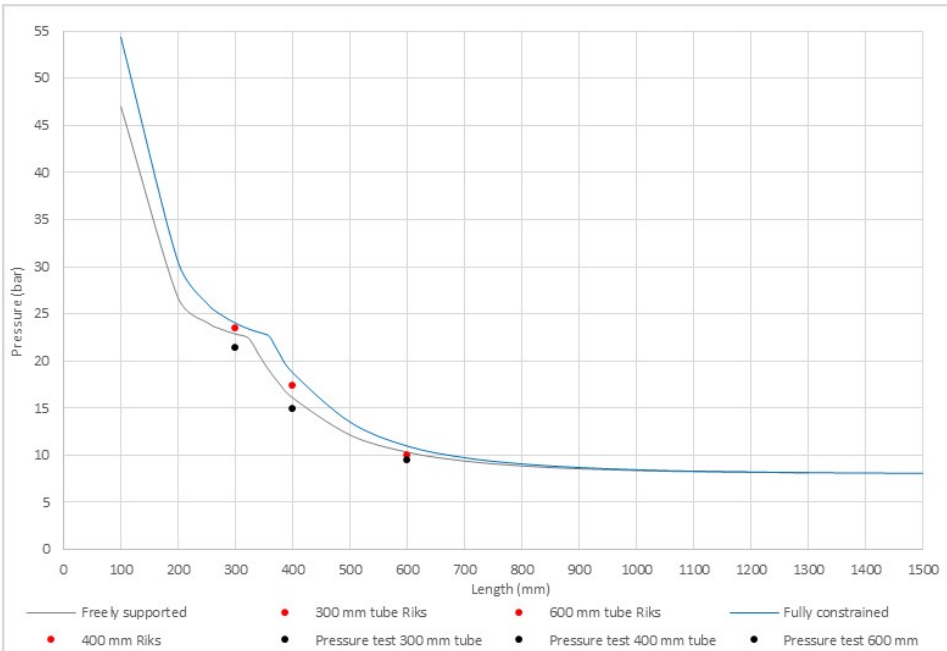


Figure 6.14: Length sensitivity analysis with both fixed and freely supported constraints.

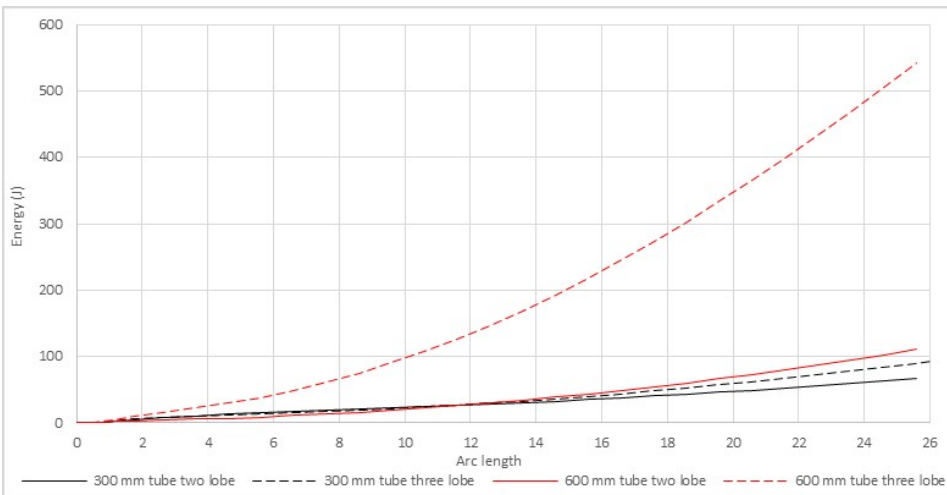


Figure 6.15: Comparison between strain energy with different buckling modes. As can be seen, the three lobe buckling mode requires a lot more work on the 600 mm long tube than the two lobe, likewise for the two lobe on the 300 mm long tube. However, the difference is a lot less on the 300 mm long tube due to the buckling pressure being closer to the buckling mode transition lengths buckling pressure, as can be seen in Figure 6.14.

Discussion

7.1 Optimal layup behavior

Based on the pressure tests, the $[89^{\circ}_2/12.7^{\circ}_1/89^{\circ}_2]$ layup can be said to perform better than the $[89^{\circ}_1/12.7^{\circ}_1/45^{\circ}_1]$ layup tested in the project thesis. The most striking difference between the two, besides the obvious buckling pressure, is when the buckling occurred. For the $[89^{\circ}_1/12.7^{\circ}_1/45^{\circ}_1]$ layup the buckling occurred at 80.8 % of the predicted Riks analysis buckling pressure and at 81.1 % of the predicted failure pressure. For the $[89^{\circ}_2/12.7^{\circ}_1/89^{\circ}_2]$ layup the deviation in failure and buckling pressure was much less with buckling and failure occurring at 97.1 % of the FEA predicted pressures. Even though the tests show that there is a substantial difference between the predictability between the two layups, only one tube was produced of each, therefore the statistical confidence is low, as mentioned in the results chapter, Section 6.2.2. Even though the statistical confidence is low, the results have been discussed with the assumption that the results are absolute due to the fact that its the only results available.

The reason for the good FEA correlation for the $[89^{\circ}_2/12.7^{\circ}_1/89^{\circ}_2]$ layup is likely due to the outer layer being oriented so as to have the fiber and matrix direction in the direction of the principal stresses at the most critical spot, the top layer at the top of the lobes. When the fiber orientation makes for a strain state approaching a principal

strain state it simplifies the stress state along the weakest direction, the matrix direction, making for a more direct application of the failure stresses. Since the failure stresses used were found through testing of vacuum infused samples and then scaled with the same factor as for the E-moduli, as done by G. Perillo [21] described in Section 5.4, they haven't been directly experimentally proven for filament wound tubes. Therefore, they likely apply best when the fibers are oriented in a fashion resembling a simple vacuum infused sample while at the same time being loaded in a simple as possible fashion. Indication of that a principal strain state occurs at the lobes for the $[89^\circ_2/12.7^\circ_1/89^\circ_2]$ layup can be seen in Figure 7.1. In Figure 7.1 the shear strain at the FEA predicted buckling pressure and at the increment closest to buckling in the tests (called failure for convenience) for the $[89^\circ_2/12.7^\circ_1/89^\circ_2]$ layup and the $[89^\circ_1/12.7^\circ_1/45^\circ_1]$ layup is plotted. Due to the fact that a principal strain state is characterized by zero shear strain [19], the shear strain was investigated to assess if a principal strain state occurred in the layups. For the $[89^\circ_2/12.7^\circ_1/89^\circ_2]$ layup, it can be seen that the shear strain at failure is at its lowest at the lobes (at 10 mm and 170 mm in the graph). This indicates that the strain state around the middle circumference at the top of the top layer is closest to a principal strain state at the lobes. Furthermore, when the deformation continues towards buckling, the shear strain at the lobes approaches zero shear strain, making the principal strain state even more pronounced. For the $[89^\circ_1/12.7^\circ_1/45^\circ_1]$ layup, it can be seen that the shear strain propagation is somewhat opposite. For the $[89^\circ_1/12.7^\circ_1/45^\circ_1]$ layup the shear strain at the lobes during failure is low, however, it increases drastically as the deformation and pressure approaches buckling, making for a very non-principal strain state for high deformation.

Another reason for the good correlation with the predicted FEA buckling and failure pressures for the $[89^\circ_2/12.7^\circ_1/89^\circ_2]$ layup, can be the LPF curve shape. The LPF curve for the $[89^\circ_2/12.7^\circ_1/89^\circ_2]$ layup has, as also mentioned as a reason for good performance in the optimal layup assessment, a long arc length increment with high increase in deformation close to the buckling pressure. In other words, there is a substantial difference in the deformation between the buckling pressure and pressures just below the buckling pressure. The LPF curves for the different lengths from the matched Riks

analysis can be seen in Figure B.20 (for convenience, scaled so as to reveal pressure). To further support this, reading from the Riks analysis for the 600 mm long tube at 9.77 bar, the Tsai-Wu failure criterion reveals a max exposure factor of only 0.32, even though being just 0.27 bar from the buckling pressure and just 0.02 bar above the test's buckling pressure. Even though the layup likely developed a matrix failure enabling water to penetrate, it must be pointed out that the matrix failure strength is based on fracture strength. This means that the matrix can have developed cracks long before reaching the matrix failure strength, as indicated by the low exposure factor at the test's buckling pressure.

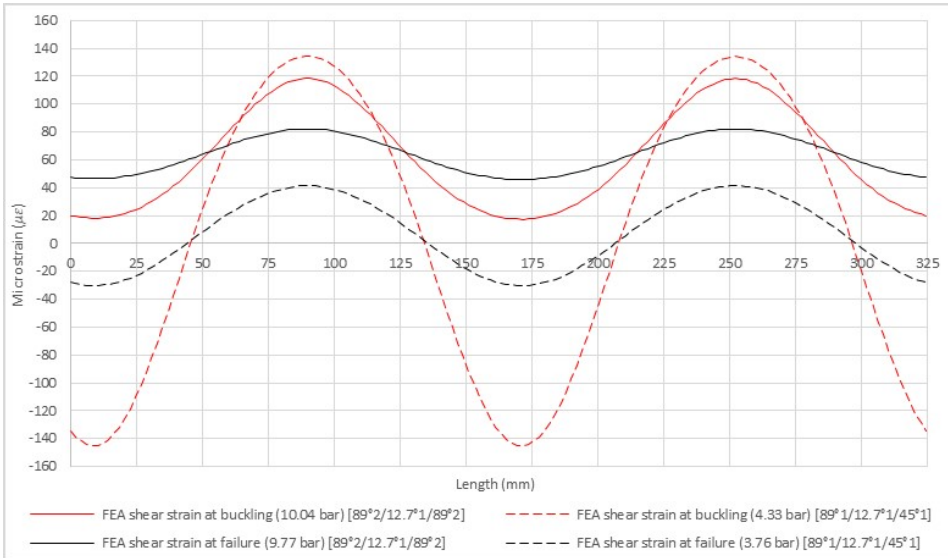


Figure 7.1: Shear strain at 300 mm on the 600 mm long tubes for the $[89^{\circ}_2/12.7^{\circ}_1/89^{\circ}_2]$ and the $[89^{\circ}_1/12.7^{\circ}_1/45^{\circ}_1]$ layup at the FEA predicted buckling pressure and at the increment closest to the buckling/failure pressure of the tests (9.75 bar and 3.5 bar).

Even though the optimal layup proved to perform better than the $[89^{\circ}_1/12.7^{\circ}_1/45^{\circ}_1]$ layup, it still developed a pressure dependent leakage, as described for all the tubes. Based on the test results it is clear that the extent of the leakage increases with decreasing tube length. However, compared to the $[89^{\circ}_1/12.7^{\circ}_1/45^{\circ}_1]$ layup, the leakages on the $[89^{\circ}_2/12.7^{\circ}_1/89^{\circ}_2]$ layup were smaller, meaning that the pressure dropped more slowly. An intuitive reason for this is the higher number of layers and the increased thickness

resulting in that the water had to penetrate more material to reach through.

As can be seen in the failure plots (failure in the top ply at the lobes) and based on the axial strain graph in Figure 2.3 showing positive strain (tension) through the whole thickness at the lobes, the layup is supposed to fail in the top layer at the lobes by matrix cracking at the buckling pressure. The failure plot and the axial strain graph can explain the pressure dependent leakage as a matrix crack mechanism in the 89° layer which closed under the stable post buckling pressure. However, even though a matrix crack occurred in the top layer, this alone is not enough to allow water to penetrate the layup. For full penetration to happen, the underlying layers also will have to fail. For the tube tested in the project thesis, which was tested until failure, it was discovered that delamination had occurred together with matrix cracking. The delamination had occurred between all the layers together with fiber buckling in the bottom layer and matrix cracking in the top layer. Preceding the failure test, several tests were run where a pressure dependent leakage occurred, as can be found described in the paper in Appendix A. To make the layup in the project thesis fail completely, an external plastic liner was used and the compressor had to be run at max capacity. Due to the plastic liner and the compressor running at max, the actual pressure required for complete failure was difficult to determine and therefore the tubes in the master's thesis was not attempted tested in this way. It was concluded that the matrix cracking had initiated delamination at a small scale during the tests prior to the failure test, resulting in that water could penetrate the layup above the threshold pressure for the pressure dependent leakage. The delamination from matrix cracking is a known effect and described by Kollár et. al. [19]. Seeing as the layup in the project thesis had the same underlying layers as the $[89^\circ_2/12.7^\circ_1/89^\circ_2]$ layup, a matrix crack in the top layer should therefore initiate the same mechanisms leading to a pressure dependent leakage. Supporting matrix cracking in the top layer is the noise on the 21.50 bar strain reading on the 300 mm long tube's strain graph in Figure 6.11 indicating that the underlying material have developed cracks, as mentioned in the results chapter. Further supporting that material damage causing a pressure dependent leakage occurred is the reduced stiffness in test nr. 2 of the 600 and 400 mm long tubes, as also mentioned in the results chapter.

From a production point of view, the $[89^{\circ}_2/12.7^{\circ}_1/89^{\circ}_2]$ layup came out with a thickness 0.405 mm thicker than predicted in the optimal layup assessment, based on the layer thicknesses measured on the $[89^{\circ}_1/12.7^{\circ}_1/45^{\circ}_1]$ layup. Due to the $[89^{\circ}_2/12.7^{\circ}_1/89^{\circ}_2]$ layup having more layers, it took more time to wind compared to the $[89^{\circ}_1/12.7^{\circ}_1/45^{\circ}_1]$ layup. Based on the findings of D. Cohen [13], who found that production time greatly affects the wall thickness, this might be a reason for why the $[89^{\circ}_2/12.7^{\circ}_1/89^{\circ}_2]$ layup ended up being thicker than predicted. Also, as a consequence of the thicker than predicted thickness is the lower volume fraction compared to the $[89^{\circ}_1/12.7^{\circ}_1/45^{\circ}_1]$ layup, also reported as a consequence of longer winding time by D. Cohen. Even though the volume fraction is lower, it does not seem to have affected the longitudinal E-modulus as scaled with the volume fraction in the material investigation in Chapter 5. This is indicated by the good match for the 600 mm long tube with an E-modulus corresponding to a volume fraction of 0.605, much higher 0.54, as found in the material investigation. However, the need for a high E-modulus can come from that the 600 mm long tube was run with freely supported constraints giving low structural stiffness, as opposed to the fixed constraints of the 300 mm and 400 mm long tubes. On the other hand, the good match for the 150 mm and 450 mm readings on the 600 mm long tube indicate that the use of freely supported constraints is a correct simulation of the end constraints. Further supporting that the higher E-modulus is correct is the subsequent good FEA match for the 300 mm and 400 mm long tubes.

A factor that can have contributed to weigh up for decreased volume fraction with respect to the E-moduli, is the void content. S. R. Ghiorse [23] stated that a 2 % increase in void content will lead to a 10 % decrease in flexural modulus. Considering that peel ply was applied by hand with high tension straight after the winding was done, this can have squeezed out potential air voids in the matrix, giving a lower void content. For the tubes tested by G. Perillo [21] to attain the material data used for the scaling of material properties, the peel ply method was not used. It is important to keep in mind when assessing void content and volume fraction that a high void content will give less epoxy content and thus a higher fiber volume fraction in a burn-off test. If a burn-off test's volume fraction from a material with high void content compared to the material

data is used for scaling, artificially high E-modulus can result due to the void content greatly affecting the mechanical behavior. The effect of the void content comes to show in the tubes tested by G. Perillo to attain the material data. Even though the volume fraction in Perillo's tubes were as high as 0.62, the E-modulus in fiber direction had to be decreased by 13.8 % from 44.8 GPa in vacuum infused samples (low void content) to 38.6 GPa, as mentioned in the scaling of the material properties in Section 5.4. The E-moduli decrease was necessary even though the vacuum infused plates had a volume fraction as low as 0.54. It was concluded by Perillo, as also mentioned in the material scaling, that the decrease in E-modulus for the filament wound tubes was caused by the void content being higher than for the vacuum infused plates. Based on the work by G. Perillo and S. R. Ghiorse, if using peel ply decreases the void content by just a small percentage it is therefore likely that it is enough to weigh up for a lower volume fraction of fibers.

Concerning the sandwich inspired layup, having a thicker than predicted layup is not negative even though the volume fraction is lower. Ideally, if the material had been isotropic, the increased thickness would have increased the resistance against buckling in the power to three through an increased area moment of inertia. This comes to show through the higher buckling pressure in the matched Riks analysis compared to the analysis with the predicted layer thicknesses in the optimal layup assessment. Compared to the predicted thickness, the real layup's matched Riks analysis showed a buckling pressure twice that of the predicted, with only 33.6 % increased thickness.

7.2 FEA comparison and length sensitivity

The imperfections needed to induce buckling on the tubes can be seen to vary a lot between the different tube lengths. However, even though there is apparently no similarities between the imperfections, it can be seen that the 600 mm and 300 mm long tubes needs a relatively small imperfection compared to the imperfection needed to achieve matching for the 400 mm long tube. The likely reason is that the 400 mm long tube needs a bigger imperfection to be compliant enough to match the strain readings considering it has got fixed constraints. At 300 mm tube length, the fixed constraints

are likely more consistent with the end caps' effect considering the shorter tube length. However, at 400 mm tube length, modeling the end caps with a damping instead of fixed would probably yield a smaller imperfection to achieve a good match while also being more consistent with the actual end cap effect.

An important fact to keep in mind when comparing FEA results and test results with the goal to find a matching method is within which boundaries it is acceptable to tweak the FEA to achieve a match. In the work presented in this master's the approach to FEA matching have been to first adjust FEA parameters so the tangential strain curves fit the tests and then try to find why exactly those parameters were needed to achieve a good match, as discussed in this chapter. However, during the process of finding the right parameters, a critical view has been applied to avoid overcompensation and use of illogical parameters. Additionally, when assessing the length sensitivity and the matching for different tube lengths it is important to keep in mind that tubes used in practical applications will be much longer than the tested tubes. Due to this, the most critical question to be answered is how it is possible to predict the behavior of longer tubes through FEA by using input parameters from testing of shorter tubes.

Due to the fact that a longer than 600 mm long tube will be more structurally compliant, it will likely need a higher ovality than 0.01 %. However, since a length of 600 mm is close to where the linear buckling analysis curves flatten in Figure 6.14, the ovality for longer tubes will likely not be much higher than 0.01 %. When considering other layups and thicker tubes it is clear that to get an idea of what ovality to use to analyze long tube sections, the test tube has to be of a length longer than that the tube needs to be modeled as fixed to achieve a good match. To find the right ovality for other layups, the test tube should be of a length not much shorter than where the graphs from the fixed and freely supported tubes in the length sensitivity analysis coincides, as for the 600 mm long tube.

When comparing the required ovality for the $[89^{\circ}_1/12.7^{\circ}_1/45^{\circ}_1]$ layup with that of the $[89^{\circ}_2/12.7^{\circ}_1/89^{\circ}_2]$ layup, the $[89^{\circ}_1/12.7^{\circ}_1/45^{\circ}_1]$ layup requires a much higher ovality. The difference in ovality between these two is likely due to the fact that the $[89^{\circ}_1/12.7^{\circ}_1/45^{\circ}_1]$ layup is a lot more compliant, yielding less resistance to developing

a buckling pattern at relatively low pressures. On the opposite end of the scale for the $[89^\circ_1/12.7^\circ_1/45^\circ_1]$ layup is the layups tested by D. Choqueuse et. al. [15] which had a high relative thickness and thus buckled very suddenly, as for normal euler buckling. Riks analysis of such tubes would very likely require a very small ovality due to the very sudden onset of buckling caused by the high structural stiffness.

The reason for that the shorter tubes needed the end caps modeled as fixed to be stiff enough to achieve matching probably comes from the relation between the stick out of the end caps, the tube length and the wall thickness. At 300 mm, the end caps take up twice as much of the tube length as on the 600 mm long tube while at the same time the thickness/length ratio is doubled.

Besides giving a good indication of how the Riks analysis can be run to predict the strain and buckling pressure on longer tubes, the buckling pressures and modes from the tests of the different lengths also gave a good indication of the reliability of the linear buckling analysis. For less detailed analysis, where only the buckling pressure is of interest or where analysis time is critical, linear buckling analysis is a good alternative to a full Riks analysis. The linear buckling analysis pressure prediction can, as shown in the length sensitivity graph, be used to predict buckling pressures of longer tubes provided that an error margin of about 5 % is used, based on the results from the pressure tests. However, as mentioned before, the statistical confidence is low due to few tests. Besides the fact that the buckling pressures of the linear buckling analysis were quite compliant with the tests, the strongest indicator of the validity of the linear buckling analysis for long tubes was the mode change prediction. Since the mode change prediction is dependent on the end effect/tube length, the fact that the 300 mm long tube had a three lobe buckling pattern indicates that the linear buckling analysis prediction of end effect is consistent with test results. Since the end effect prediction is correct for shorter tubes it is therefore likely to be correct also for longer tubes.

As can be seen from the strain energy plot in Figure 6.15, the strain energy differs quite a lot between the different buckling modes and the different lengths. At an arc length of 24.5 the strain energy for the three lobe buckling mode on the 600 mm long tube is 505 J, 490 % higher than for the naturally occurring two lobe mode at 102 J. On

the 300 mm long tube the two lobe buckling mode has got a strain energy of 84 J, only 133 % higher than for the natural three lobe buckling mode at 63 J. The reason for the higher difference between the two modes on the 600 mm long tube compared to the 300 mm long tube likely comes from the distance from the mode transition length in the length sensitivity analysis, as seen in Figure 6.14. Looking at the curve for the freely constrained analysis, which has got a mode transformation length of 320 mm, the 600 mm long tube is 280 mm longer than the mode transition length, whereas the 300 mm long tube is only 20 mm shorter. The reason for that the 300 mm long tube has got a lower overall strain energy for both modes compared to the 600 mm long tube is due to it having less strain due to shorter length. Considering the findings above, the reason for the tubes to buckle as either two lobe or three lobe is due to the fact that the naturally occurring buckling modes requires less energy input. Besides explaining the reason for the occurrence of the different modes, the most important aspect of the strain energy plot is that it gives an indication of how physically meaningful the imperfections are. The fact that it is possible to render unnatural buckling modes on the tubes in FEA by using imperfections, indicates that the actual imperfections used to achieve buckling behavior might be analysis parameters more than existing imperfections on the tubes. In other words and as an example, the 600 mm long tube likely has not got an ovality of exactly 0.01 %/0.005 mm from production. However, by modeling the tube with this ovality a good match is found between FEA and tests due to factors that has more to do with manipulating the FEA analysis method than the actual geometry of the tube to be tested. This implication means that the predictability of the FEA likely is independent of production irregularities, such as the ovality of a produced tube, which can vary to some degree if many tubes are produced.

Conclusion and recommendations for further work

8.1 Conclusion

In this master's thesis an assessment has been made of what is the most optimal layup for achieving high buckling pressures for thin walled filament wound tubes subjected to external hydrostatic pressure. The most optimal layup was found to be that of $[89^{\circ}_2/12.7^{\circ}_1/89^{\circ}_2]$ based on a FEA assessment of seven tubes with different layups together with a detailed investigation of the strain states on the tubes. Besides, a method has been found to achieve a good match between FEA and strains measured on the tubes during pressure testing.

During the preparational project thesis a 600 mm long tube of 100 mm in diameter with a layup of $[89^{\circ}_1/12.7^{\circ}_1/45^{\circ}_1]$ was instrumented with optical fiber to measure strain and pressure tested until buckling. During the first part of the master's thesis it was found that modelling the tube elliptic in FEA gave a very good match between FEA Riks analysis and strain measurements from testing of the tubes. The elliptic shape was introduced by adding and subtracting 0.46% of the mean diameter (so called 0.46% ovality for convenience) to the major and minor diameter of the ellipse respectively.

The same ovality was used to simulate the buckling behaviour of the seven tubes in the optimal layup assessment. To further investigate the matching method and to validate the optimal layup assessment result, the $[89^{\circ}_2/12.7^{\circ}_1/89^{\circ}_2]$ layup was pressure tested in three different tube lengths, 600 mm 300 mm and 400 mm, all with a 100 mm tube diameter and instrumented with optical fiber. The buckling pressure of the 600 mm long tube was found to be 9.75 bar, 2.79 times that of the $[89^{\circ}_1/12.7^{\circ}_1/45^{\circ}_1]$ layup despite being just 33 % thicker, validating the predicted high performance of the optimal layup assessment. To achieve a good match in the FEA of the 600 mm long tube, an ovality of 0.01 % had to be used. Additionally, to achieve a stiff enough tube, an E-modulus in the fiber direction of 37738 MPa had to be used, 9.7 % higher than what was predicted through scaling with volume fraction found through burn-off testing. The reason for the higher than predicted E-modulus was concluded to be caused by a relatively low void content due to peel ply being applied with high tension post winding, squeezing out air voids. The match in buckling pressure between the test and the analysis was also good, with the 600 mm long tube buckling at 97.1 % of the predicted pressure. In order to render the 300 mm and 400 mm long tubes substantially stiff in the FEA for a good match, they had to be constrained as fixed. The fixed constraints differed from the 600 mm long tube, which had a very good match with freely supported constraints. The need for fixed constraints was concluded as arising from a greater end effect from the end caps for the shorter tubes. Since the 600 mm long tube achieved a good match without fixed constraints, indicating little end effect, it was concluded that for tubes longer than 600 mm with the same layup the imperfection required for correct strain prediction will likely be close to 0.01 % ovality.

The reason for the good performance of the $[89^{\circ}_2/12.7^{\circ}_1/89^{\circ}_2]$ layup was concluded as being due to a high bending stiffness in the tubes' tangential direction caused by the outer 89° layers. Secondly, it was concluded that the 12.7° layers kept the layup substantially stiff in the axial direction to hinder build up of strains in the weak transverse direction of the 89° layers. The layup acted therefore as a sandwich structure in the tangential direction with stiff outer layers and a more compliant core.

8.2 Recommendations for further work

As proved in this work, composite tubes with layups that have a high bending stiffness in the tangential direction is beneficial for achieving high buckling pressure from external hydrostatic pressure. However, finding methods to replace the middle layer of such layups with a more lightweight material with high strength in one direction, the axial direction, will be beneficial for several factors. Firstly, for long tube sections, having a lightweight core material will give a much lighter tube. Secondly it is much easier to wind 89° layers than 12.7° layers from a machine and production complexity viewpoint, requiring less sophisticated machines and shorter production time. Therefore, avoiding winding of the 12.7° layer will cut costs and production time.

Relevant considering increasing the strength and stiffness of the tubes is to further investigate the void content's influence. Investigating how the peel ply method described and used in this thesis influence the void content, volume fraction and strength/stiffness will then be very relevant and a good starting point.

From an analysis and buckling pressure prediction viewpoint, more layups should be tested to further validate the matching method. Also, thicker layups should be investigated to assess at what point the tubes go from gradually developing a buckling shape before losing structural stiffness to where they undergo sudden collapse.

Bibliography

- [1] *Leo 3 Datasheet*. Keller AG.
- [2] *OBR 4600 User Manual*. Luna Technologies.
- [3] *Offshore Standard DNV-OS-C501 Composite Components*. DNV.
- [4] *Release fabrics and peel plies product catalogue*. Tygvac.
- [5] *Vacuum bag sealant types product catalogue*. Tygvac.
- [6] (2006). *Technical Datasheet EPIKOTE Resin MGS RIMIR 135 and EPIKURE Curing Agent MGS RIMH 134-RIMH 137*. Number PDS-8246- (Rev. 11/5/2013 7:15:30 AM). Momentive.
- [7] (2009). *HiPer-Tex W2020 Rovings Datasheet*. 3B.
- [8] (2010). *Wind power industry selector guide*. Huntsman.
- [9] (2012a). *Abaqus Analysis User Manual, 29.6 Shell elements*. Dassault Systèmes.
- [10] (2012b). *Abaqus Analysis User Manual, 6.2.3 Eigenvalue buckling prediction*. Dassault Systèmes.
- [11] (2012c). *Abaqus Analysis User Manual, 6.2.4 Unstable collapse and postbuckling analysis*. Dassault Systèmes.

- [12] (2013). *FLEX-Z 3 Product Datasheet/User manual*. Zywx Inc.
- [13] Cohen, D. (1997). Influence of filament winding parameters on composite vessel quality and strength. *Composites Part A*, pages 1035–1047.
- [14] D. Choqueuse, B. Bigourdan, A. D. B. D. L. Q. Hydrostatic compression behaviour of steel-composite hybrid tubes.
- [15] D. Choqueuse, P. D. (2014). Durability of composite materials for underwater applications. *Solid Mechanics and Its Applications*, 208:200–201.
- [16] Haaheim, M. Health monitoring of composites using optical fibers.
- [17] Hugaas, E. Buckling of thin walled composite tubes.
- [18] Johannessen, J. *Tekniske Tabeller*.
- [19] Lázlo P. Kollár, G. S. S. (2003). *Mechanics of Composite Structures*. Cambridge University Press.
- [20] Mikrosam. *MAW 20 LS 4/1 Filament Winding machine User Manual*.
- [21] Perillo, G. *Numerical and Experimental Investigation of Impact Behaviour of GFRP Composites*.
- [22] Peters, S. (2011). *Composite filament winding / edited by S.T. Peters*. Materials Park, Ohio : ASM International.
- [23] R., G. S. Effect of void content on the mechanical properties of carbon/epoxy laminates.
- [24] T. Messenger, M. Pyrz, B. G. P. C. (2002). Optimal laminations of thin underwater composite cylindrical vessels. *Composite Structures*, 58:529–537.
- [25] Vedvik, N. P. Essential mechanics of composites. Release 01 - 2013.

Appendix **A**

Paper

Abstract

A filament wound tube of 100 mm diameter and 600 mm length, with a thickness of 1.675 mm, was exposed to external hydrostatic pressure in an autoclave to test the buckling behavior. Since the autoclave was closed from visual inspection of the tube, alternative methods have been explored to monitor the tubes' behavior during testing without making modifications to the autoclave. Optical fiber glued to the outer surface of the tube was found to be an efficient method of measuring and monitoring strain fields on the tube. Before testing, one continuous optical fiber was glued circumferentially on to the outer surface of the tube with intervals of 150 mm along the longitudinal axis, thus measuring tangential strain fields around three circumferences on the tube. By matching FEA strain results with the optical fiber strain measurements a method was found that gave good correlation between FEA and the optical fiber strain measurements. The method was based on using Riks analysis with the tube modelled as slightly elliptic. The FEA predicted buckling at 4.33 bar, however; the tube got non visible failure causing leakage, likely by matrix cracking and delamination, just above 3.5 bar, reducing the stiffness and causing buckling earlier than predicted. After buckling, the optical fibers showed a lot of noise.

Introduction

Composite tubes see many different applications today due to high strength to weight ratio. There is an increasing interest in replacing steel tubes that operate in high pressure and high temperature environments with composite tubes [1]. Such applications can include drilling risers and drill strings for the oil industry [2]. Replacing steel risers and steel drill strings with composite tubes will greatly cut the weight of the equipment, and will have the benefit of requiring less buoyancy elements built into the structures. Although composite tubes have been used a lot as pressure pipes, little use has been seen when the greater pressure is from external pressure, as is often a design case at deep waters. In order for composite tubes to be qualified for such environments they need to be thoroughly tested to qualify not only the material, but also the analysis tools, design methodology and condition monitoring. Of relevant earlier studies, D. Choquose et. Al [3] concluded that predicting the behavior and buckling pressures of cylindrical deep sea containers is difficult. The work in this paper seeks to get a step closer to understanding the behavior of composite tubes when subjected to external pressure. To investigate the behavior, FEA in combination with condition monitoring during testing, by the use of optical fibers, was carried out.

Materials and methods

Tube design, material and winding layup

To manufacture the composite tube, filament winding with glass fiber reinforced polymer was used. The fiber used for the winding was HiPer-Tex W2020 from 3B [4] and the epoxy was EPIKOTE Resin MGS RIMR 135 with curing agent EPIKURE Curing agent RIMH 137. The epoxy and curing agent was mixed and cured according to the corresponding datasheet [5]. The inner diameter of the tube was 100 mm and the length of the tube was 600 mm, wound with a layup of $[89^\circ/\pm 12.7^\circ/\pm 45^\circ]$ with the hoop (89°) layer as the inner layer. The thickness of the tube was measured with a micrometer to be 1.675 mm and the thickness of the individual layers was found through studying the cross section in a microscope, the layer thicknesses can be found in Table 3.

A burn off test was carried out to find the volume fraction of the tube to verify and adjust the material properties, which assumed a volume fraction of 0.62. The volume fraction was found to be 0.60 and the material data in the fiber direction was scaled accordingly, as can be seen in Table 2. Scaling was carried out linearly with the material data for the matrix material [5] as reference.

Fiber instrumentation and equipment

Much work has been done regarding embedding optical fiber into composite structures. Most relevant for this study is D. Choqueuse et. al. [1]. D. Choqueuse et. al. embedded optical fiber bragg gratings into a CFRP layer filament wound onto a steel tube before exerting the tube to external hydrostatic pressure in an autoclave. The study concluded that the fibers performed well up to 200 bar, whereafter the fiber likely sustained damage at the micro level.

While the optical fiber bragg gratings used by D. Choqueuse et. al. measure strain at given spots on the fiber, like traditional strain gauges, the optical fiber used in this study is capable of giving continuous strain readings (strain fields) along the whole length of the fiber. The end result is that very accurate strain data can be measured that is easily comparable with strain fields in FEA, provided that the optical fiber's functionality can be verified for the structure and condition it is applied to. To verify and explore the fiber's functionality when glued to a submerged filament wound tube and exerted to direct water pressure, placing the fibers on the outer surface of the tube was chosen. An additional benefit of placing the fibers on the outer surface was that it made for a good reference plane for the FEA. Since this strain measurement method is new, confidence needs to be built in it. Besides measuring strain during buckling, building confidence in the method was therefore also part of the goal of the work in this paper.

The equipment used to interpret the reflections from the optical fiber in this study is called Optical Backscatter Reflectometry OBR and is made and sold by Luna Technologies. The fiber itself is a standard telecom fiber.

Regarding verifying the functionality and performance of the OBR in combination with optical fiber applied to composites, M. Haaheim investigated this in his publically available master thesis, see [6]. Haaheim embedded optical fiber into hand layup CRFP structures to thoroughly test the performance and strain measuring accuracy compared with FEA and other more traditional strain measurement methods. The conclusion of Haaheim was that the optical fiber corresponded well with both FEA and other methods, as also found and verified in this paper.

The Optical Backscatter Reflectometry OBR works by interpreting the Rayleigh backscatter reflections from optical fiber. In short, when an optical fiber is produced the fiber gets it's own "fingerprint" of roughnesses that reflects light in a distinct way. When the fiber is stretched or compressed, the distance between the roughnesses change slightly, yielding a different light fingerprint. The Optical Backscatter Reflectometry OBR compares the reflected light of the fingerprint before the fiber is put under strain with the reflection from when the fiber is strained. Subsequently it calculates the amount and location of the strain along the fiber [7]. In the case of this study, the "zero point" fingerprint was read from the fiber after the optical fiber had been glued to the tube, before submerging it. Reading the "zero point" fingerprint at this point led to that any small strains introduced when gluing the fiber to the tube was cancelled out. Even though the strain output is a continuous curve it is a result of many small virtual strain gauges. In the OBR's software, the distance between the strain gauges and the length of the strain gauges can be set. By increasing the distance between the gauges, less data points are attained. Increasing the length of the gauges gives more accurate measurements provided that the strain field is

relatively even. Setting a long gauge length will give less scatter of the results, but might overlook local variations in strain, the gauges can also overlap each other. Both the gauge length and the gauge distance is set during post processing of the results and they are chosen based on what gives the best results with the least scatter and noise [6].

A single fiber with a diameter of 165 micron was glued on the tube with cyanide optic fiber glue as shown in Figure 1. A close up picture of the fiber as glued onto the tube can be seen in Figure 2. To smoothen the surface of the tube before applying the optical fiber it was sanded with 400 grit sand paper. The tube had the fiber applied circumferentially at three locations with 150 mm spacing as shown in Figure 1, thus only measuring tangential strain. Between the circumferences the fiber was left free, unglued, so as not to cause any disturbance. An isolated signal wire was joined to the optical measurement fiber with a fiber heat-shrink joint after the last turn, as can be seen in Figure 2. The joint was submerged during testing. The signal wire exited the autoclave through a water tight T-fitting on the pressure supply line, shown in Figure 3. During post processing of the data from the fiber in the OBR software the gauge length was set to 5 mm and the spacing was set to 1 mm, giving 4 mm overlap of the virtual strain gauges.

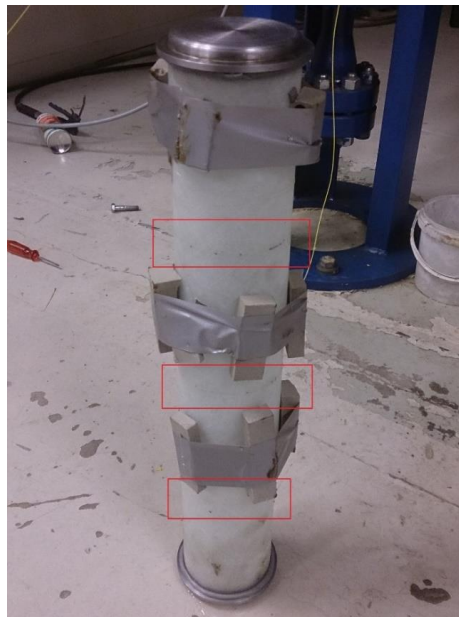


Figure 1 Tube with endcaps and fiber protection (Styrofoam) glued and taped lightly onto the tube. The red squares outlines the fiber at 150 mm (bottom), 300 mm (middle) and 450 mm (top).



Figure 2 Close up of the optical fiber glued onto the tube (left) and the fiber heat-shrink tube (right) joining the signal wire and the optical fiber

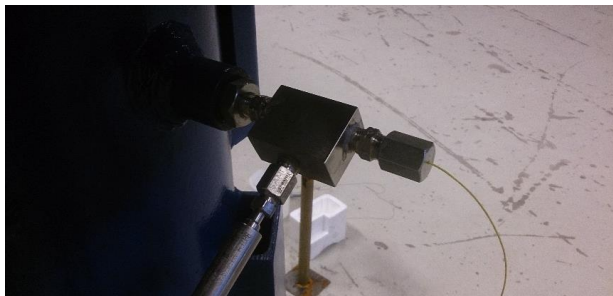


Figure 3 T-fitting on the pressure supply line on the autoclave with the fiber escaping through an endcap made watertight with silicon.

FE model

To model and analyze the tube, Abaqus/CAE 6.12-1 was used. The tube was modeled as a shell profile of 600 mm length with 100 mm in diameter and it was meshed with SR4 elements set to 2.0 mm in size, as shown in Figure 4. Abaqus' Composite Layup with Conventional Shell was used together with the scaled (only E_1) material properties in Table 2. The (unscaled) material data shown in Table 2 were found by G. Perillo in his PhD thesis [8] by matching material data in a FEA with a filament wound tube subjected to a radial point load, as shown in Figure 5. In order to model the tube's wound pattern as closely as possible, several balanced layers were used for each winding angle on the tube, apart from the hoop layer due to that it was wound in one go. A graphical representation of the layup can be seen in Figure 6.

A mesh sensitivity analysis was run based on linear buckling analysis and the results can be seen in Table 1. The results from the mesh sensitivity analysis show that the mesh size to a very little degree affected the predicted buckling pressure. The buckling mode was also the same for all mesh sizes (two lobes). To assess whether or not the end effect from the sealing end caps would be very pronounced at the tube's length of 600 mm, a length sensitivity analysis was also run based on linear buckling analysis. The end effect affected to some extent the buckling pressure, but not the buckling mode (two lobe versus three lobe at shorter lengths, Figure 8 shows the two lobe buckling mode).

Table 1 Mesh Sensitivity Analysis.

Mesh size (mm)	Buckling pressure (bar)
2.0	4.7598
8.0	4.8091
16.0	4.9379

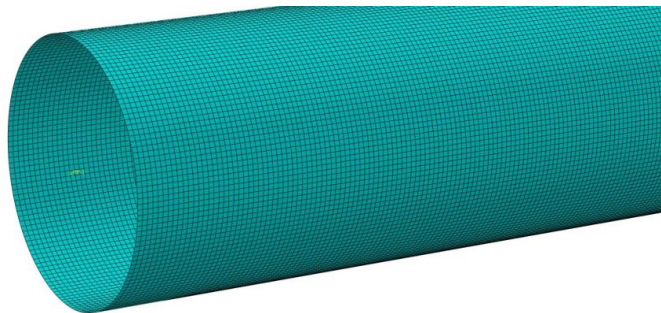


Figure 4 2.0 mm Mesh.

Table 2 Material Properties, E_1 is scaled with a volume fraction of 0.602 as opposed to 0.62, which the original data from G. Perillo [8] assumed. Material data has been found through matching FEA with a filament wound tube subjected to a radial point load, see Figure 5.

Parameter	Scaled value (unscaled value)	Unit
E_1	37.537 (38.6)	GPA
E_2	11.0	GPA
ν_{12}	0.3	-
G_{12}	3.07	GPA

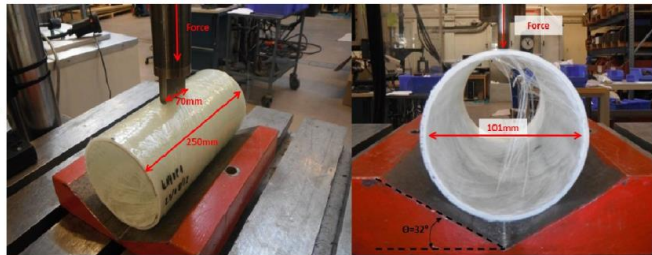
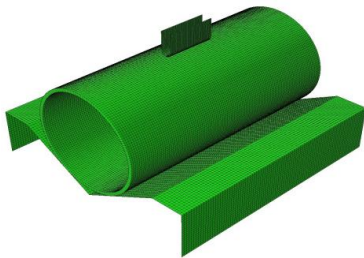


Figure 5 By carrying out experiments with a point load on short sections of filament wound tubes and matching the force/displacement curves with FEA by adjusting the material data, the material properties in Table 2 was found.

Table 3 Layout in Abaqus and measured thickness in the microscopy.

FEM ply number	Orientation (winding angle)	FEM ply thickness (mm)	Measured thickness (mm)
1	89°	0.262653	0.262653
2 - 9	±12.7°	0.088750	0.710002
10 - 17	±45°	0.087793	0.702345

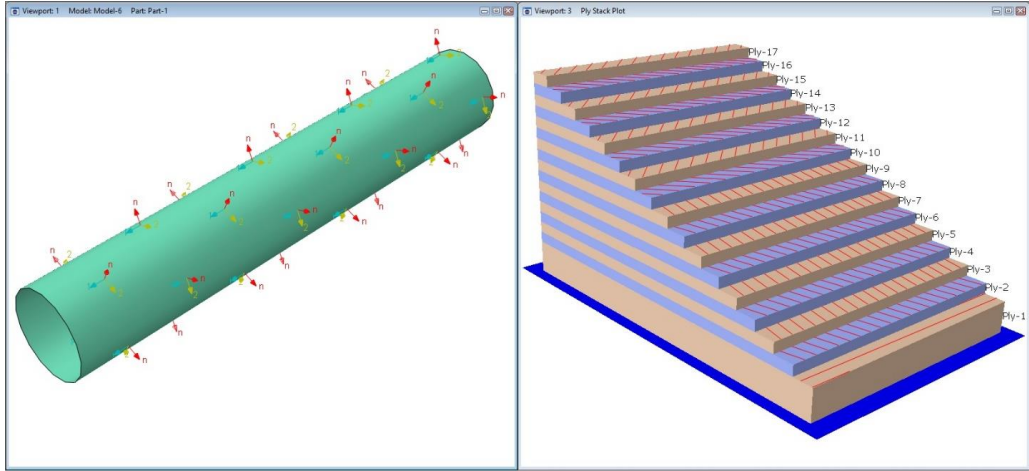


Figure 6 Layout in Abaqus showing the direction of the material coordinate system and orientation of each ply.

The tube's ends were both pinned (freely supported) to two reference points set one at each end of the tube along the central axis using a Rigid Body constraint. Besides the Rigid Body constraints, one side was constrained to absolute translation in all directions. The two reference points can be seen in Figure 7 as RP-1 and RP-2, and the absolute constraint can be seen around the edge at the RP-1 side of the tube. The tube had an external pressure of 10 bar (1 MPa) applied on the outer surface, as well as a point load of 8364.68 N applied in RP-2 to simulate the pressure on the end caps, both loads are visible in Figure 7. The force of 8364.68 N was calculated by multiplying the pressure with the projected area as shown in Equation 1.

$$F(t) = (\pi \cdot (r + t)^2 \cdot 10 \text{ bar}) = (\pi \cdot (50 \text{ mm} + 1.6 \text{ mm})^2 \cdot 10 \text{ bar}) = 8364.68 \text{ N} \quad (1)$$

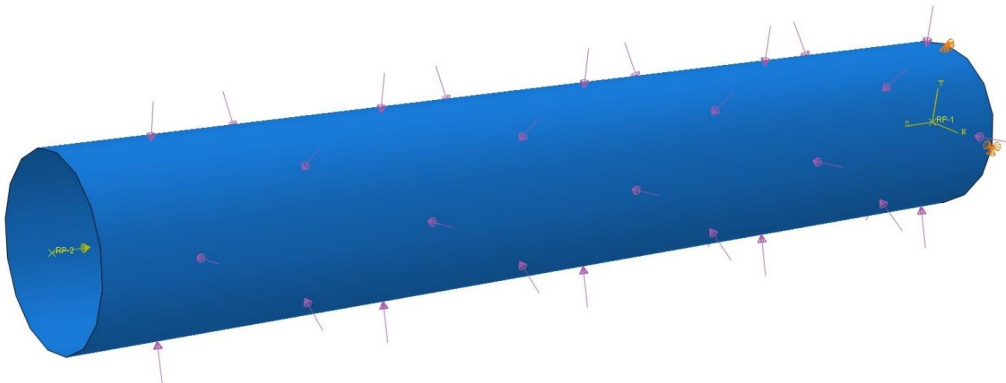


Figure 7 The tube as constrained with all loads applied. The yellow arrow is the point load and the purple arrows indicate the pressure load. The orange cones at the right end indicates the absolute translation constraint while the constraints hindering the ends of the tube rotating is not visible, but acts from RP-1 and RP-2 as a Rigid Body constraint with the ends of the tube.

Results

The pressure in the autoclave was increased in intervals of 0.5 bar and an optic fiber strain reading was carried out after each increase. Pressure stopped increasing above 3.5 bar even though the pump was still running, indicating a leakage. The leakage, once initiated, only acted at pressures above 3.0 bar, making any pressure above 3.0 bar unstable and unsustainable. After the test there was however no visible failure on the tube indicating leakage. The temperature of the water was constant throughout the test at about 7 °C, so the measured strain was not in any way affected by temperature change, see [6] for effects of temperature on optic fiber. Figure 9, Figure 10 and Figure 11 shows the optic fiber strain readings and FEA results up to 3.5 bar, but does not include any measurements after the pressure dependent leakage occurred. One optic fiber strain reading was carried out after the leakage occurred, but at 2.3 bar and not at the leakage threshold value of 3.0 bar. The 2.3 bar reading can be seen in Figure 12.

As can be seen in the strain graphs, the match between the FEA and the optical fiber for corresponding pressure readings is very good on a general basis, despite that the optical fiber readings have some noise. A good example of a good match is the 3.5 bar reading from the middle (300 mm) of the tube indicated with brown color in Figure 9 having a good match with the brown dashed FEA strain curve. To achieve the good match between the FEA and the optic fiber readings, several methods were explored. The method that proved to give the best match was using Riks analysis with buckling initiated by a geometrical imperfection on the tube. The imperfection needed to induce buckling was introduced by modelling the tube slightly elliptic in the extrusion sketch. By matching the FEA tangential strain results with that from the optical fibers by adjusting the degree of ovality, an ovality of 0.46% of the nominal diameter (100 mm) was found to give the best match. 0.46% ovality means that 0.46 mm (0.46% x 100 mm) was subtracted and added to the minor and major diameter of the ellipse in the extrusion sketch respectively.

The Riks analysis gave a buckling pressure of 4.33 bar, a lower value than for the linear buckling analysis in Table 1, which was expected due to the elliptic shape of the tube in the Riks analysis. Due to the leakage, the pressure in the tube never reached the FEA predicted buckling pressure even though, as mentioned, it followed the predicted strain values.

For visual reference of the deformation, Figure 8 shows the radial displacement of the tube at 3.41 bar in the Riks analysis with a max absolute radial displacement of -0.79 mm. Also visible is the starting point for the path in the strain graph at 300 mm, the starting point for the 450 and 150 mm readings are along the same longitudinal axis. As can be seen in the deformation plot is the tube's two lobe buckling mode. The two lobe mode is also clearly present in the strain graphs with the the "valleys" in the graphs being the creases and the two distinct peaks being the lobes.

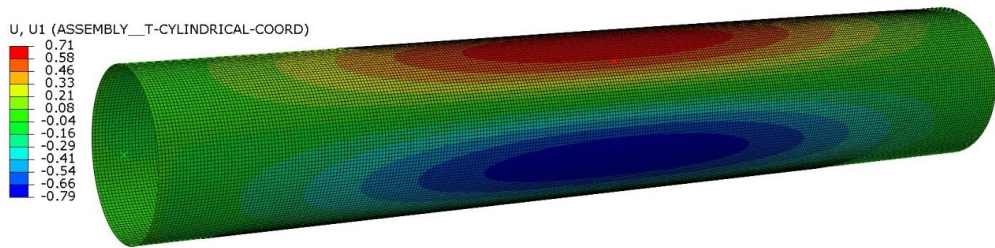


Figure 8 Radial displacement plot at 3.41 bar with a visualization deformation scale factor of 1 and units in mm. The red dot is the starting point for the tangential strain graph path for the 300 mm reading, the starting point for the 150 and 450 mm paths are along the same longitudinal axis. The two lobe buckling mode is clearly present, with the crease(s) in blue and lobe(s) in red color.

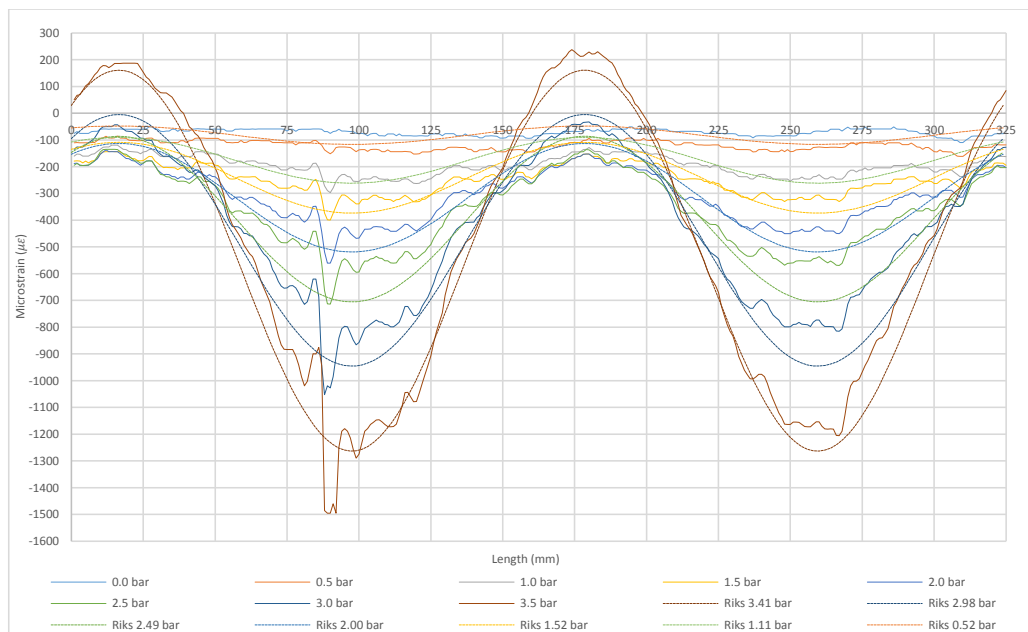


Figure 9 Optic fiber strain readings and FEA results comparison graph for the middle circumference (at 300 mm) of the tube. The dashed curves are from FEA and the continuous lines are from the optic fibers. The curves with equal color are at the same pressure.

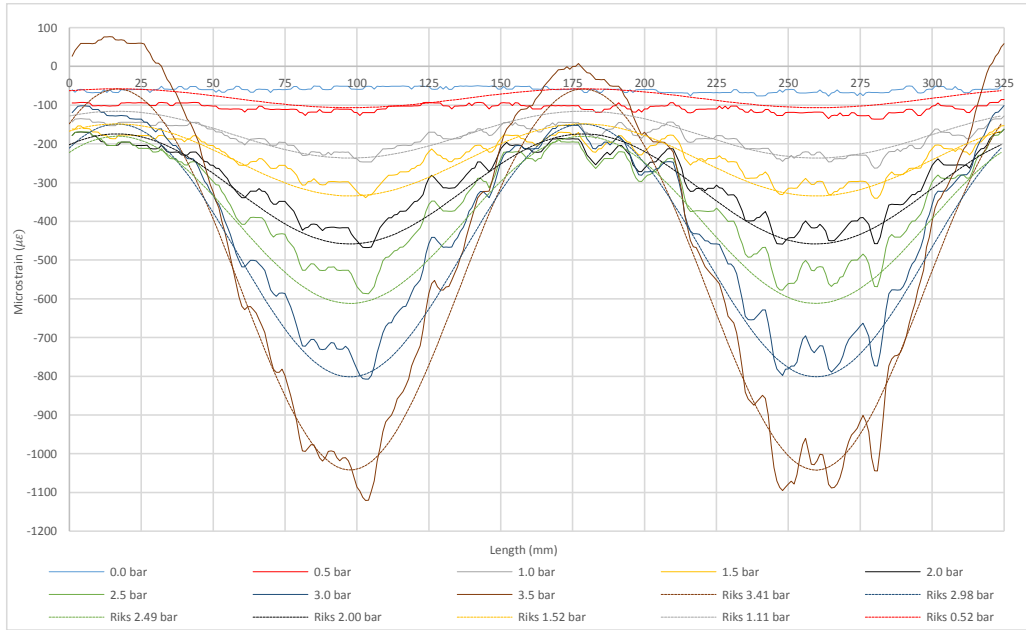


Figure 10 Optic fiber strain readings and FEA results comparison for the bottommost optic fiber circumference (at 150 mm) of the tube. The dashed curves are from FEA and the continuous lines are from the optic fibers. The curves with equal color are at the same pressure.

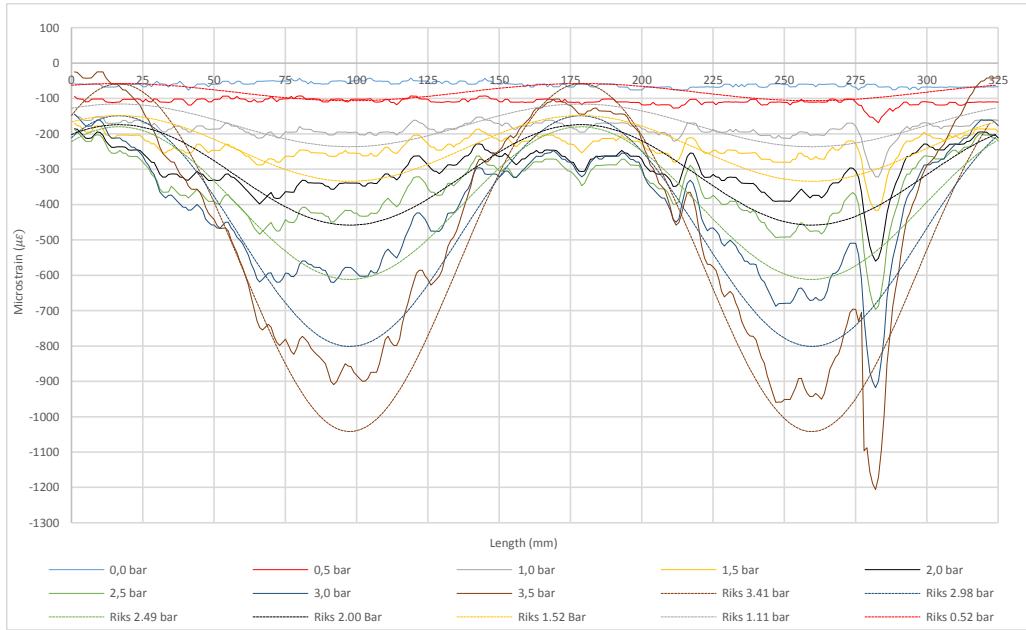


Figure 11 Optic fiber strain readings and FEA results comparison for the topmost optic fiber circumference (at 450 mm) of the tube. The striped curves are from FEA and the continuous lines are from the optic fibers. The curves with equal color are at the same pressure.

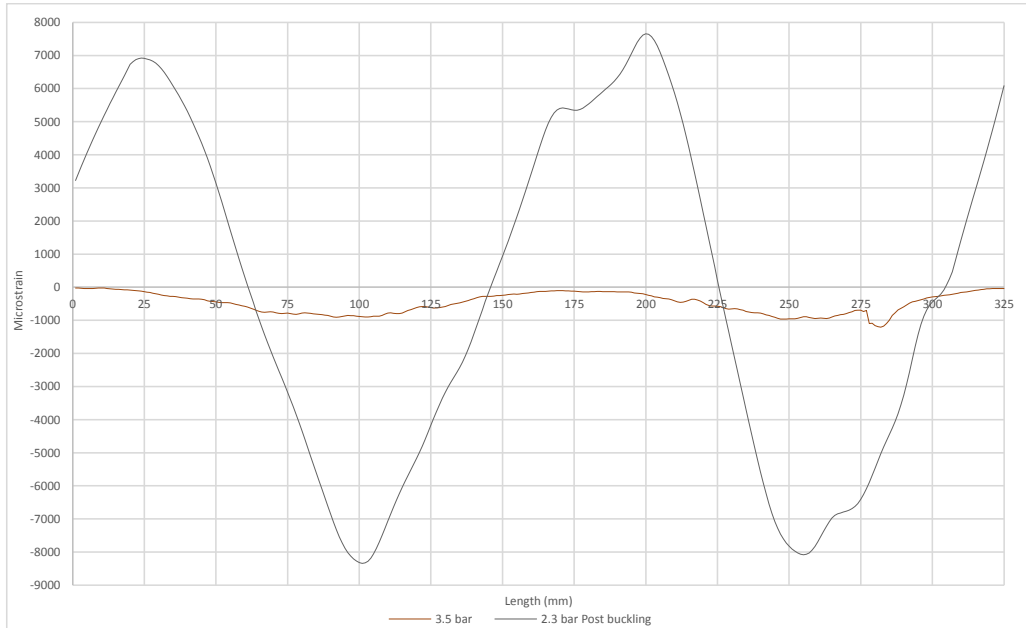


Figure 12 Optic fiber strain reading at 2.3 bar from the topmost optic fiber circumference of the tube (450 mm) after occurrence of the pressure dependent leakage, the reading has been smoothed in Matlab due to severe noise.

Discussion

The FEA results and the optic fiber readings matched very well, as seen in Figure 9, Figure 10 and Figure 11. Not captured by the FEA was the slight difference in pressure between bottom and top of the autoclave, which is the likely reason for why the 150 and 450 mm readings have a poorer match than for the 300 mm reading.

The leakage initiated just above 3.5 bar was likely caused by matrix cracking and delamination mechanisms resulting in that water could penetrate all the layers. As a consequence of the matrix cracking and delamination, the stiffness of the tube decreased so that it buckled long before the predicted pressure of 4.33 bar from the Riks analysis. A good indication of that the tube actually buckled as it lost stiffness and began leaking at 3.5 bar is the very high strains in the post leakage 2.3 bar reading in Figure 12. After the pressure dependent leakage was initiated, a lot of noise was registered in the optical fiber readings. The noise was likely caused by the high strains occurring after 3.5 bar as the tube buckled. The high strains combined with matrix cracking on the surface might have led to small radiuses being introduced on the fiber at micro level [6] or in other ways damaged the fiber so that noise resulted.

An aspect of the results, which is important to take into account for application to longer tubes, is the buckling's dependency of the tube's length. Since the tube failed before the predicted buckling pressure in both the Riks analysis and the linear buckling analysis, it is hard to tell whether the length sensitivity analysis that was carried out is correct. More research has to be done so that test results for short tubes can be extrapolated to also be valid for longer tubes.

Conclusion

There was found that optical fiber glued to the outer surface of a filament wound tube subjected to external pressure is a good way of monitoring the deformations and strains on the tube. Monitoring with optical fiber has the advantage over normal strain gauges and optical fiber bragg gratings that strain fields are monitored instead of strain at single points. Therefore, using optical fiber on submerged structures can give a very complete picture of the deformations on pair with visual inspection during testing. In addition to give good results for post processing and analyzing of the behavior, live monitoring of the strain from the tube is also possible. The optical fiber readings from the test tube gave strain measurements that matched very well with strain results from FEA Riks analysis of a corresponding tube in Abaqus/CAE 6.12-1. The good match was achieved through having the tube in the FEA modeled with a slight elliptic shape with 0.46% of the nominal diameter of the tube added and subtracted to the major and minor diameter of the ellipse respectively. During testing, a non-visible failure of the tube occurred at just above 3.5 bar, resulting in leakage and a stiffness reduction of the laminate, causing buckling at a lower pressure than what was predicted by the FEA, at 4.33 bar. The non-visible failure caused a pressure dependent leakage that only acted above 3.0 bar, yielding any pressure above 3.0 bar unsustainable. After the failure occurred the preceding optical fiber strain readings contained a lot of noise, likely due to high strains during buckling combined with matrix cracking on the outer surface, where the fiber was glued on.

Bibliography

- [1] B. B. A. D. B. D. L. Q. D. Choqueuse, "Hydrostatic compression behaviour of steel-composite hybrid tubes".
- [2] Composite filament winding / edited by S.T. Peters, Materials Park, Ohio : ASM International, 2011.
- [3] P. D. D. Choquese, "Durability of Composite Materials for Underwater Applications," *Durability of Composites in a Marine Environment, Solid Mechanics and Its Applications 208*, 2014.
- [4] 3B, "HiPer-Tex W2020 Rovings Datasheet," 3B-fibreglass, 2009.
- [5] Momentive, "Technical Datasheet EPIKOTE Resin MGS RIMIR 135 and EPIKURE Curing Agent MGS RIMH 134-RIMH 137," Momentive, 2006.
- [6] M. L. Håheim, Health monitoring of Composites using Optical Fibers, Trondheim: NTNU Norwegian University of Science and Technology, 2012.
- [7] D. Samiec, "Distributed fibre-optic temperature and strain measurement with extremely high spatial resolution," *Photonik international*, 2012.
- [8] G. Perillo, Numerical and Experimental Investigation of Impact Behaviour of GFRP Composites, Trondheim: NTNU, 2014.
- [9] Mikrosam, "MAW 20 LS 4/1 Filament Winding machine User Manual," 2011.

- [10] Tygvac, "Release fabrics and peel plies product catalogue".
- [11] Dassault Systèmes, Abaqus Analysis User Manual, 6.2.4 Unstable collapse and postbuckling analysis, 2012.
- [12] R. Z. F. C. P. O. Y.-H. G. M. Mulle, "Thermal expansion of carbon–epoxy laminates measured with embedded FBGS - Comparison with other experimental techniques and numerical simulation," *Composites: Part A*, 2007.
- [13] "Produkter (Products), Melbye AS," Melbye AS, [Online]. Available: <http://www.melbye.com/no/no/produkter/fibernett-1/fiberkabel-1/>. [Accessed March 2014].
- [14] Momentive, "Technical Datasheet EPIKOTE Resin MGS RIMIR 135 and EPIKURE Curing Agent MGS RIMH 134-RIMH 137," 2006.

Appendix **B**

Graphs

B.1 Strain measurements from 600 mm long tube test nr.

1

Optic fiber at 150 mm

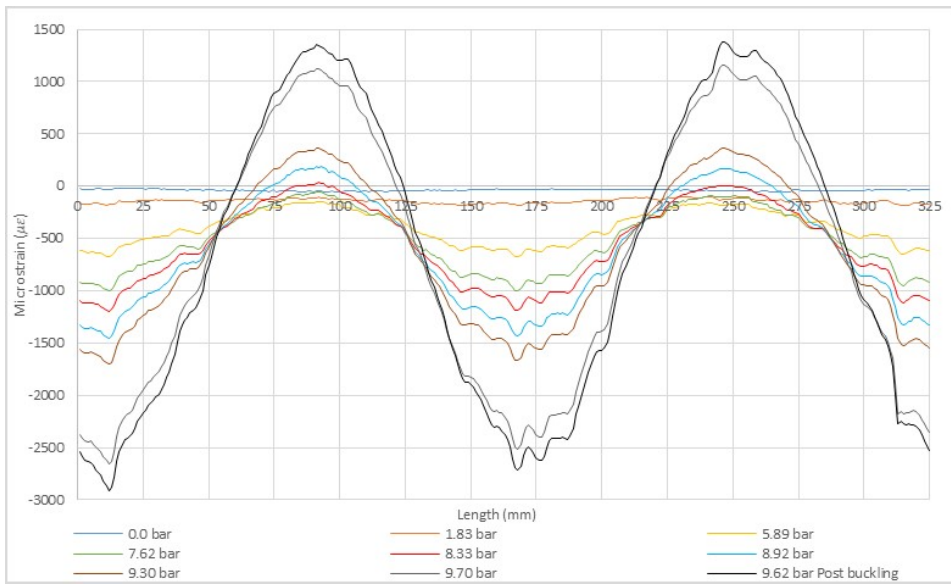


Figure B.1: Strain measurements from optic fiber at 150 mm on the 600 mm long tube from test nr. 1.

Optic fiber at 300 mm

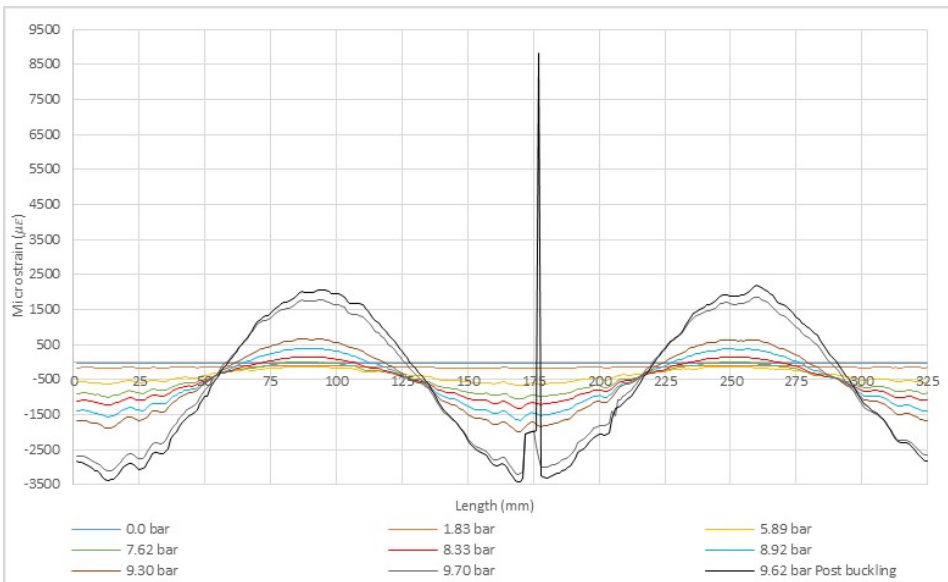


Figure B.2: Strain measurements from optic fiber at 300 mm on the 600 mm long tube from test nr. 1.

Optic fiber at 450 mm

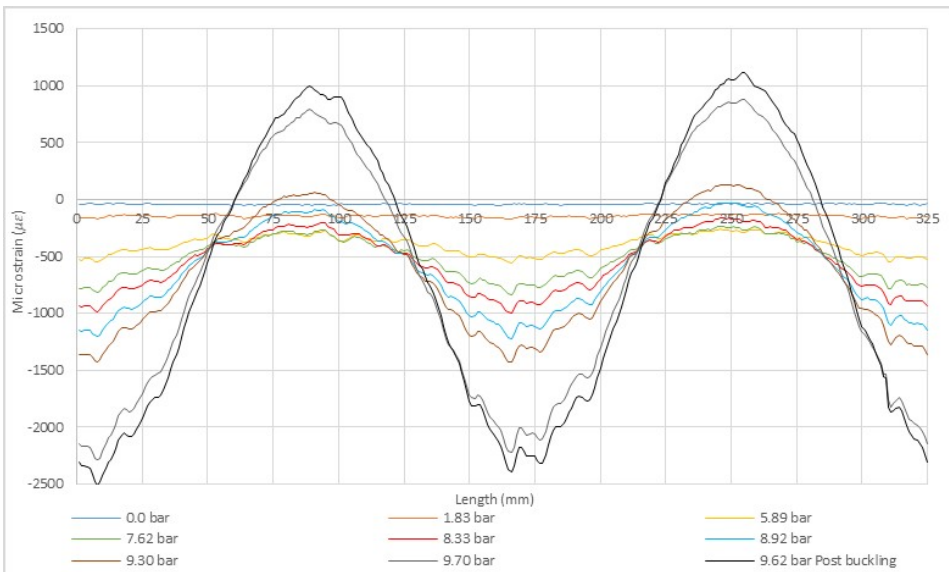


Figure B.3: Strain measurements from optic fiber at 450 mm on the 600 mm long tube from test nr. 1.

B.2 Strain measurements from 600 mm long tube test nr. 2

Optic fiber at 150 mm

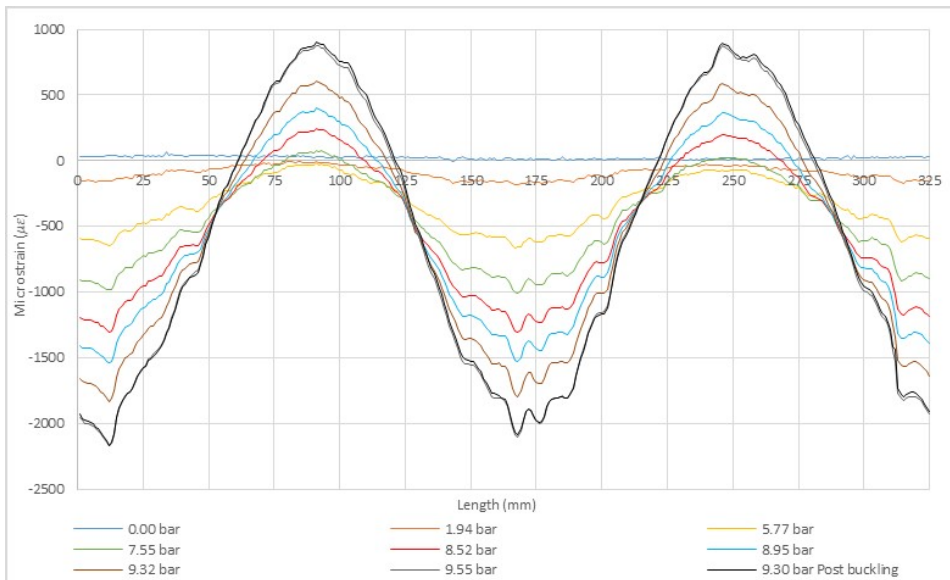


Figure B.4: Strain measurements from optic fiber at 150 mm on the 600 mm long tube from test nr. 2.

Optic fiber at 300 mm

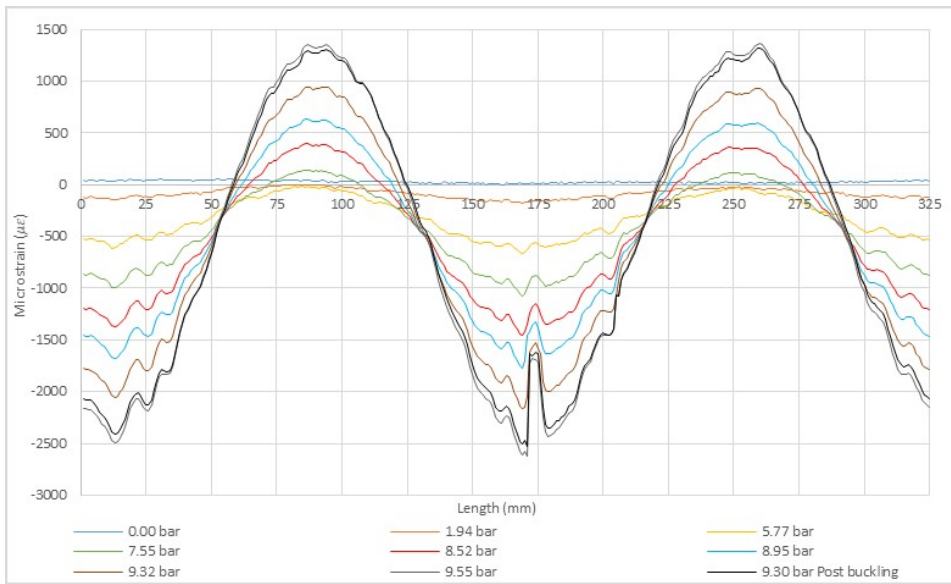


Figure B.5: Strain measurements from optic fiber at 300 mm on the 600 mm long tube from test nr. 2.

Optic fiber at 450 mm

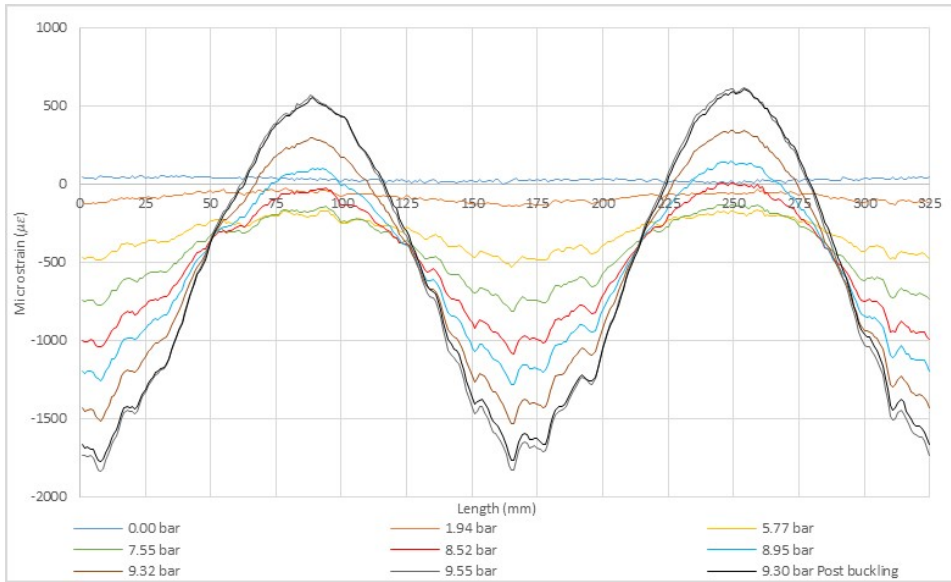


Figure B.6: Strain measurements from optic fiber at 450 mm on the 600 mm long tube from test nr. 2.

B.3 Strain measurements from 400 mm long tube test nr.

1

Optic fiber at 200 mm

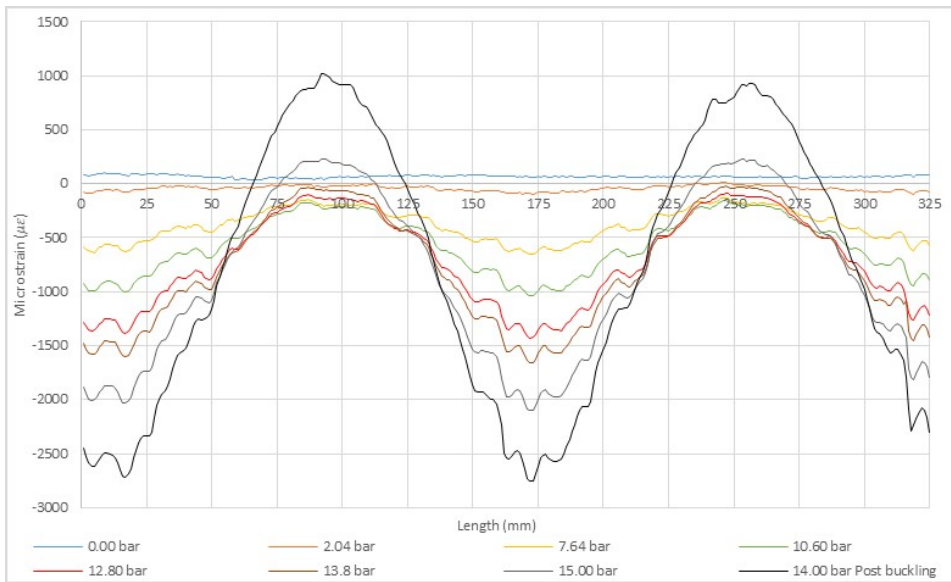


Figure B.7: Strain measurements from optic fiber at 200 mm on the 400 mm long tube from test nr. 1.

B.4 Strain measurements from 400 mm long tube test nr. 2

Optic fiber at 200 mm

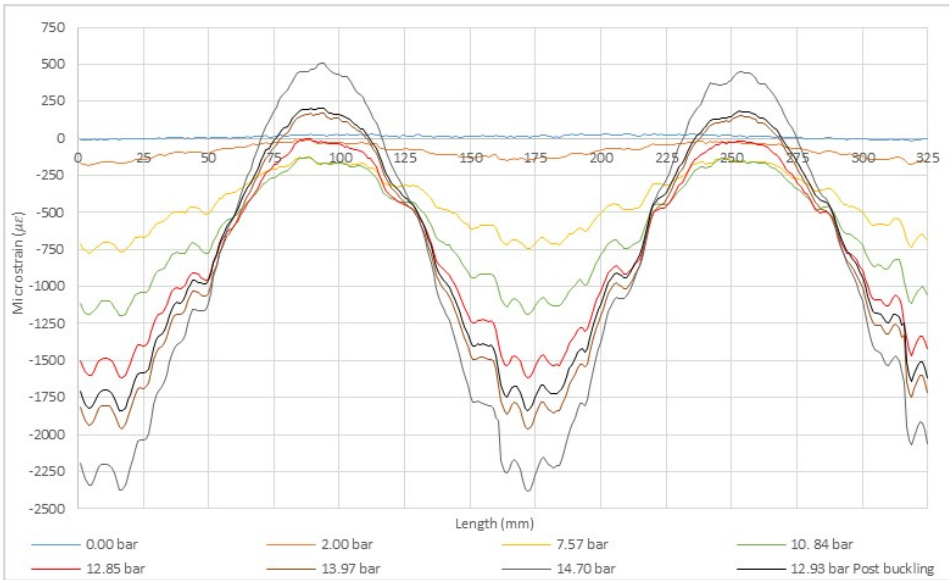


Figure B.8: Strain measurements from optic fiber at 200 mm on the 400 mm long tube from test nr. 2.

B.5 Strain measurements from 300 mm long tube

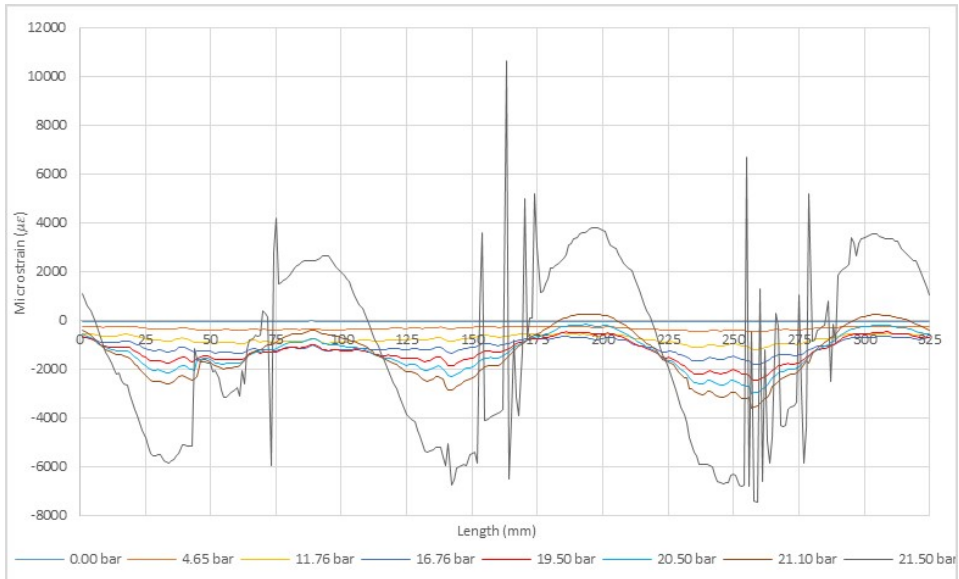


Figure B.9: Strain measurements from optic fiber at 150 mm on the 300 mm long tube.

B.6 Pressure readings from the 600 mm long tube

Pressure readings from test nr. 1

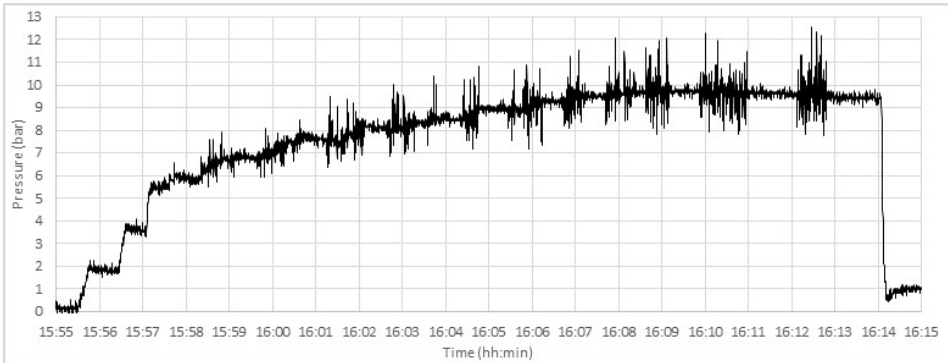


Figure B.10: Pressure reading from test nr. 1 of the 600 mm long tube.

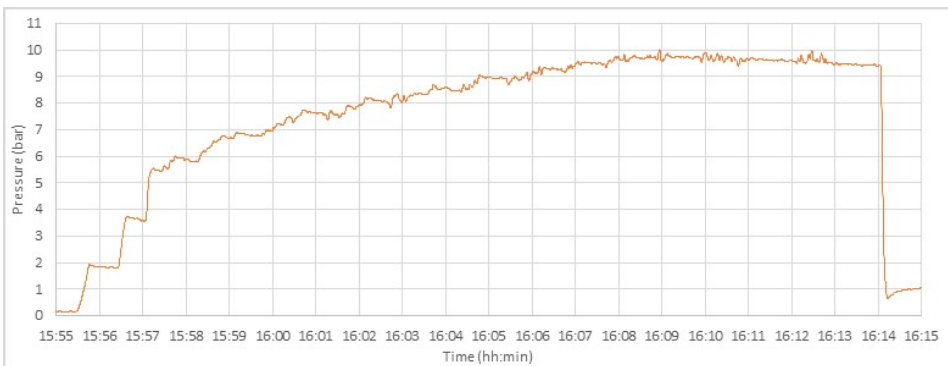


Figure B.11: Pressure reading from test nr. 1 of the 600 mm long tube, smoothed using Matlab.

Pressure readings from test nr. 2

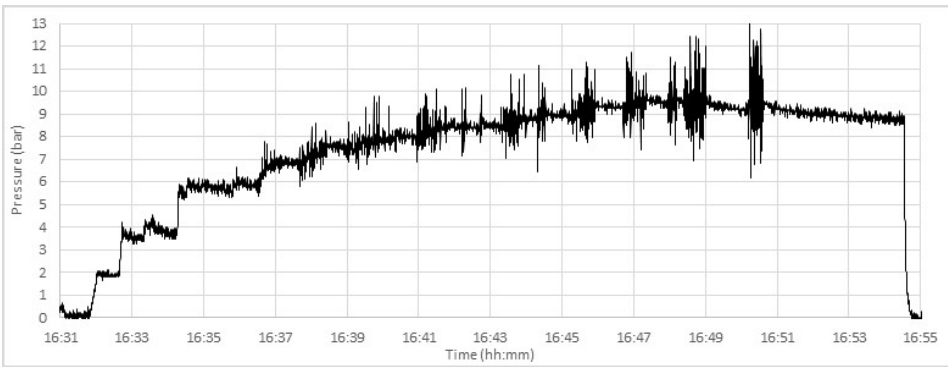


Figure B.12: Pressure reading from test nr. 2 of the 600 mm long tube.

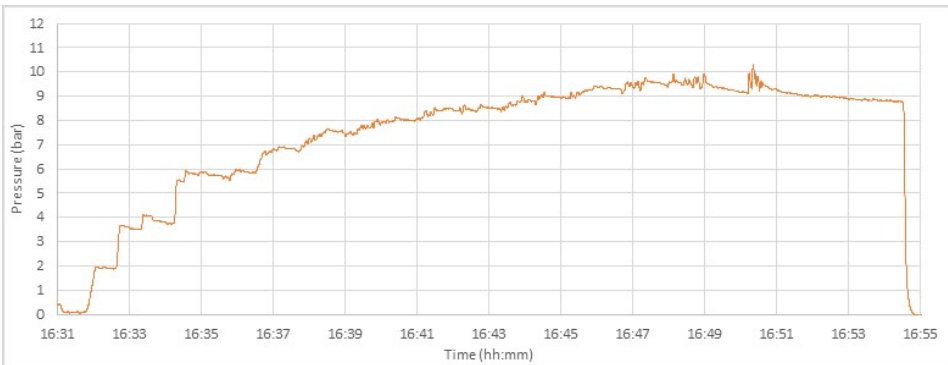


Figure B.13: Pressure reading from test nr. 2 of the 600 mm long tube, smoothed using Matlab.

B.7 Pressure readings from the 400 mm long tube

Pressure readings from test nr. 1



Figure B.14: Pressure reading from test nr. 1 of the 400 mm long tube.



Figure B.15: Pressure reading from test nr. 1 of the 400 mm long tube, smoothed using Matlab.

Pressure readings from test nr. 2



Figure B.16: Pressure reading from test nr. 2 of the 400 mm long tube.



Figure B.17: Pressure reading from test nr. 2 of the 400 mm long tube, smoothed using Matlab.

B.8 Pressure readings from the 300 mm long tube

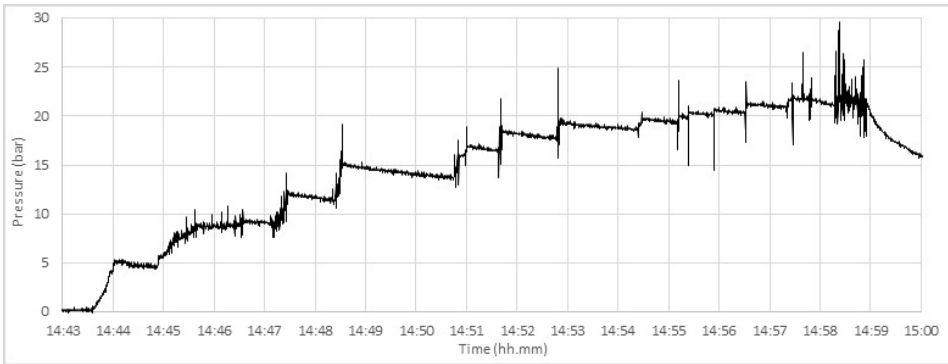


Figure B.18: Pressure reading from the 300 mm long tube.

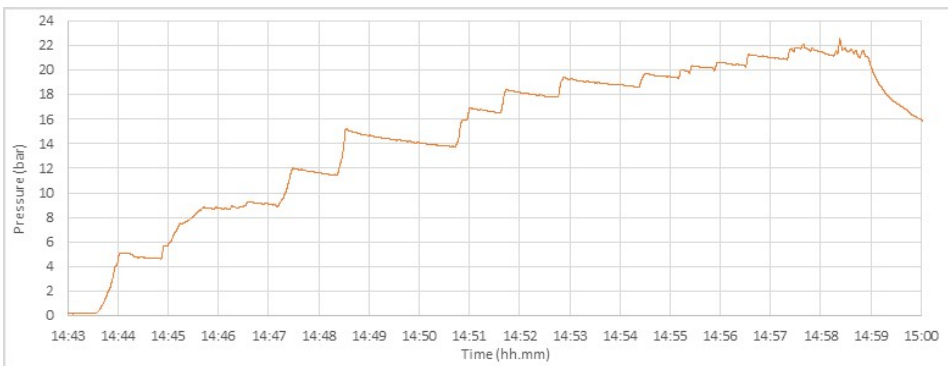


Figure B.19: Pressure reading from the 300 mm long tube, smoothed using Matlab.

B.9 LPF curve

Pressure vs Arc length

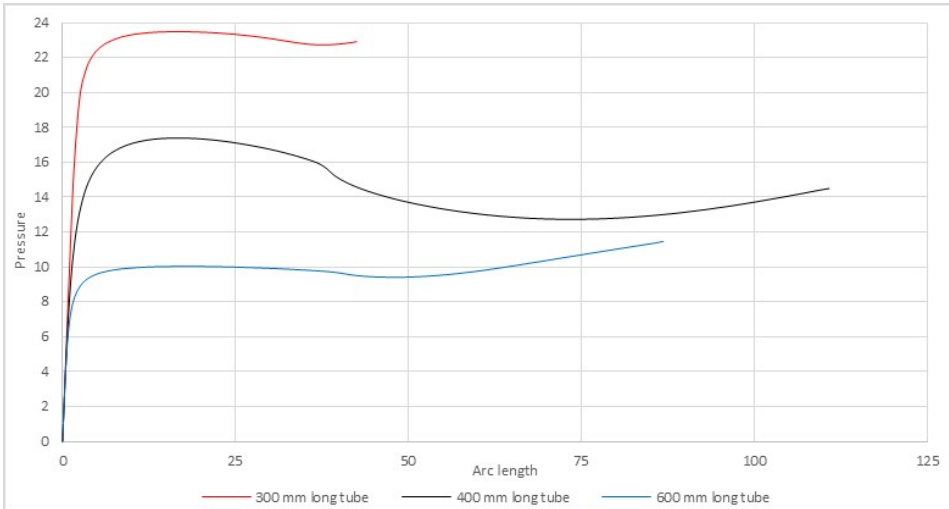


Figure B.20: The Load proportionality factor scaled so as to reveal pressure set against the arc length of the tubes.

Appendix **C**

Tables

C.1 Layer thickness

Table C.1: Each layers fraction of the total thickness in the microscopy pictures.

Picture nr.	89° inner	12.7°	89° outer
1	0.0.306	0.319	0.375
2	0.300	0.369	0.330
3	0.0.301	0.314	0.384
4	0.274	0.347	0.367
5	0.301	0.317	0.382
6	0.300	0.323	0.377
7	0.310	0.325	0.365
8	0.327	0.310	0.364
9	0.297	0.292	0.369
10	0.297	0.341	0.362
Avareage	0.303	0.327	0.370
Standard deviation	0.013	0.022	0.015

C.2 Material properties

Table C.2: Material properties for HiPer-Tex W2020 + Momentive Epikote MGS 135 (Epikure MGS 137) at volume fraction of 0.620 from Perillo [21]. For explanation on how they were acquired, see the paper in Appendix A.

Parameter	Value	Unit
E_1	38.6	GPA
E_2	11.0	GPA
E_3	11.0	GPA
ν_{12}	0.3	-
ν_{13}	0.3	-
ν_{23}	0.5	-
G_{12}	3.07	GPA
X_T	855.0	MPA
X_C	414.0	MPA
Y_T	39.0	MPA
Y_C	112.0	MPA
S_{12}	42.0	MPA
S_{13}	42.0	MPA
S_{23}	42.0	MPA

C.3 Material background information

Table C.3: The table contains information for the composite used (EPIKOTE Resin MGS RIMR 135 with Curing agent EPIKURE Curing agent RIMH 137 and HiPer-tex W2020 fiber). The blank fields were not to be found.

Generic fiber type	R-glass [7].
Bundle type	
Fiber trade name	HiPer-tex [7].
Fiber manufacturer	3B [7].
Type of weave	
Type of sizing	
Weaver	
Fabric trade name	
Generic resin type	Epoxy
Trade name of resin	EPIKOTE Resin MGS RIMR [6].
Catalyst	

C.4 Clock times for optical fiber strain readings readings

Table C.4: Clock times in (mm:ss) for when the optic fiber strain readings were taken referring to the time axis in the pressure graphs in Appendix B.6.

Test nr. 1 Pressure	Optical fiber reading time (mm:ss)	Test nr. 2 Pressure	Optical fiber reading time (mm:ss)
0 bar	Outside pressure graph	0.00 bar	Outside pressure graph
1.83 bar	56:02	1.94 bar	32:19
5.89 bar	58:00	5.77 bar	35:13
7.62 bar	01:02	7.55 bar	38:47
8.33 bar	03:23	8.52 bar	42:59
8.92 bar	05:11	8.95 bar	44:53
9.30 bar	06:27	9.32 bar	46:18
9.70 bar	09:42	9.55 bar	47:43
9.62 bar Post buckling	11:36	9.30 bar Post buckling	49:33

Table C.5: Clock times in (mm:ss) for when the optic fiber strain readings were taken referring to the time axis in the pressure graphs in Appendix B.7.

Test nr. 1 Pressure	Optical fiber reading time (mm:ss)	Test nr. 2 Pressure	Optical fiber reading time (mm:ss)
0.00 bar	Outside pressure graph	0.00 bar	Outside pressure graph
2.04 bar	29:00	2.00 bar	00:19
7.64 bar	32:30	7.57 bar	06:29
10.80 bar	35:50	10.84 bar	11:31
12.80 bar	03:23	12.85 bar	13:47
13.80 bar	40:26	13.97 bar	15:32
15.00 bar	41:59	14.70 bar	16:24
14.00 bar Post buckling	42:52	12.93 bar Post buckling	17:55

Table C.6: Clock times in (mm:ss) for when the optic fiber strain readings were taken referring to the time axis in the pressure graphs in Appendix B.8.

Pressure	Optical fiber reading time (mm:ss)
0.00 bar	Outside pressure graph
4.65 bar	44:40
11.76 bar	49:37
16.76 bar	52:10
19.50 bar	52:28
20.50 bar	56:17
21.10 bar	56:53
21.50 bar	58:00

Appendix **D**

Pictures

D.1 Microscopy pictures

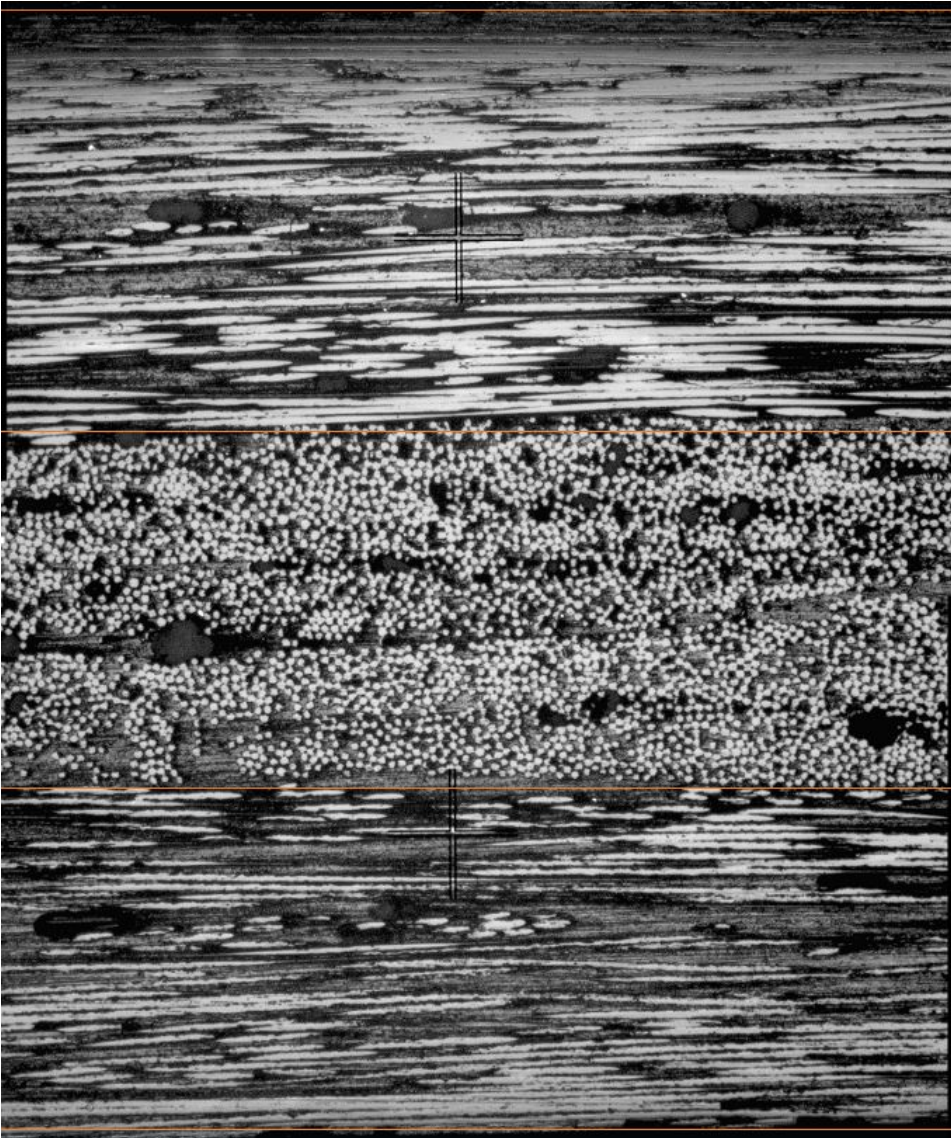


Figure D.1: Picture nr. 1.

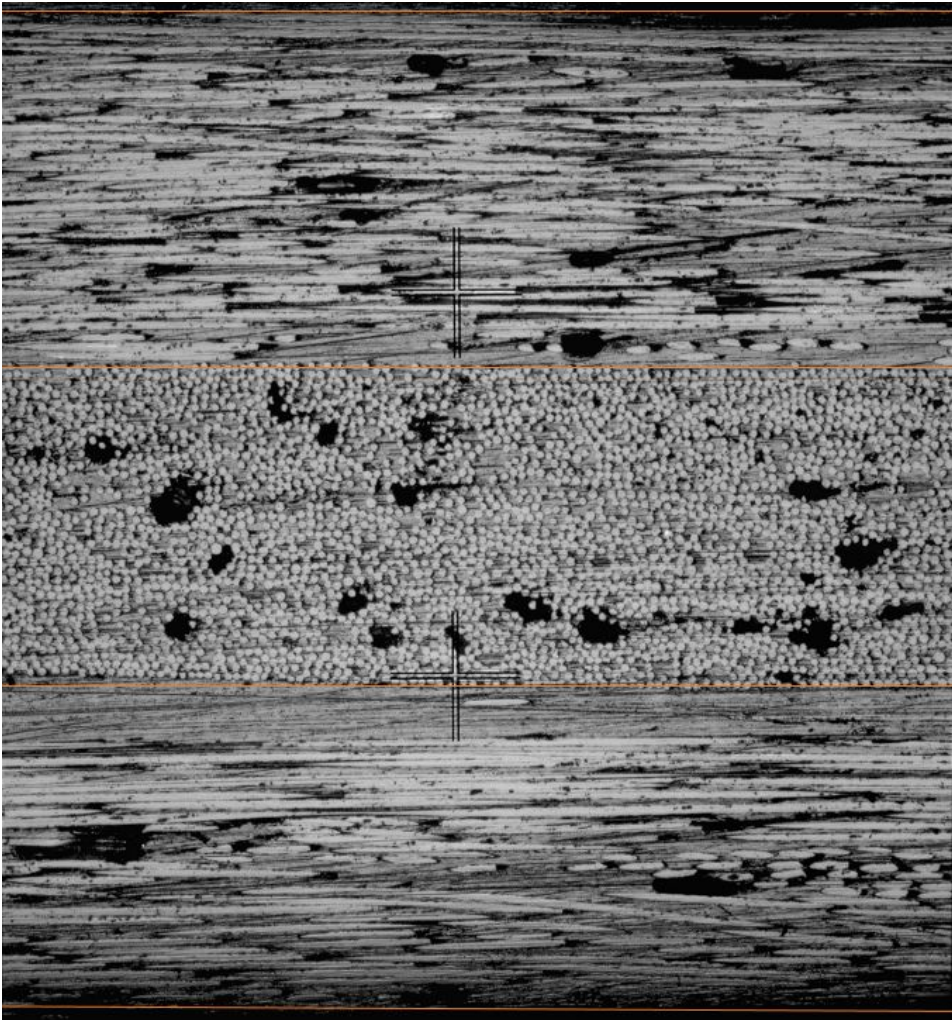


Figure D.2: Picture nr. 2.

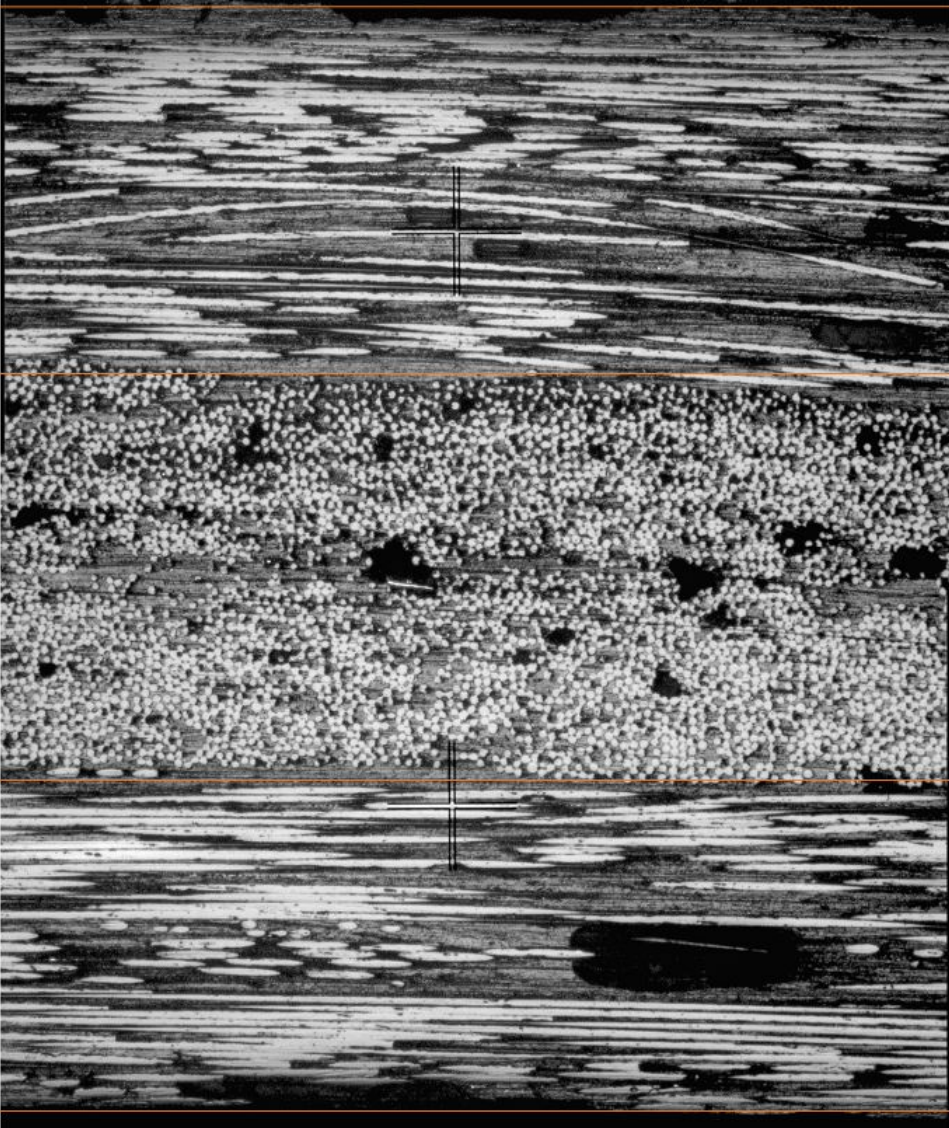


Figure D.3: Picture nr. 3.

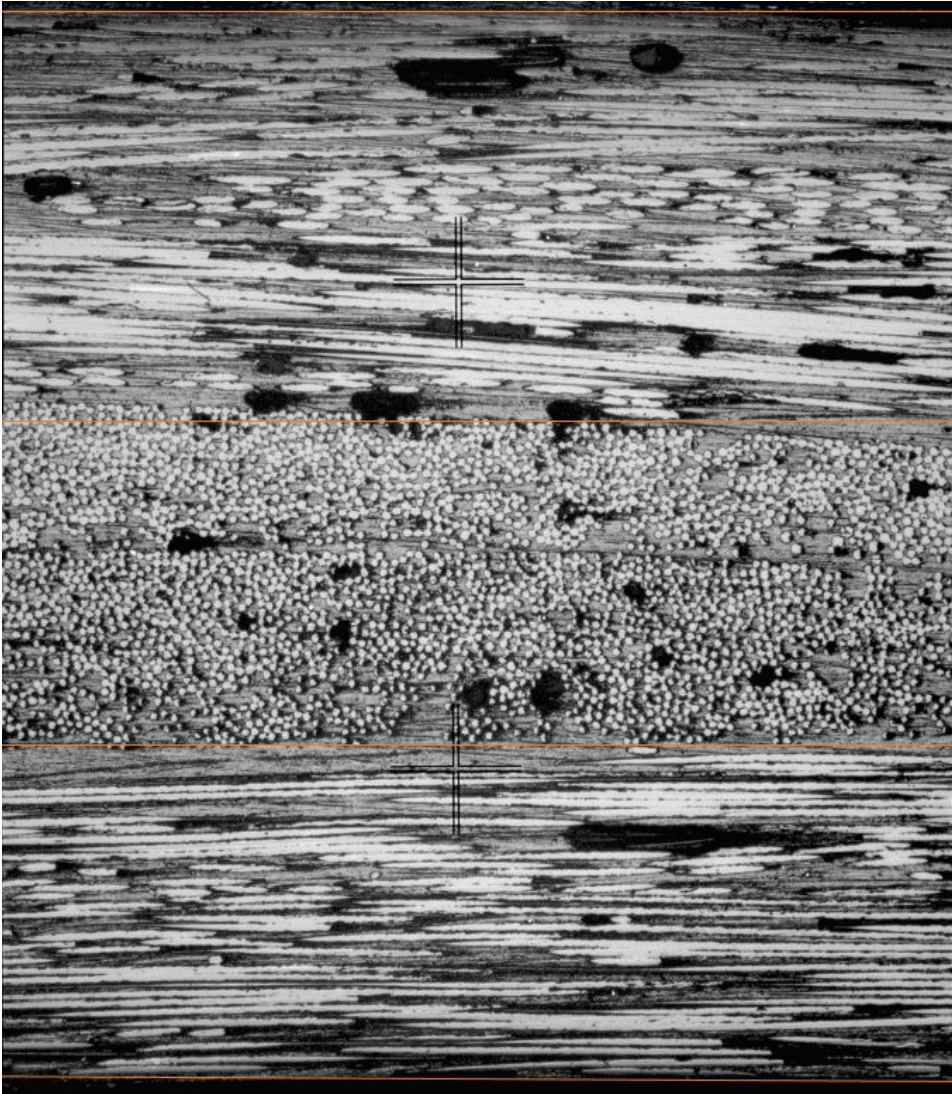


Figure D.4: Picture nr. 4.

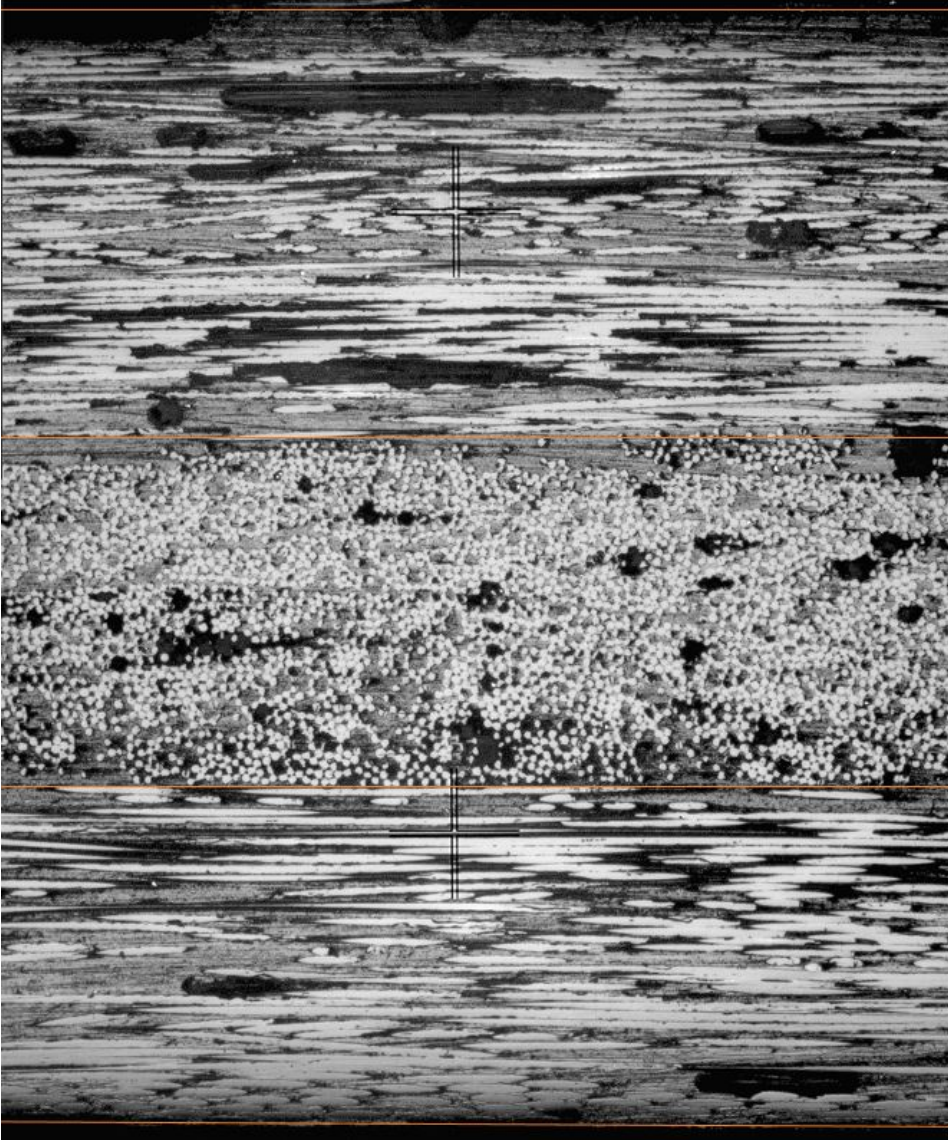


Figure D.5: Picture nr. 5.

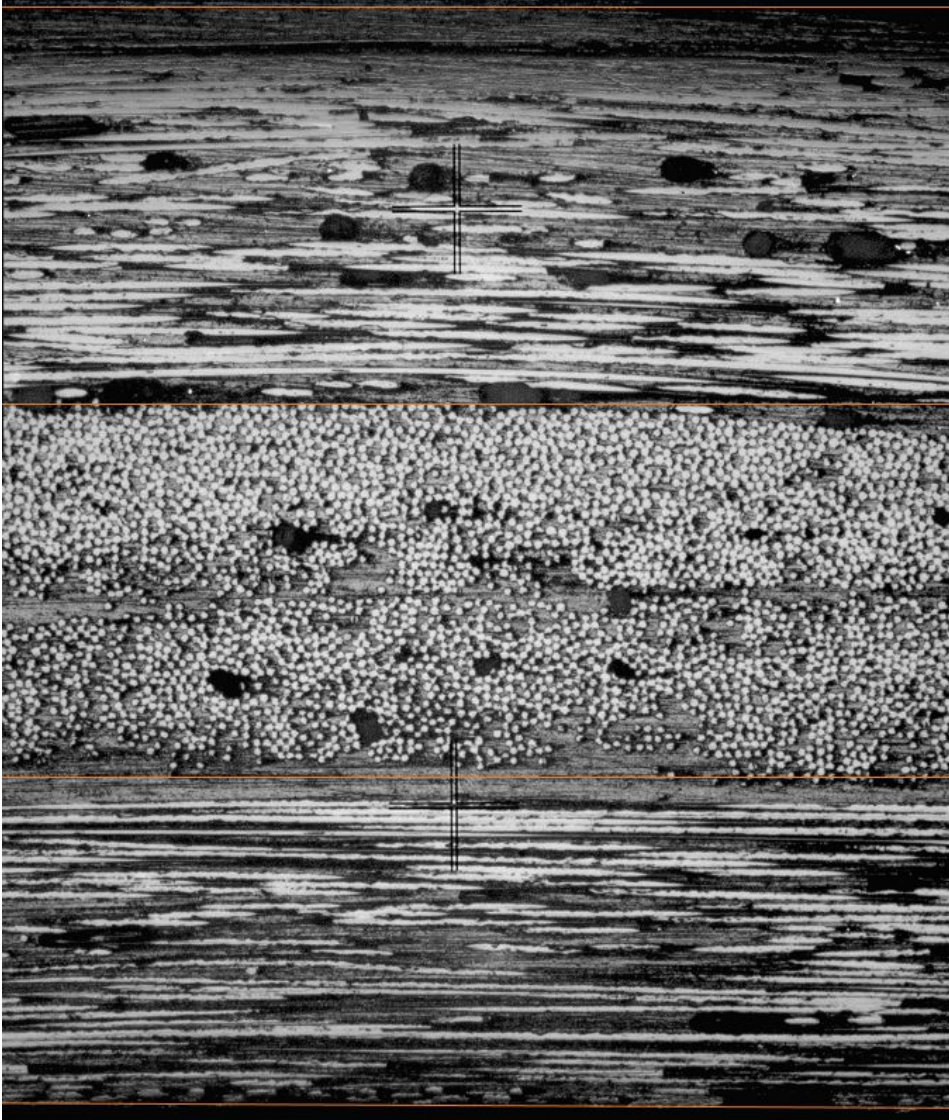


Figure D.6: Picture nr. 6.

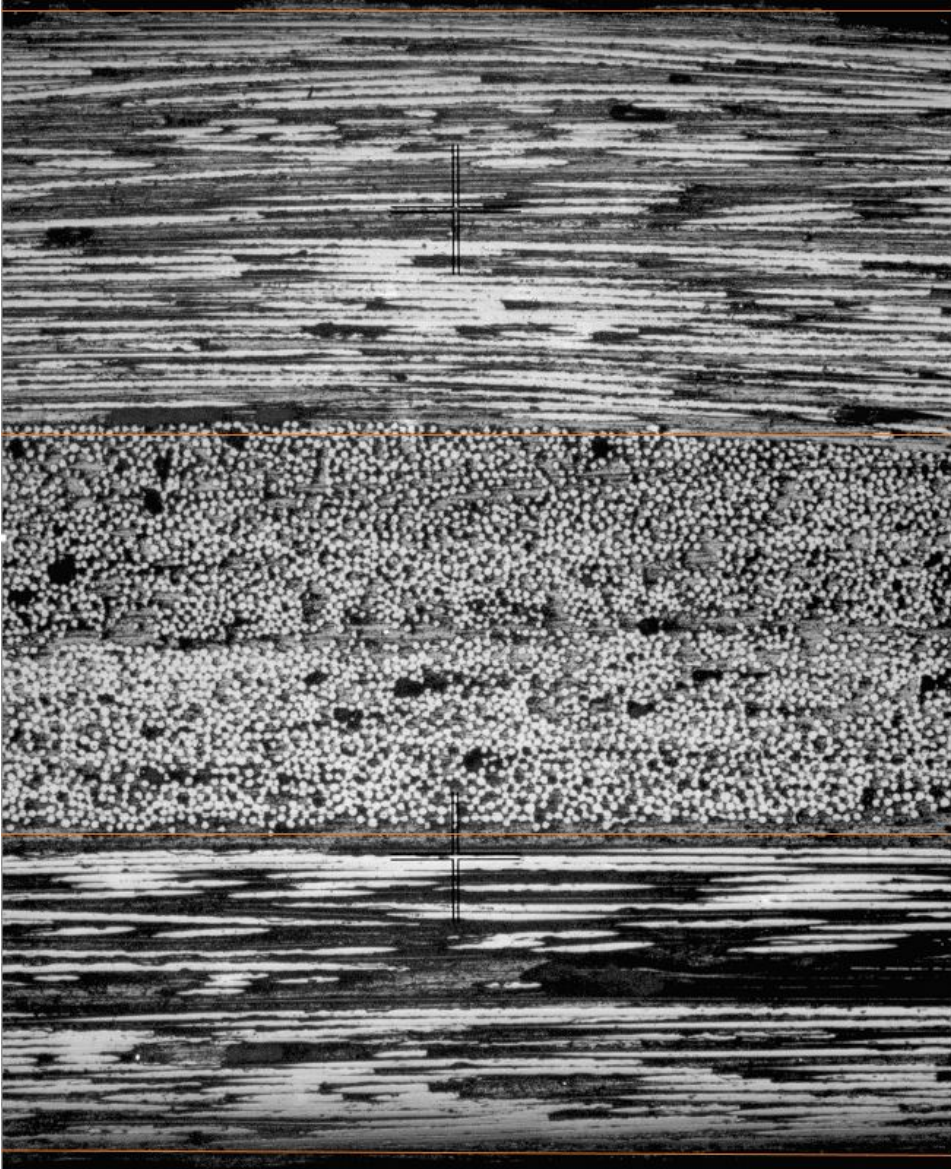


Figure D.7: Picture nr. 7.

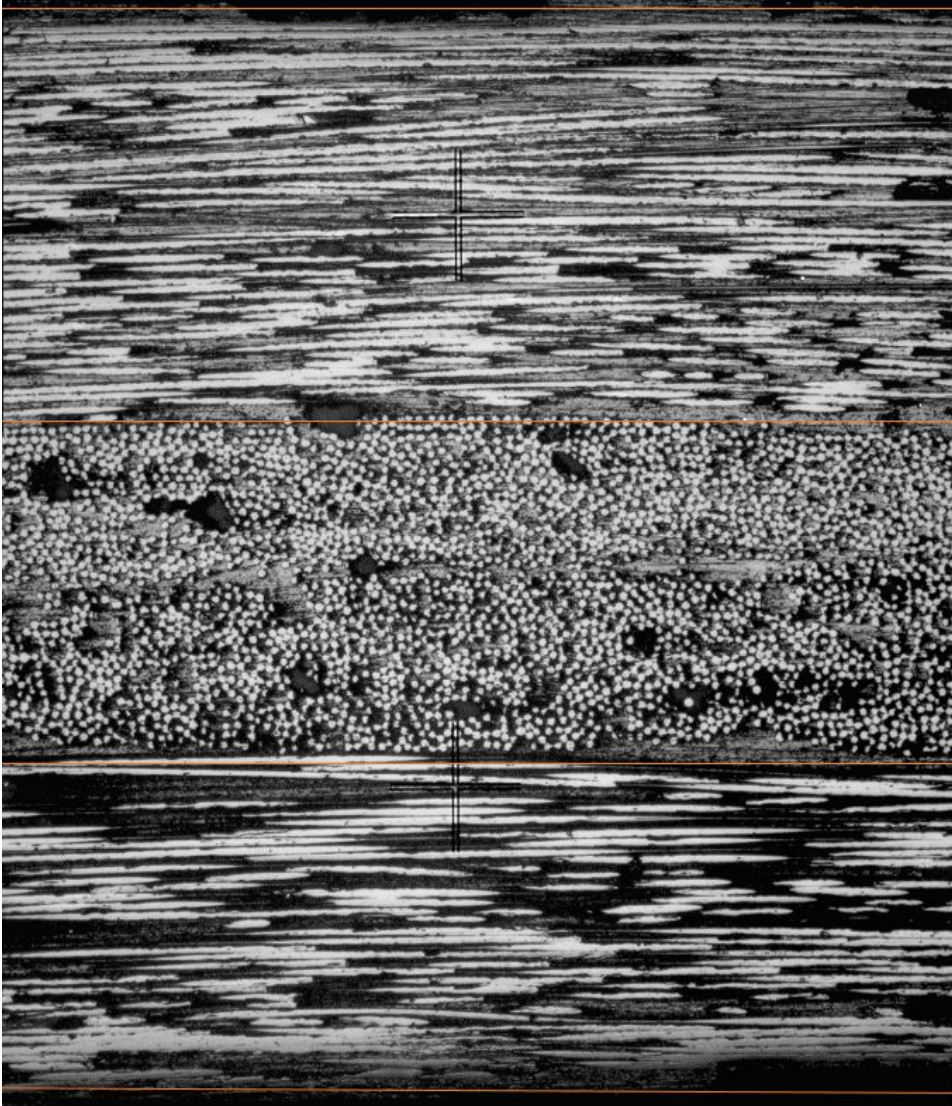


Figure D.8: Picture nr. 8.

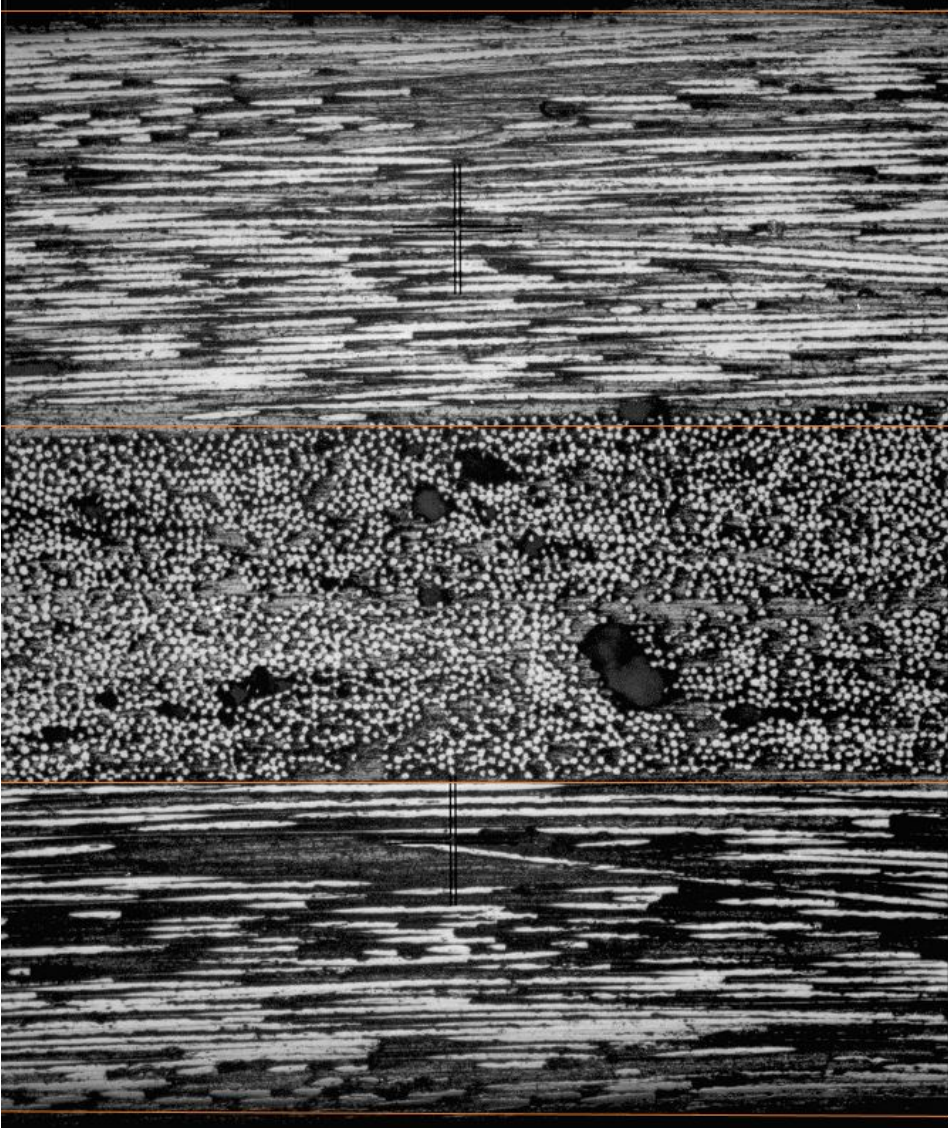


Figure D.9: Picture nr. 9.

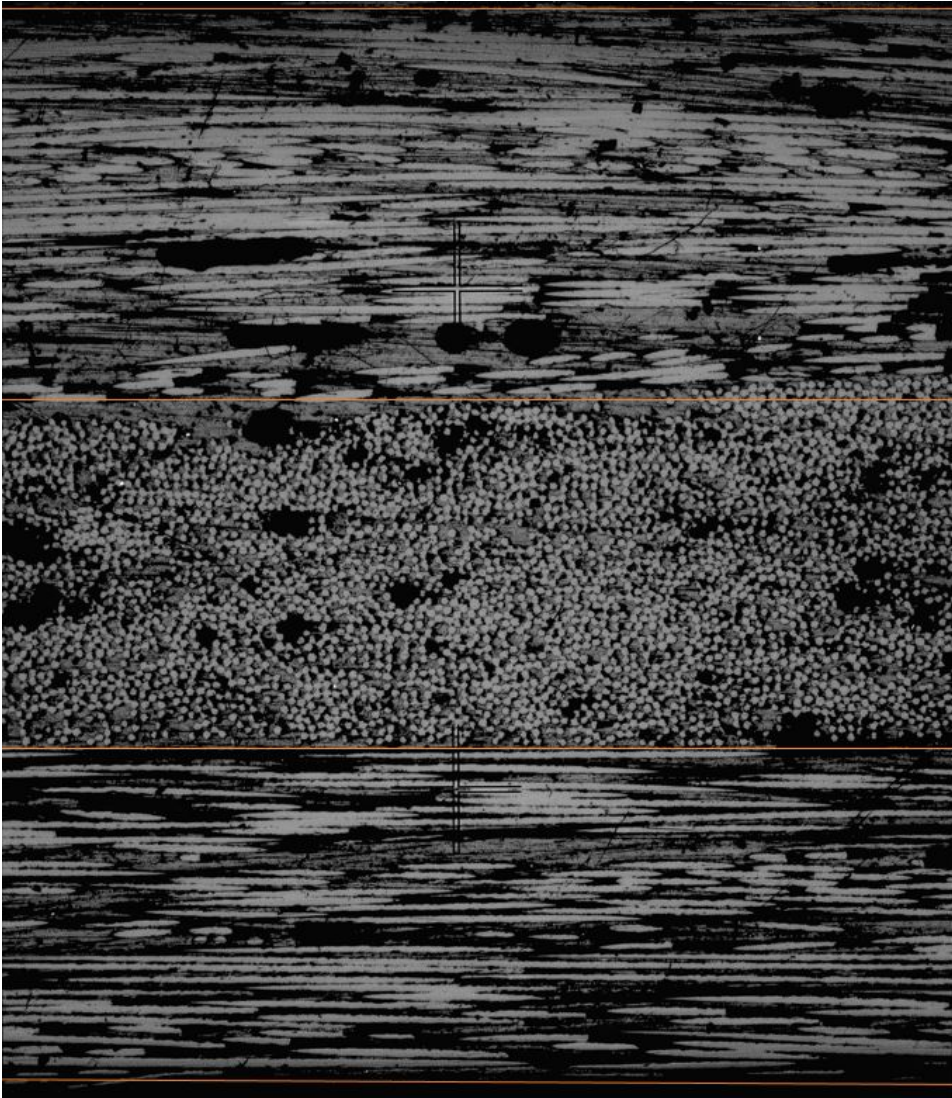


Figure D.10: Picture nr. 10.

D.2 layups for the optimal layup assessment

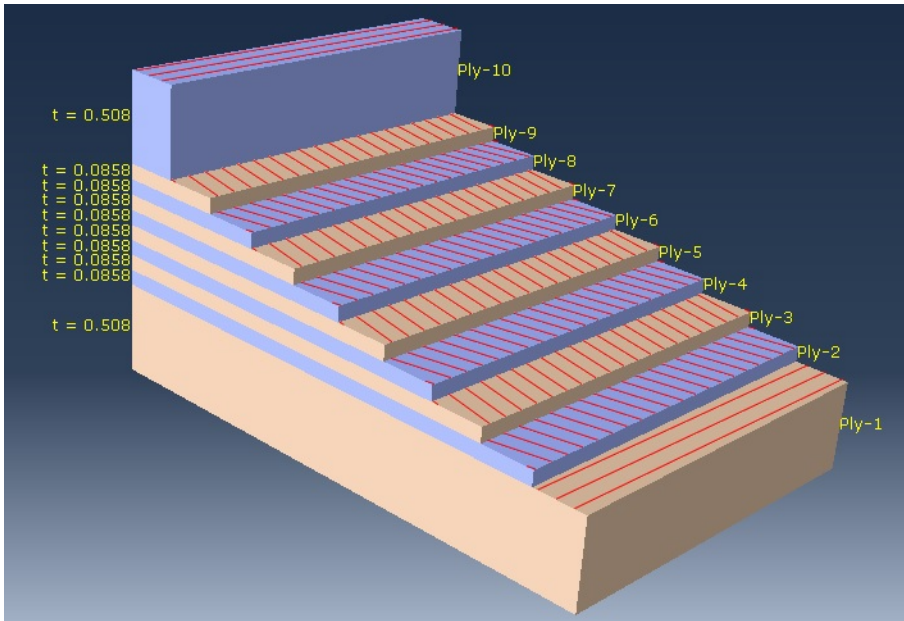


Figure D.11: Layup nr. 1, $[89^{\circ}_2/12.7^{\circ}_1/89^{\circ}_2]$, in Table 2.3.

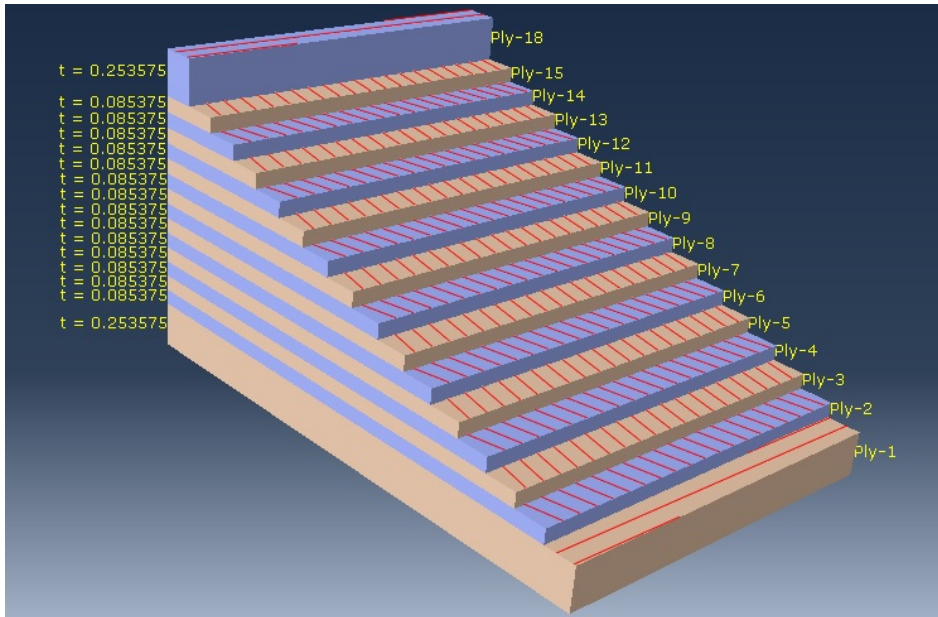


Figure D.12: Layup nr. 2, $[89^{\circ}_1/12.7^{\circ}_n/89^{\circ}_1]$ in Table 2.3.

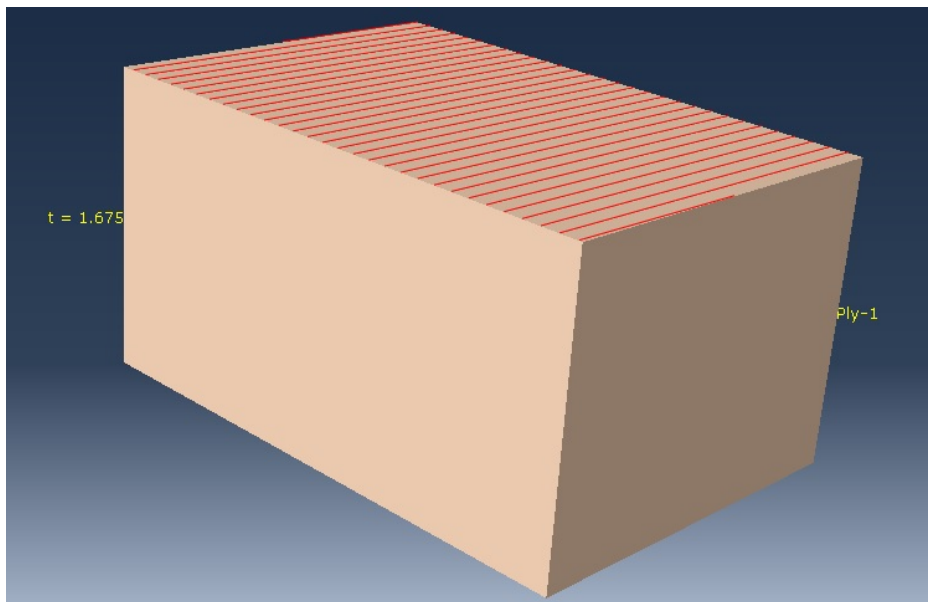


Figure D.13: Layup nr. 3, $[89^{\circ}_n]$, in Table 2.3.

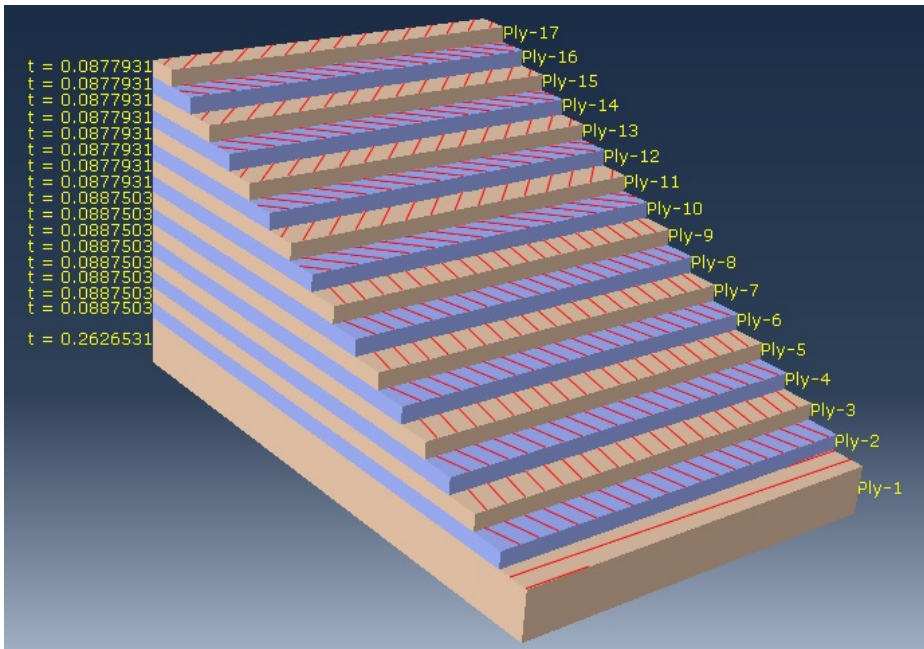


Figure D.14: Layup nr. 4, $[89^{\circ}_1/12.7^{\circ}_1/45^{\circ}_1]$, in Table 2.3.

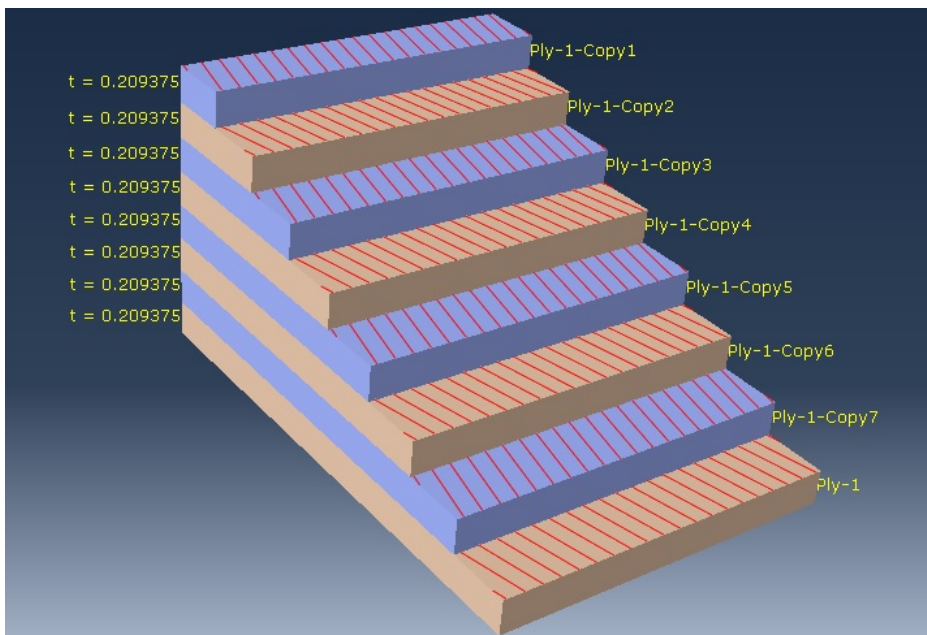


Figure D.15: Layup nr. 5, $[12.7^{\circ}_n]$, in Table 2.3.

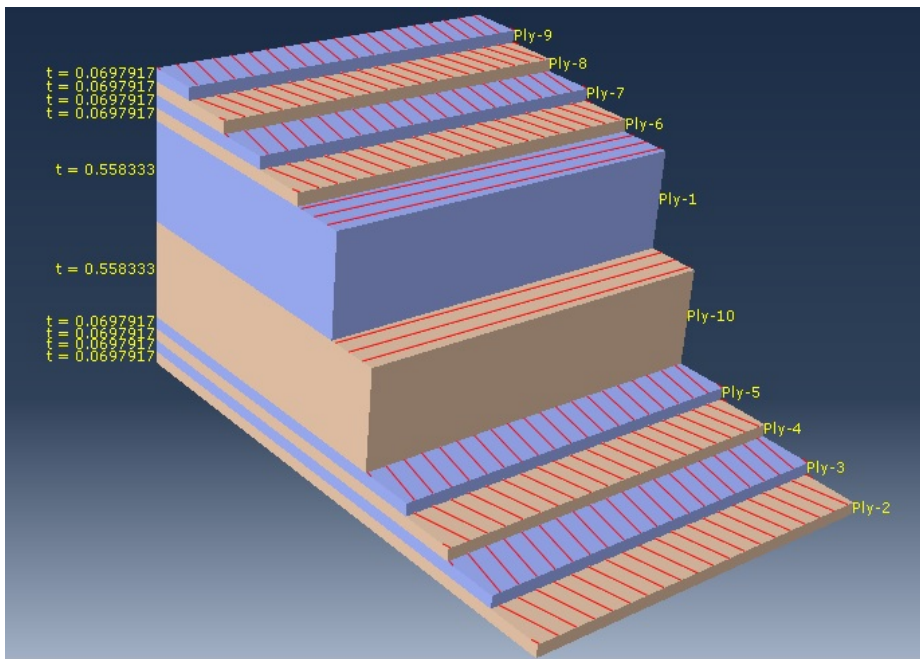


Figure D.16: Layup nr. 6, $[12.7^\circ_n/89^\circ_2/12.7^\circ_n]$, in Table 2.3.

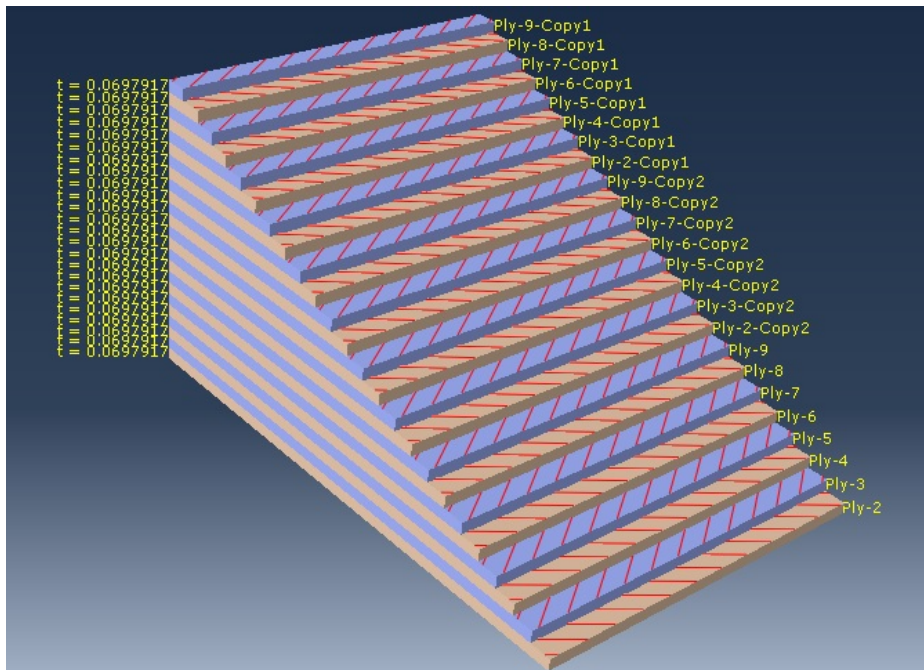


Figure D.17: Layup nr. 7, $[55^\circ_n]$, in Table 2.3.

D.3 Failure Criteria

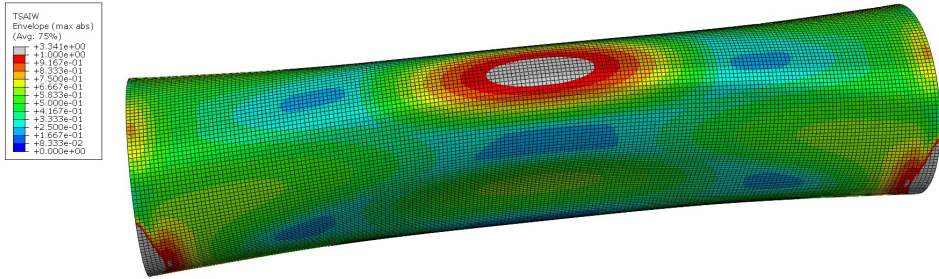


Figure D.18: Max exposure factor of the Tsai-Wu failure criterion through the thickness of the 400 mm long tube. The scaling factor is set to 5 and the failure pressure is 17.39 bar.

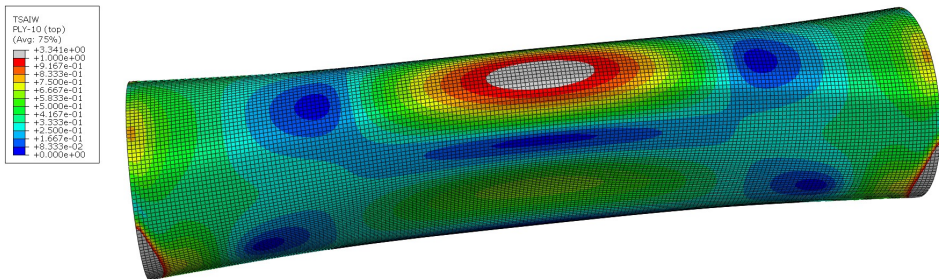


Figure D.19: Tsai-Wu failure criterion at the top of the top ply on the 400 mm long tube. The scaling factor is set to 5 and the failure pressure is 17.39 bar. As can be seen, the top of the lobe corresponds with the max exposure factor plot in Figure D.18, making it the most critical spot.

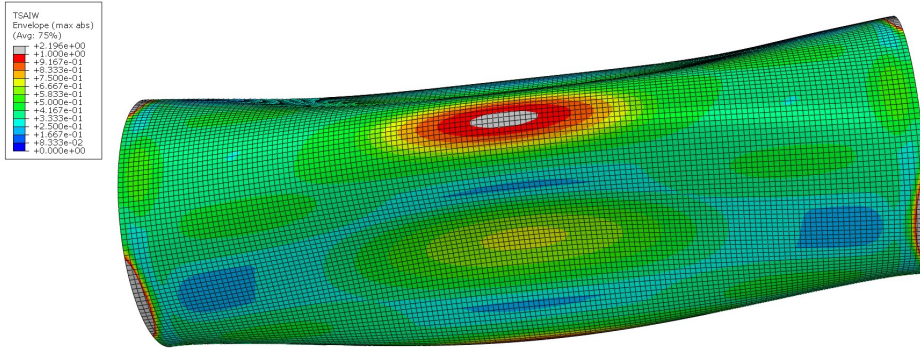


Figure D.20: Max exposure factor of the Tsai-Wu failure criterion through the thickness of the 300 mm long tube. The scaling factor is set to 5 and the failure pressure is 23.49 bar.

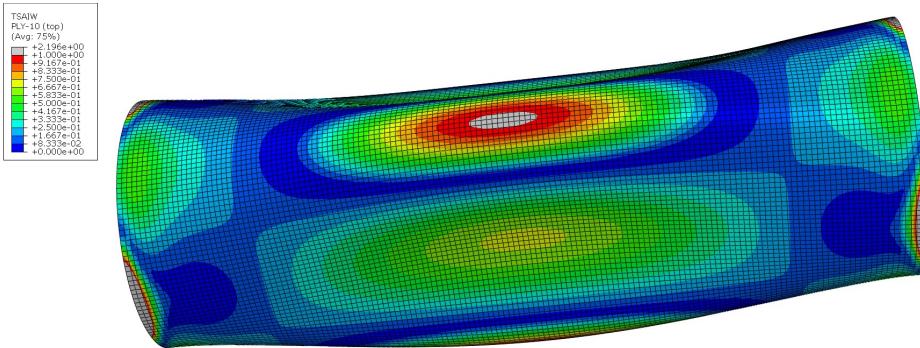


Figure D.21: Tsai-Wu failure criterion at the top of the top ply on the 300 mm long tube. The scaling factor is set to 5 and the failure pressure is 23.49 bar. As can be seen, the top of the lobe corresponds with the max exposure factor plot in Figure D.18, making it the most critical spot.

D.4 Deformation plots and tangential strain path start points

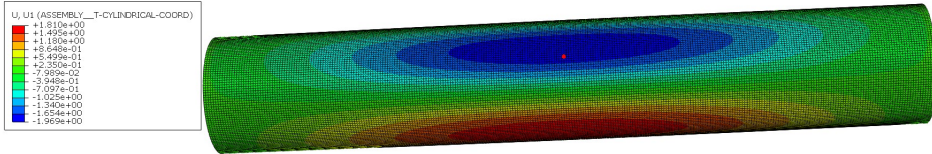


Figure D.22: Radial deformation plot on the 600 mm long tube at 9.67 bar together with the starting point of the path for the tangential strain graphs, indicated by the red dot. As can be seen the max radial deformation is -1.97 mm occurring in the creases. The deformation scale factor is set to 1.

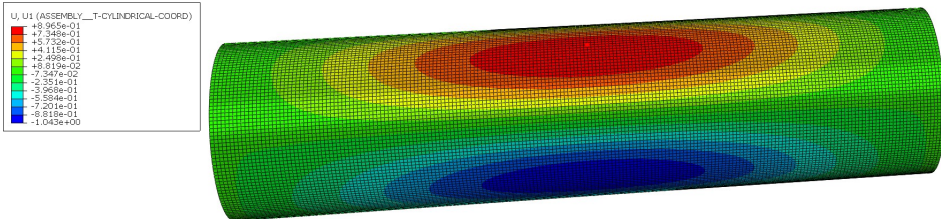


Figure D.23: Radial deformation plot on the 400 mm long tube at 15.23 bar together with the starting point of the path for the tangential strain graphs, indicated by the red dot. As can be seen the max radial deformation is -1.04 mm occurring in the creases. The deformation scale factor is set to 1.

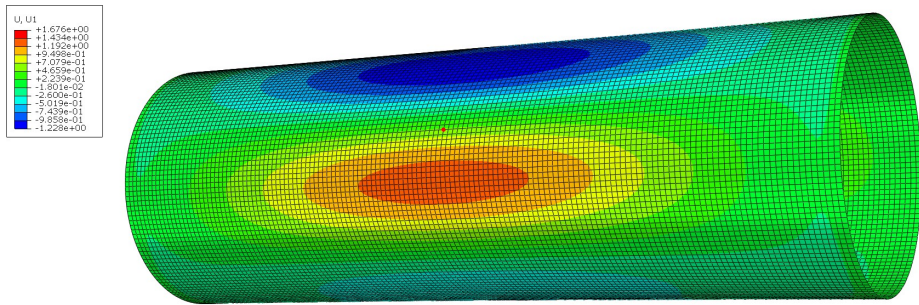


Figure D.24: Radial deformation plot on the 300 mm long tube at 23.27 bar together with the starting point of the path for the tangential strain graphs, indicated by the red dot. As can be seen the max radial deformation is 1.68 mm occurring at the lobes. The deformation scale factor is set to 1.

paper

Appendix **E**

Risk assessments

E.1 Risk assessment of thesis

NTNU	Kartlegging av risikofyllt aktivitet	Utarbeidet av	Nummer	Dato	
		HMS-avd.	HMSRV2601	22.03.2011	
HMS		Godkjent av	Side	Erstatter	
		Rektor	1 av 1	01.12.2006	



Enhet: IPM

Dato: 05.09.13

Deltakere ved kartleggingen (m/ funksjon): Eivind Hugaas (student), Andreas Echtermeyer (Veileder)

Kort beskrivelse av hovedaktivitet/hovedprosess: Prosjektoppgave: Buckling of thin walled composite tubes

ID nr.	Aktivitet/prosess	Ansvarlig	Eksisterende dokumentasjon	Eksisterende sikringstiltak	Lov, forskrift o.l.	Kommentar
1	Skriving av oppgave	Eivind Hugaas		Sikre nok søvn, Forebygge slitasjeskader i hånd	Arbeidsmiljøloven	
2	Bygging av testrig	Eivind Hugaas	Verkstedskurs	Vernesko, briller, Labfrakk, hansker, verkstedskurs		
3	Produksjon av komposittrør med NTNU's <i>Filament winding machine (FWM)</i>	Eivind Hugaas, Nils Petter Vedvik	MAW 20 LS 4/1 Filament Winding Machine User Manual	Vernesko, briller, Labfrakk, hansker, spesifikt <i>FWM kurs.</i>		
4	Testing	Eivind Hugaas		Vernesko, briller, Labfrakk, hansker, sperringer og sikring av testrig		

NTNU	Risikovurdering	utarbeidet av	Nummer	Dato	
		HMS-avd.	HMSRV2603	04.02.2011	
HMS/KS		godkjent av	side	Erstatter	
		Rektor	1 av 3	9.2.2010	

Enhet: IPM


Dato: 30.8.2013

Linjeleder:

Deltakere ved risikovurderingen (m/ funksjon): Eivind Hugaas (student), Andreas Echtermeyer (veileder)

ID nr	Aktivitet fra kartleggings-skjemaet	Mulig uønsket hendelse/ belastning	Vurdering av sannsynlighet	Vurdering av konsekvens:				Risiko-verdi	Kommentarer/status Forslag til tiltak
			(1-5)	Menneske (A-E)	Ytre miljø (A-E)	Øk/ materiell (A-E)	Om-dømme (A-E)		
1	Skriving av oppgave	Stressrelaterte plager	2	B				2B	Sikre nok søvn og passe på at arbeidsmengden blir jevn
		Musesyke	2	B				2B	Klatre hardt nok til at fingrene holder seg i god form.
2	Produksjon av testrig	Uheldig interaksjon mellom maskiner og menneske	1	C				1C	Vernesko, Briller, labfrakk og hjelm ved tunge løft.
3	Produksjon av komposittrør	Uheldig interaksjon mellom maskiner og menneske	1	B				1B	Vernesko, Briller, labfrakk
		Kjemikaliesøl på menneske	2	B				2B	Briller, labfrakk, ryddig lab, sikring av løse gjenstander.
		Kjemikaliesøl på utstyr	2			C		2C	Ryddig lab, sikring av løse gjenstander
4	Testing	Ukontrollert avblødning av trykk	1	B				1B	Gjennomgang av test før start, påse at rig tåler makstrykk med sikkerhetsmargin, sikre testrig mot eventuelle trykkakselererte løse gjenstander.

E.2 Risk assessment of filament winding

Sikkerhets- og kvalitetsgjennomgang av laboratorietester og verkstedsarbeid <i>Safety and Quality Evaluation of Activities in the Laboratory and Workshop</i>		 Perleporten	
1 Identifikasjon - Identification		Dokumentnr. - Document no.:	
Kundenavn – Customer name Eivind Hugaas	Prosjektnavn – Project name Optimize resistance to buckling under external hydrostatic pressure of thin walled composite tubes	Prosjektnr. – Project no. 69450723	
Beskrivelse av arbeid – Description of job Filament winding of 100 mm diameter glass fiber tube on the FWM at NTNU.		Dato – Date 29.04.2014	
2 Prosjekt - Team			
Prosjektleder og organisasjon – Project manager and organisation	Eivind Hugaas - NTNU	Ansvarlig for instrumentering – Responsible for instrumentation.	Eivind Hugaas
Leiestedsansvarlig – Laboratory responsible	Nils Petter Vedvik	Operatør – Operator	Eivind Hugaas
Auditør for sikkerhets og kvalitetsgjennomgang – Auditor for safety check	Nils Petter Vedvik	Ansvarlig for styring av forsøk – Responsible for running the experiment.	Eivind Hugaas
Ansvarlig for eksperimentelt faglig innhold – Responsible for experimental and scientific content	Nils Petter Vedvik	Ansvarlig for logging av forsøksdata – Responsible for logging and storing experimental data	Eivind Hugaas
Ansvarlig for dimensjonering av last og trykkpåkjennte komponenter – Responsible for dimensioning load bearing and pressurized components	Nils Petter Vedvik	Ansvarlig for montering av testrigg – Responsible for building the rig	Eivind Hugaas
3 Viktig!! – Important!!			J: Ja – Yes / N: Nei - No
Er arbeidsordren signert? – Is the work order signed?			J
Har operatøren nødvendig kurs/trening i bruk av utstyret? - Has the operator the required courses/training on the equipment?			J
Har operatøren sikkerhetskurs? (påbudt) – Has the operator followed the safety courses? (mandatory)			J
Kan jobben gjøres alene? - Can the work be done alone?			J
- Dersom ja, er det med visse forbehold (for eksempel, må bruke alarm, ha avtale med noen som kommer innom med jevne mellomrom eller lignende). Dette må vurderes i Seksjon 5. If yes, the work may have to be done under special conditions (e. g. must use the alarm, have agreement with some coming back periodically or similar). This shall be evaluated in Section 5.			
4.1 Sikkerhet – Safety (Testen medfører – The test contains)			J: Ja – Yes / N: Nei - No
Stor last – Big loads	J	Brannfare – Danger of fire	N
Tunge løft – Heavy lifting	J	Arbeid i høyden – Working at heights	N
Hengende last – Hanging load	J	Hydraulisk trykk – Hydraulic pressure	N
Gasstrykk – Gas pressure	N	Vanntrykk – Water pressure	N
Høy temperatur – High temperature	J	Lav temperatur – Low temperature	N
Deler i høy hastighet – Parts at high velocity	J	Farlige kjemikalier – Dangerous chemicals	J
Sprutakselerasjon ved brudd – Sudden acceleration at fracture/failure	J	Forspente komponenter – Pre-tensioned components	N
Farlig støv – Dangerous dust	N	Kraftig støy – Severe noise	N
Klemfare – Danger of pinching	J	Roterende deler – Rotating parts	J
4.2 Påkrevet verneutstyr – Required safety equipment			J: Ja – Yes / N: Nei - No
Briller (påbudt) – Glasses (mandatory)	J	Vernesko – Safety shoes	J
Hjelm – Helmet	N	Hansker – Gloves	J
Skjerm – Screen	N	Visir – Visir	N
Hørselsvern – Ear protection	N	Løfteredskap – Lifting equipment	N

Sikkerhets- og kvalitetsgjennomgang av laboratorietester og verkstedsarbeid

5.1 Beskrivelse av aktivitet – Description of the activity (see Appendix)

Vurdering skal være basert på en skriftlig prosedyre for bruk av maskinen. I enkelte tilfeller kan prosedyre bli beskrevet direkte i tabellen nedenfor.

The evaluation shall be based on a written operating procedure for the machine. For simple cases the procedure can be directly described in the tables below.

Nr.	Beskrivelse av aktivitet – Description of activity	Fare - Danger	Lov, forskrift o.l. – Legal requirements	Prosedyre nr. – Procedure no.	Sannsynlighet – Probability	Konsekvens – Consequence	Risiko – Risk
1	Lifting of mandrel	Dropping mandrel			2	A	2A
2	Handling of epoxy	Spilling epoxy			2	B	2B
3	Running the FWM	Pinching			1	B	1B
4	Heat treatment	Burns			1	B	1B
5	Entanglement	Pinching			1	B	1B

5.2 Korrigerende Tiltak – Corrective Actions

Nr.	Korrigerende tiltak – Corrective action	Sannsynlighet – Probability	Konsekvens – Consequence	Risiko – Risk	Utført dato – Date of action
1	Use lifting equipment for mandrel when lifting	1	A	1A	29.04.2013
2	Use gloves and safety glasses	1	A	1A	29.04.2013
3	Mark up the machine's perimeter of movement	1	A	1A	29.04.2013
4	Use heat resistant gloves	1	A	1A	29.04.2013
5	Use periemeter laser	1	A	1A	29.04.2013

Sikkerhets og kvalitetsgjennomgang av laboratorietester og verkstedsarbeid



5.3 Feilkilder – Reasons for mistakes/errors

Sjekkliste: Er følgende feilkilder vurdert? – Check list: Is the following considered?

J: Ja – Yes / N: Nei - No

Tap av strøm – Loss of electricity	N	Overspenning – Voltage surge	N
Elektromagnetisk støy – Electromagnetic noise	N	Manglende aggregatkapasitet av hydraulikk – Insufficient power of the machine	N
Jordfeil – Electrical earth failure	N	Vannsprut – Water jet	N
Ustabil trykk av hydraulikk/kraft – Unstable pressure or hydraulic force	J	Tilfeldig avbrudd av hydraulikk/kraft – Unintended interruption of power supply	J
Last-/ forskyvnings grenser etablert? – Are load and displacement limits established?	J	Lekkasjer (slanger/koblinger, etc.) – Leakage of pipes, hoses, joints, etc.	N
Mulige påvirkninger fra andre aktiviteter – Possible interference from other activities	N	Mulige påvirkninger på andre aktiviteter – Possible interference towards other activities	N
Problemer med datalogging og lagring – Troubles in loading and storage	N	Brann i laboratoriet – Fire in the laboratory	J

6 Kalibreringsstatus for utstyr – Calibration of equipment

(ex: load cell, extensometer, pressure transducer, etc)

I.D.	Utstyr - Equipment	Gyldig til (dato) – Valid until (date)
1	Eye	Next winding

7 Sporbarhet – Traceability

Eksisterer – Is there

J: Ja – Yes / N: Nei - No

Er alle prøvematerialene kjente og identifiserbare? – Are all experimental materials known and traceable?	J
Eksisterer det en plan for markering av alle prøvene? – Is there a plan for marking all specimens?	J
Er dataloggingsutstyret identifisert? – Is the data acquisition equipment identified?	J
Er originaldata lagret uten modifikasjon? – Are the original data stored safely without modification?	J
Eksisterer det en backup-prosedyre? – Is there a back-up procedure for the data (hard disk crash)?	N
Eksisterer det en plan for lagring av prøvestykker etter testing? – Is there a plan for storing samples after testing?	J
Eksisterer en plan for avhending av gamle prøvestykker? – Is there a plan for disposing of old samples?	J


8 Kommentarer – Comments

9 Signaturer – Signatures

Godkjent (dato/sign) – Approved (date/signature)

Prosjektleder – Project leader	Verifikatør – Verifier	Godkjent – Approved by

E.3 Risk assessment of testing

Sikkerhets- og kvalitetsgjennomgang av laboratorietester og verkstedsarbeid <i>Safety and Quality Evaluation of Activities in the Laboratory and Workshop</i>		 Perleporten	
1 Identifikasjon - Identification		Dokumentnr. - Document no.:	
Kundenavn – <i>Customer name</i> Eivind Hugaas	Prosjektnavn – <i>Project name</i> Optimize resistance to buckling under external hydrostatic pressure of thin walled composite tubes	Prosjektnr. – <i>Project no.</i> 69450723	
Beskrivelse av arbeid – <i>Description of job</i> Pressure testing of 100 mm diameter tubes in the Autoclave at IPM.		Dato – <i>Date</i> 29.04.2014	
2 Prosjekt - Team			
Prosjektleder og organisasjon – <i>Project manager and organisation</i>	Eivind Hugaas - NTNU	Ansvarlig for instrumentering – <i>Responsible for instrumentation.</i>	Eivind Hugaas
Leiestedsansvarlig – <i>Laboratory responsible</i>	Nils Petter Vedvik	Operatør – <i>Operator</i>	Eivind Hugaas
Auditør for sikkerhets og kvalitetsgjennomgang – <i>Auditer for safety check</i>	Nils Petter Vedvik	Ansvarlig for styring av forsøk – <i>Responsible for running the experiment.</i>	Eivind Hugaas
Ansvarlig for eksperimentelt faglig innhold – <i>Responsible for experimental and scientific content</i>	Nils Petter Vedvik	Ansvarlig for logging av forsøksdata – <i>Responsible for logging and storing experimental data</i>	Eivind Hugaas
Ansvarlig for dimensjonering av last og trykkpåkjennte komponenter – <i>Responsible for dimensioning load bearing and pressurized components</i>	Nils Petter Vedvik	Ansvarlig for montering av testrigg – <i>Responsible for building the rig</i>	Eivind Hugaas
3 Viktig!! – Important!!			J: Ja – Yes / N: Nei - No
Er arbeidsordren signert? – <i>Is the work order signed?</i>			J
Har operatøren nødvendig kurs/trening i bruk av utstyret? – <i>Has the operator the required courses/training on the equipment?</i>			J
Har operatøren sikkerhetskurs? (påbudt) – <i>Has the operator followed the safety courses? (mandatory)</i>			J
Kan jobben gjøres alene? – <i>Can the work be done alone?</i>			J
- Dersom ja, er det med visse forbehold (for eksempel, må bruke alarm, ha avtale med noen som kommer innom med jevne mellomrom eller lignende). Dette må vurderes i Seksjon 5. <i>If yes, the work may have to be done under special conditions (e. g. must use the alarm, have agreement with some coming back periodically or similar). This shall be evaluated in Section 5.</i>			
4.1 Sikkerhet – Safety (Testen medfører – <i>The test contains</i>)			J: Ja – Yes / N: Nei - No
Stor last – <i>Big loads</i>	J	Brannfare – <i>Danger of fire</i>	N
Tunge løft – <i>Heavy lifting</i>	J	Arbeid i høyden – <i>Working at heights</i>	N
Hengende last – <i>Hanging load</i>	J	Hydraulisk trykk – <i>Hydraulic pressure</i>	N
Gasstrykk – <i>Gas pressure</i>	J	Vanntrykk – <i>Water pressure</i>	J
Høy temperatur – <i>High temperature</i>	N	Lav temperatur – <i>Low temperature</i>	N
Deler i høy hastighet – <i>Parts at high velocity</i>	N	Farlige kjemikalier – <i>Dangerous chemicals</i>	N
Sprutakselerasjon ved brudd – <i>Sudden acceleration at fracture/failure</i>	J	Forspente komponenter – <i>Pre-tensioned components</i>	J
Farlig støv – <i>Dangerous dust</i>	N	Kraftig støv – <i>Severe noise</i>	J
Klemfare – <i>Danger of pinching</i>	J	Roterende deler – <i>Rotating parts</i>	N
4.2 Påkrevet verneutstyr – Required safety equipment			J: Ja – Yes / N: Nei - No
Briller (påbudt) – <i>Glasses (mandatory)</i>	J	Vernesko – <i>Safety shoes</i>	J
Hjelm – <i>Helmet</i>	J	Hansker – <i>Gloves</i>	J
Skjerm – <i>Screen</i>	N	Visir – <i>Visir</i>	N
Hørselsvern – <i>Ear protection</i>	J	Løfteredskap – <i>Lifting equipment</i>	J

Sikkerhets og kvalitetsgjennomgang av laboratorietester og verkstedsarbeid



5.3 Feilkilder – Reasons for mistakes/errors

Sjekkliste: Er følgende feilkilder vurdert? – Check list: Is the following considered?

J: Ja – Yes / N: Nei - No

Tap av strøm – Loss of electricity	N	Overspenning – Voltage surge	N
Elektromagnetisk støy – Electromagnetic noise	N	Manglende aggregatkapasitet av hydraulikk – Insufficient power of the machine	N
Jordfeil – Electrical earth failure	N	Vannsprut – Water jet	J
Ustabil trykk av hydraulikk/kraft – Unstable pressure or hydraulic force	J	Tilfeldig avbrudd av hydraulikk/kraft – Unintended interruption of power supply	J
Last-/ forskyvnings grenser etablert? – Are load and displacement limits established?	J	Lekkasjer (slanger/koblinger, etc.) – Leakage of pipes, hoses, joints, etc.	J
Mulige påvirkninger fra andre aktiviteter – Possible interference from other activities	N	Mulige påvirkninger på andre aktiviteter – Possible interference towards other activities	N
Problemer med datalogging og lagring – Troubles in loading and storage	J	Brann i laboratoriet – Fire in the laboratory	J

6 Kalibreringsstatus for utstyr – Calibration of equipment

(ex: load cell, extensometer, pressure transducer, etc)

I.D.	Utstyr - Equipment	Gyldig til (dato) – Valid until (date)
1	Manometre	Next test

7 Sporbarhet – Traceability

Eksisterer – Is there

J: Ja – Yes / N: Nei - No

Er alle prøvematerialene kjente og identifiserbare? – Are all experimental materials known and traceable?	J
Eksisterer det en plan for markering av alle prøvene? – Is there a plan for marking all specimens?	J
Er dataloggingsutstyret identifisert? – Is the data acquisition equipment identified?	J
Er originaldata lagret uten modifikasjon? – Are the original data stored safely without modification?	J
Eksisterer det en backup-prosedyre? – Is there a back-up procedure for the data (hard disk crash)?	J
Eksisterer det en plan for lagring av prøvestykker etter testing? – Is there a plan for storing samples after testing?	J
Eksisterer en plan for avhending av gamle prøvestykker? – Is there a plan for disposing of old samples?	J

8 Kommentarer – Comments

9 Signaturer – Signatures

Godkjent (dato/sign) – Approved (date/signature)

Prosjektleder – Project leader	Verifikatør – verifier	Godkjent – Approved by

E.4 Risk assessment explanation

Sikkerhets og kvalitetsgjennomgang av laboratorietester og verkstedsarbeid



APPENDIX Bakgrunn - Background

Sannsynlighet vurderes etter følgende kriterier:

Probability shall be evaluated using the following criteria:

Svært liten Very unlikely 1	Liten Unlikely 2	Middels Probable 3	Stor Very Probable 4	Svært stor Nearly certain 5
1 gang/50 år eller sjeldnere – Once per 50 years or less	1 gang/10 år eller sjeldnere – Once per 10 years or less	1 gang/år eller sjeldnere – Once a year or less	1 gang/måned eller sjeldnere – Once a month or less	Skjer ukentlig – Once a week

Konsekvens vurderes etter følgende kriterier:

Consequence shall be evaluated using the following criteria:

Gradering – Grading	Menneske – Human	Ytre miljø, Vann, jord og luft – Environment	Øk/materiell – Financial/Material	Omdømme – Reputation
E Svært Alvorlig – Very critical	Død – Death	Svært langvarig og ikke reversibel skade – Very prolonged, non-reversible damage	Drifts- eller aktivitetsstans >1 år. – Shutdown of work >1 year.	Troverdighet og respekt betydelig og varig svekket – Trustworthiness and respect are severely reduced for a long time.
D Alvorlig – Critical	Alvorlig personskade. Mulig uførhet. – May produce fatality/ies	Langvarig skade. Lang restitusjonstid – Prolonged damage. Long recovery time.	Driftsstans > ½ år Aktivitetsstans i opp til 1 år – Shutdown of work 0,5-1 year.	Troverdighet og respekt betydelig svekket – Trustworthiness and respect are severely reduced.
C Moderat – Dangerous	Alvorlig personskade. – Permanent injury, may produce serious health damage/sickness	Mindre skade og lang restitusjonstid – Minor damage. Long recovery time	Drifts- eller aktivitetsstans < 1 mnd – Shutdown of work < 1 month.	Troverdighet og respekt svekket – Troverdighet og respekt svekket.
B Liten – Relatively safe	Skade som krever medisinsk behandling – Injury that requires medical treatment	Mindre skade og kort restitusjonstid – Minor damage. Short recovery time	Drifts- eller aktivitetsstans < 1 uke – Shutdown of work < 1 week.	Negativ påvirkning på troverdighet og respekt – Negative influence on trustworthiness and respect.
A Sikker – Safe	Injury that requires first aid	Insignificant damage. Short recovery time	Shutdown of work < 1 day	

Risikoverdi = Sannsynlighet X Konsekvenser

Beregn risikoverdi for menneske. IPM vurderer selv om de i tillegg beregner risikoverdi for ytre miljø, økonomie/ material og omdømme. I så fall beregnes disse hver for seg.

Risk = Probability X Consequence

Calculate risk level for humans. IPM shall evaluate itself if it shall calculate in addition risk for the environment, economic/material and reputation. If so, the risks shall be calculated separately.

Risikomatrisen

Risk Matrix

I risikomatrisen er ulike grader av risiko merket med rødt, gul eller grønn:

Rødt: Uakseptabel risiko. Tiltak skal gjennomføres for å redusere risikoen.

Gul: Vurderingsområde. Tiltak skal vurderes.

Grønn: Akseptabel risiko. Tiltak kan vurderes ut fra andre hensyn.

Når risikoverdien havner på rødt felt, skal altså enheten gjennomføre tiltak for å redusere risikoen. Etter at tiltak er iverksatt, skal dere foreta ny risikovurdering for å se om risikoen har sunket til akseptabelt nivå.

For å få oversikt over samlet risiko: Skriv risikoverdi og aktivitetens IDnr. i risikomatrise (docx) / risikomatrise (odt). Eksempel: Aktivitet med IDnr. 1 har fått risikoverdi 3D. I felt 3D i risikomatrisen skriver du IDnr. 1. Gjør likedan for alle aktiviteter som har fått en risikoverdi. En annen måte å skaffe oversikt på, er å fargelegge feltet med risikoverdien i skjemaet for risikovurdering. Dette tydeliggjør og gir samlet oversikt over risikoforholdene. Ledelse og brukere får slik et godt bilde av risikoforhold og hva som må prioriteres.

In the risk matrix different degrees of risk are marked with red, yellow or green;

Red: Unacceptable risk. Measures shall be taken to reduce the risk.

Yellow: Assessment Area . Measures to be considered.

Green: Acceptable risk. Measures can be evaluated based on other considerations.

When a risk value is red, the unit shall implement measures to reduce risk. After the action is taken, you will make a new risk assessment to see if the risk has decreased to acceptable levels.

To get an overview of the overall risk: Write the risk value and the task ID no . the risk matrix (docx) / risk matrix (odt) . Example : Activity with ID no . 1 has been risk value 3D. In the field of 3D risk matrix type ID no . 1 Do the same for all activities that have been a risk . Another way to get an overview is to color the field of risk value in the form of risk assessment . This clarifies and gives overview of the risk factors . Management and users get such a good picture of the risks and what needs to be prioritized.

KONSEKVENNS	Svært alvorlig	E1	E2	E3	E4	E5
	Alvorlig	D1	D2	D3	D4	D5
	Moderat	C1	C2	C3	C4	C5
	Liten	B1	B2	B3	B4	B5
	Svært liten	A1	A2	A3	A4	A5
		Svært liten	Liten	Middels	Stor	Svært stor
		SANNSYNLIGHET				

Prinsipp over akseptkriterium. Forklaring av fargene som er brukt i risikomatriksen.

Farge	Beskrivelse
Rød	Uakseptabel risiko. Tiltak skal gjennomføres for å redusere risikoen.
Gul	Vurderingsområde. Tiltak skal vurderes.
Grønn	Akseptabel risiko. Tiltak kan vurderes ut fra andre hensyn.

Til Kolonnen "Korrigerende Tiltak":

Tiltak kan påvirke både sannsynlighet og konsekvens. Prioriter tiltak som kan forhindre at hendelsen inntreffer, dvs sannsynlighetsreducerende tiltak foran skjerpene beredskap, dvs konsekvensreducerende tiltak.

For Column "Corrective Actions"

Corrections can influence both probability and consequence. Prioritize actions that can prevent an event from happening.

Oppfølging:

Tiltak fra risikovurderingen skal følges opp gjennom en handlingsplan med ansvarlige personer og tidsfrister.

Follow Up

Actions from the risk evaluation shall be followed through by an action plan with responsible persons and time limits.

Etterarbeid #

- Gå gjennom aktiviteten/prosessen på nytt.
- Foreta eventuell ny befaring av aktiviteten/prosessen for enten a) å få bekreftet at risikoverdiene er akseptable eller b) for å justere risikoverdiene.
- Gå gjennom, vurder og prioriter tiltak for å forebygge uønskede hendelser. Først skal dere prioritere tiltak som reduserer sannsynlighet for risiko. Dernest skal dere ta for dere tiltak som reduserer risiko for konsekvenser.
- Tiltakene skal føres inn i handlingsplanen. Skriv fristen for å gjennomføre tiltaket (dato, ikke tidsrom) og navn på den / de som har ansvar for tiltakene.
- Foreta helhetsvurdering for å avgjøre om det nå er akseptabel risiko.
- Ferdig risikovurdering danner grunnlag for å utarbeide lokale retningslinjer og HMS-dokumenter, opplæring og valg av sikkerhetsutstyr.
- Ferdig risikovurdering og eventuelle nye retningslinjer gjøres kjent/tilgjengelig for alle involverte.
- Sett eventuelt opp kostnadsoverslag over planlagte tiltak.